TRIARYLBORON-FUNCTIONALIZED 8-HYDROXYQUINOLINE AND THEIR RESPECTIVE ALUMINUM (III) AND DIBORON COMPOUNDS

by

Vladimir Zlojutro

A thesis submitted to the Department of Chemistry

In conformity with the requirements for

the degree of Master of Science

Queen's University

Kingston, Ontario, Canada

(September, 2011)

Abstract

The purpose of this thesis was to develop the first examples of multifunctional triarylboron-functionalized 8-hydroxyquinoline, their respective aluminum (III) complexes, Al($\mathbf{1}$)$_3$ and Al($\mathbf{2}$)$_3$, and diboron analogues, **B1** and **B2**. There was particular focus in investigating the electron accepting characteristics of these systems for potential use as electron transport materials (ETMs) in organic light emitting diodes (OLEDs).

The first part of the thesis will discuss the aluminum complexes. Through the introduction of the triarylboron moiety these derivatives of the well-known ETM tris(8-hydroxyquinoline)aluminum (Alq$_3$) exhibited better electron accepting properties than the parent compound. Furthermore, the complexes were able to act as sensors and indicators towards soft Lewis acids such as CN$^-$ and hard Lewis acids such as F$^-$, respectively.

First the structures of the compounds were investigated using COSY NMR, leading to the discovery that similar to Alq$_3$ the new aluminum complexes possessed the commonly observed *mer*-isomeric form. Furthermore, their photophysical characteristics were investigated using UV-Vis and fluorescence spectroscopic measurements. The solid state fluorescence quantum yield of Al($\mathbf{1}$)$_3$ ($\Phi=0.06$) and Al($\mathbf{2}$)$_3$ ($\Phi=0.02$) were measured and compared to Alq$_3$ ($\Phi=0.14$). In order to better understand these results and gain insight into the electronic transitions of the aluminum complexes, DFT calculations were employed using the B3LYP/6-31G* level of theory.

The second part of the thesis will discuss the only examples of diboron-functionalized 8-hydroxyquinoline complexes to date, with one three-coordinate and one four-coordinate boron moiety. Based on CV measurements and DFT calculations, it was discovered that the LUMO of the diboron compounds were lowered substantially compared to their aluminum analogues discussed earlier. More interestingly, it was found that only **B1** has any contributions to its

LUMO from the triarylboron moiety, leading to the slightly stronger electron accepting ability of **B1** compared to **B2**. Furthermore, these compounds were both able to act as sensors towards small anions such as F$^-$.

Acknowledgements

First of all, I would like to thank my parents, my brother and the rest of my family for all of their support throughout my studies. In particular, Mama and Daja you have been the most loving, supportive and encouraging parents a son could ask for and none of this would have been possible without you. Posebno, Tata, uvjek ču da zapamtim tvoju reči "Ne predaj se!". To my brother Zoki, thank you for being the best brother anyone could ask for, you have always been there and I couldn't have done it without you. IEE guys.

I would like to express my immense gratitude to my supervisor, Dr. Suning Wang, for all of her encouragement and guidance throughout my entire project. I know that there were days that I tested her patience and I want to thank her for never faltering and always believing in me. It has been a privilege to work for someone who is not only a model scientist and professor, but also a supervisor who works so tirelessly to mold her students into confident and successful people/scientists. It is with her support and guidance that I was able to accomplish this thesis.

Many thanks are in order to a number of the faculty members in the Chemistry Department at Queen's University for their time both in class and during office hours. In addition, I would like to thank Dr. Jean-Michel Nunzi and Dr. Donal Macartney for taking time out of their busy schedules to be on my committee. No matter how busy Dr. Francoise Sauriol was she would always drop everything immediately to assist me in obtaining a NMR spectra and to answer any questions I had regarding the data, and for that I have always been extremely grateful.

Thank you to the entire Wang group, past and present. Dr. Yi Sun who was my mentor in the lab and spent countless hours helping me reach my research goals. In addition, I would like to thank him for allowing me to use two of his compounds for my thesis, **2** and Al(**2**)$_3$. Dr. Chul Baik and Zachary M. Hudson for making me a master at Sonogashira and Suzuki coupling

Table of Contents

List of Figures

List of Tables

List of Symbols and Abbreviations

A	absorbance
Abs	absorbance
Al	aluminum
Anal	analytical
Alq_3	tris(8-hydroxyquinoline)
B3LYP	Becke 3-Parameter Exchange, Lee, Yang, Parr
br	broad
˚C	degrees Celsius
c	conventration
calcd	calculated
$CDCl_3$	deuterated chloroform
CD_2Cl_2	deuterated dichloromethane
cm	centimeters
CH_2Cl_2	dichloromethane
COSY	Correlation Spectroscopy
CT	charge transfer
CV	cyclic voltammetry
d	doublet
dd	doublet of doublet
DIPEA	diisopropylamine
DFT	density functional theory
ε	molar absorptivity

$E_{1/2}$	Half-reduction potential
E_a	electron affinity
EBL	electron blocking layer
EDG	electron donating group
EL	electroluminescent, emissive layer
Em	emission
EML	emissive layer
ETL	electron transport layer
ETM	electron transport material
eq.	equivalents
eV	electron volt
EWG	electron withdrawing group
fac	facial
g	grams
HBL	hole-blocking layer
HOMO	highest occupied molecular orbital
HQC	high- concentration quenching
HRMS	high resolution mass spectrometry
HTL	hole transport layer
HTM	hole transport material
hv	light
Hz	hertz
ICT	intramolecular charge transfer

ISC	intersystem crossing
ITO	indium tin oxide
J	coupling constant
kJ	kilojoules
l	path length
L	liter
LC	ligand centered
^{3}LC	triplet state ligand centered
LUMO	lowest unoccupied molecular orbital
m	meter, multiplet
M	Molar
mer	meridional
mg	milligram
mL	millilitres
μL	microliter
MLCT	metal to ligand charge transfer
mmol	millimole
μmol	micromole
MO	molecular orbital
mol	mole
m.p.	melting point
mV	millivolts
m/z	mass-to-charge ratio

nm	nanometres
NMR	nuclear magnetic resonance
OLED	organic light emitting diode
PL	photoluminescent
p.p.m.	parts-per-million
q	8-hydroxyquinoline
red	reduction
r.t.	room temperature
s	seconds
S_0	ground state singlet
S_1	excited state singlet
T_1	1st level excited triplet state
T_2	2nd level excited triplet state
TEA	triethylamine
T_g	glass transition temperature
THF	tetrahydrofuran
TMS	trimethylsilane
UV	ultraviolet
UV-Vis	ultraviolet-visible
V	volts
δ	chemical shift
λ	wavelength
Φ	quantum yield

Chapter 1
Introduction

The discovery of electroluminescence from thin films of tris-(8-hydroxyquinoline) aluminum (Alq_3) in 1987 by Tang and van Slyke[1] has led to extensive research in the application of organic materials with optoelectronic properties in OLEDs,[2-4] solar cells[5-7] and anion sensors[8,9]. While conventional inorganic materials yield efficient PVs and LEDs, they are often bulky, brittle and expensive to manufacture. On the other hand organic materials allow for the fabrication of thin films that lend the materials a great deal of flexibility, durability and effectively lower manufacturing costs due to novel printing techniques. Furthermore, the photophysical properties of these organic materials can be easily and precisely tuned for target applications.[10-13]

Although both Alq_3 and organoboron compounds have been demonstrated to have favorable optoelectronic properties, there is limited research on the combination of these two systems for device purposes. In particular, there are no examples of 8-hydroxyquinoline (q) modified with a triarylboron moiety. This chapter will begin with an introduction to luminescence, OLEDs, Alq_3 and organoboron compounds. Drawbacks to OLED lifetime and efficiency will be discussed as well as potential solutions with respect to the electron transport layer (ETL). The remainder of the introduction will be literature review on the functionalization and photophysical properties of Alq_3 and derivatives, and triarylboron compounds. This will lead to the final chapter, which will outline the motivation of this dissertation.

1.1 Luminescence

When sufficient energy is provided to a molecule the electrons can overcome the energy barrier required to move from its ground state to a higher energy level. The excited electron may return back to the ground state by dissipating its energy in one of three ways: (1) fluorescence, where the excess energy is emitted as a photon, (2) non-radiative decay, which is the loss of energy through molecular vibrations or chemical reactions and (3) phosphorescence which requires the conversion of a singlet state to a triplet state followed by emission of a photon. There are a variety of methods to induce excitation and subsequent emission such as mechanoluminescence,[14,15] chemiluminescence,[16,17] bioluminescence,[17] thermoluminescence,[18,19] photoluminescence[20] and electroluminescence.[2] Though we will go into more detail of photo- and electroluminescence.

1.1.1 Photoluminescence (PL)

Photoluminescence is the process by which an electron absorbs a photon, electromagnetic radiation, and is subsequently promoted into an excited state. Furthermore, the energy of a photon, based on its wavelength, will dictate what excited state energy level the electron can reach. Within each energy level there are often several closely spaced vibrational states. It is common for an electron to migrate to a lower vibrational state within the excited state (S_1) before

2

returning to the ground state (S_0). As such the excitation wavelength is always slightly shorter than the emission wavelength, leading to peaks with a small separation, referred to as a Stokes shift. This mechanism is typical of fluorescence. On the other hand the mechanism behind phosphorescence is quite different.

Phosphorescence is quite rare in organic materials due to the forbidden transition of an electron from a singlet state to a triplet state. Upon excitation, the electron is excited to a higher singlet state (S_1). From here the electron undergoes an intersystem crossing (ISC) where it is converted from a singlet state (S_1) to a triplet state (T_1). The electron then relaxes to the singlet ground state (S_0) by emitting a photon. This phenomenon is common in metal complexes due to spin-orbital coupling.[21]

The difference between fluorescence and phosphorescence is illustrated in the Jablonski diagram (**Figure 1.1**). Due to the forbidden nature of phosphorescence, typical emission rates are 10^3-10^0 s^{-1} resulting in lifetimes that are typically milliseconds to seconds, while fluorescence is much quicker having an emission rate of 10^{-8} s^{-1} and a lifetime of 10 x 10^{-9} s.[20]
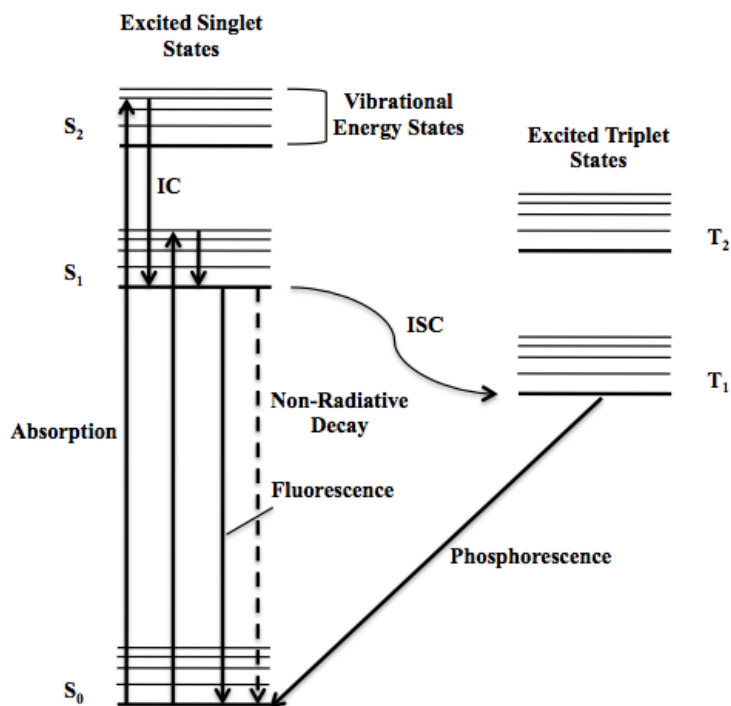
Figure 1.1 The Jablonski diagram.

1.1.2 Quantum Yield

Due to the various pathways an excited electron may take back to its ground state, both radiative and non-radiative, an important molecular characteristic is the quantum yield (Φ), which is the ratio between the number of photons absorbed and subsequently emitted by the molecule. The most efficient molecule will approach but rarely reach unity due to Stokes shift. In order to determine the quantum yield of an unknown compound a standard, such as rhodamine, 9,10-diphenylanthracene or quinine bisulfate, whose absorbance profile closely matches the unknown is used.[22] The quantum yield is then calculated using the following equation:

4

Equation 1.1

$$\phi_x = \left| \frac{\left(A_s F_x n_x^{\;2}\right)}{\left(A_x F_s n_s^{\;2}\right)} \right| \phi_s$$

where the subscript x and s denote the unknown and standard compounds, respectively, A is the absorbance, F is the integrated area of the emission peak, and n is the refractive index of the solvent.[22]

According to Beer's Law an increased concentration will result in a subsequent increase in the absorbance values as shown in equation 1-2:

Equation 1.2

$$A = \varepsilon c \ell$$

where A is the absorbance, l is the path length of the cell, c is the concentration of the solution and ε is the molar absorptivity. As the concentration exceeds a certain threshold light is simply reflected by the large number of molecules within a solution giving inaccurate absorbance values. Furthermore, there will be an increased number of molecular collisions providing an alternate pathway for excited molecules to dissipate their energy. Therefore, in order to achieve accurate quantum yield measurements the absorbance at the intersection between the absorbance peaks of the standard and the unknown compound, which will be used as the excitation wavelength, must be below 0.05.[22]

1.2 Electroluminescence and OLEDs

OLEDs and LEDs are operated according to a phenomenon known as electroluminescence (EL), whereby an electric current is passed through a luminescent material that results in the production of light. Over the past decade this technology has reached a stage where high contrast displays can now be printed on wafer-thin substrates that exhibit both a high degree of flexibility and durability. The general schematic of an OLED can be seen in **Figure 1.2**. As illustrated, the emissive layer (EML) is sandwiched between an electron-transporting layer (ETL) and a hole-transporting layer (HTL).[23]

Cathode (Al)   **Anode (ITO)**

ETL

EL

HTL

Substrate
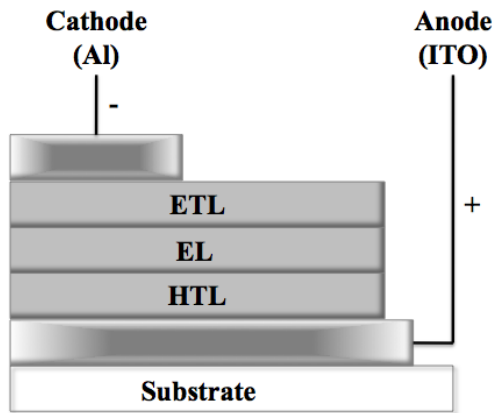
Figure 1.2 General schematic of an OLED.

The ETL promotes the migration of an electron from the cathode to the EML, while the HTL facilitates the removal of an electron from the EML to the anode leaving behind a hole, which is a positive charge. As a result, an exciton is formed, which is an entity that consists of an electron in the LUMO and a hole in the HOMO bound together by electrostatic attraction. Upon recombination energy is released in the form of visible light resulting in the luminescence observed from OLEDs. The mechanism is displayed in **Figure 1.3**.
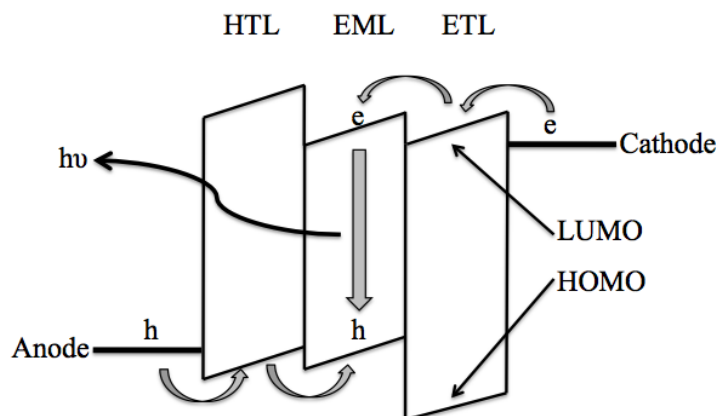
Figure 1.3. A general three layered OLED device.

The efficiency of an OLED device is heavily dependant on the relative energy levels of the HOMOs and LUMOs of the various layers. The work-function of the cathode, the LUMO energy of ETL and EML should behave as a gradient promoting the migration of an electron towards the EML, while the LUMO of the HTL must be higher in energy so as to prevent the electron from migrating to the anode. Similarly, the HOMO of the EML, HTL and the work-function of the

anode must also act as a gradient in order to facilitate the movement of the electron from the EML towards the anode, leaving behind a hole. On the other hand, the energy gap between the HOMO of the EML and ETL must be large enough to prevent the electron in the ETL from migrating to the EML and destabilizing the potential formation of an exciton. Improper alignment of the various energy levels leads to charge accumulation, emission from a layer other than the EML, and poor carrier balance which have all been linked to poor device lifetimes and efficiencies.[23]

Typically the efficiency of an OLED is determined by measuring its external quantum efficiency (EQE), which is the number of photons emitted through the front glass substrate versus the number of injected electrons. EQE (η_{ext}) can be determined using the following equation:

Equation 1.3

$$\eta_{ext} = \eta_{int}\eta_{Ph} = \gamma\eta_{ex}\Phi_P\eta_{Ph}$$

where, η_{Ph} is the out-coupling efficiency (the ratio of photons that exit the front glass substrate), η_{ex} is the fraction of total excitons that contribute to photons (for fluorescence and phosphorescence the maximum values are ~1/4 and 1, respectively), Υ is the ratio of electrons and holes injected from the electrodes (electron-hole balance factor) ($\Upsilon \leq 1$), and Φ_P is the intrinsic quantum efficiency of radiative decay (includes both fluorescence and phosphorescence).[4] Under the assumption that η_{Ph}~$1/2n^2$~20%, the maximum EQE of a device incorporating fluorescent or phosphorescent dye is 5% or 20%, respectively, where n is the refractive index and has a value of 1.5.[24,25]

8

Emitting Materials (EM)

A device requires an efficient EM that can facilitate the recombination of an electronically generated exciton. As such an EM must be able to form a stable anionic and cationic radical in order to accept both a negative and positive charge. While in PL light simply excites an electron from the S_0 to S_1 state, in EL a current generates electrons with both singlet and triplet spin states in a ratio of 1:3. As a result, during its infancy, when the display industry was using singlet emitters, such as Alq_3, devices had a maximum internal quantum efficiency (IQE) of 25% (in equation 1.3 above this variable would be η_{ex}). It was only during the past decade that this problem was overcome with the discovery that a metal center could increase the rate of ISC within an organic molecule through a phenomenon known as spin-orbital coupling.[24] This paved the way for the development of triplet emitters that could use both singlet and triplet excitons allowing IQE to approach 100%. This is in large part why the η_{ext} of an EL device with a phosphorescent dye is higher than its fluorescent counterpart.

In order to realize full-color displays, the development of efficient red, green and blue (RGB) emitters is crucial. The following sections will outline advancements of red (**1.2.1.1**)**,** green (**1.2.1.2**) and blue (**1.2.1.3**) emitters.

1.2.1.1 Red Emitters

All of the red emitters discussed will be illustrated in **Figure 1.4**. Many of the first generation red emitters, such as DCM-1 and DCM-2, were used as dopants in an Alq_3 EML.[26] In dilute solutions quantum efficiencies of the emitters were anywhere between 50-100%, while concentrated solutions or solid-state fluorescence was almost non-existent due to high concentration quenching (HCQ) properties.[27] This phenomenon is caused by the highly conjugated and polar nature of typical red emitters, which facilitates intermolecular π-π stacking making the material prone to crystallization in the solid state.[27] Therefore, significant interest was placed on the design of new non-dopant emitters that were not prone to HCQ and could survive vacuum deposition. A solution presented itself with the discovery of the spin-orbital coupling phenomenon, leading to the development of novel triplet emitters. Some of the first examples of such emitters were $Eu((DBM)_3(Phen))$ and $Eu(DBM)_3HPBM$.[28] The purpose of the phenanthroline ligand was to saturate the coordination number of Eu(III) as well as enhance fluorescence,[29] while oxadiazole derivatives were used due to their ability to act as good ETM.[30] Although these triplet emitters demonstrated promising properties and sharp red emission bands, they were not as bright as anticipated. The need for brighter non-dopant red emitters led to the discovery of NPAFN[31] and PhSPFN[32]. The brightness of $Eu((DBM)_3(Phen))$ was 460 cd/m^2 while for NPAFN and PhSPFN it was ~10000 cd/m^2 and ~11000 cd/m^2, respectively. Furthermore, the bulky nature of the amine substituents on NPAFN and PhSFN prevented intermolecular π-π stacking, inhibiting HCQ.[32]
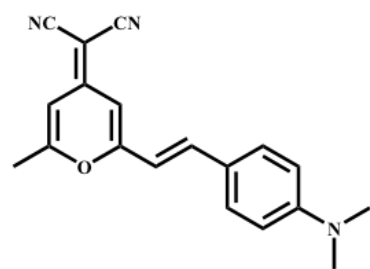
DCM-1
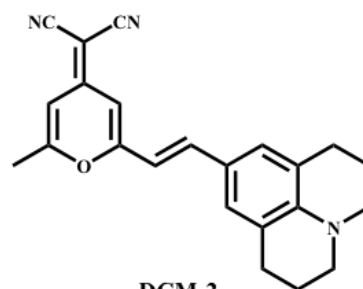
DCM-2
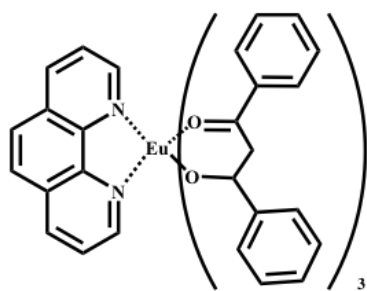
Eu((DBM)₃(Phen))
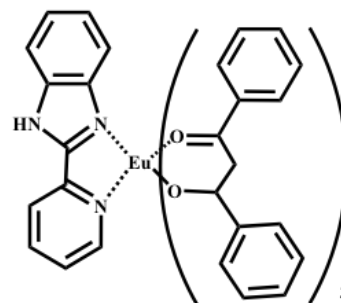
Eu(DBM)₃HPBM
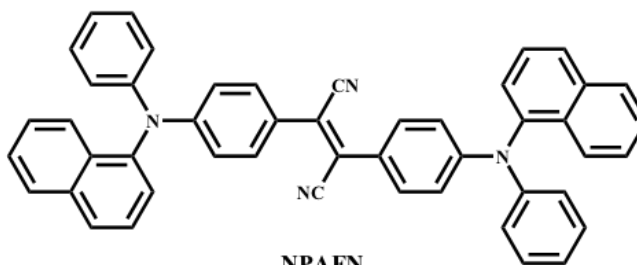
NPAFN
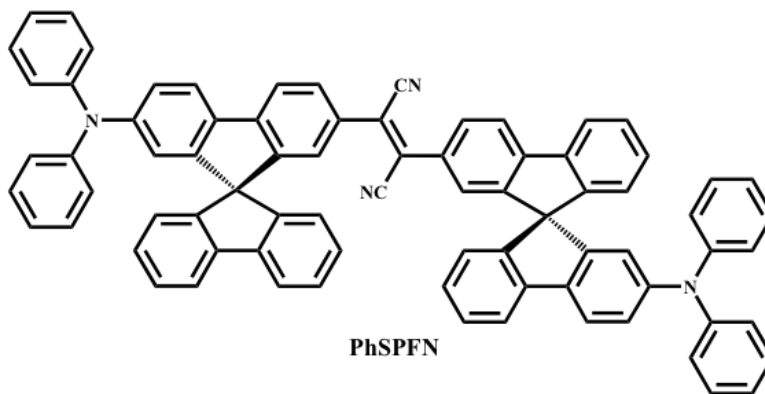
PhSPFN

Figure 1.4 Examples of red emitters.

1.2.1.2 Green Emitters

All green emitters discussed in any detail will be illustrated in **Figure 1.5**. In the earlier stages of OLED fabrication the most common green dyes used were derivatives of quinacridone,[33] quinoline,[34] quinoxaline,[35] and carbazole.[36] Unfortunately, aside from Alq_3, these systems suffered from intermolecular π-π stacking similar to DCM-1 and DCM-2. Alq_3 was the brightest non-dopant green emitter available for many years, serving as a benchmark for the development of more efficient systems. Many of the resulting materials were typically composed of a green emitting fluorene core linked to an ETL, such as DFBTA, yielding a device with an external quantum efficiency (EQE) approaching 3.7%.[37] The design and development of green triplet emitters using metal centers for electrophosphorescent devices has been more successful, yielding systems that could compete with Alq_3. Ir(III) complexes have been extensively investigated yielding highly efficient OLEDs. For instance, devices using either [Ir(ppy)$_3$] or [Ir(ppy)$_2$(acac)] had an EQE of 19%.[24,38] Another lanthanide that has had tremendous success is Tb(III). One of the most efficient green emitters, arguably better than the conventional Alq_3, is $(Tb(PPO)_2(PMIP)_3$.[39] Unfortunately, there has been limited success outside the rare earth metals. For example, Pt(II) emitters struggle from a square planar geometry that reduces luminescence intensity as a result of excimer emission.[40] The most successful Pt(II)-based green emitter to date is Pt-BppyA, which is also the only system of its kind to incorporate a triarylboron moiety. The EQE of the resulting device was 8.9%.[41]
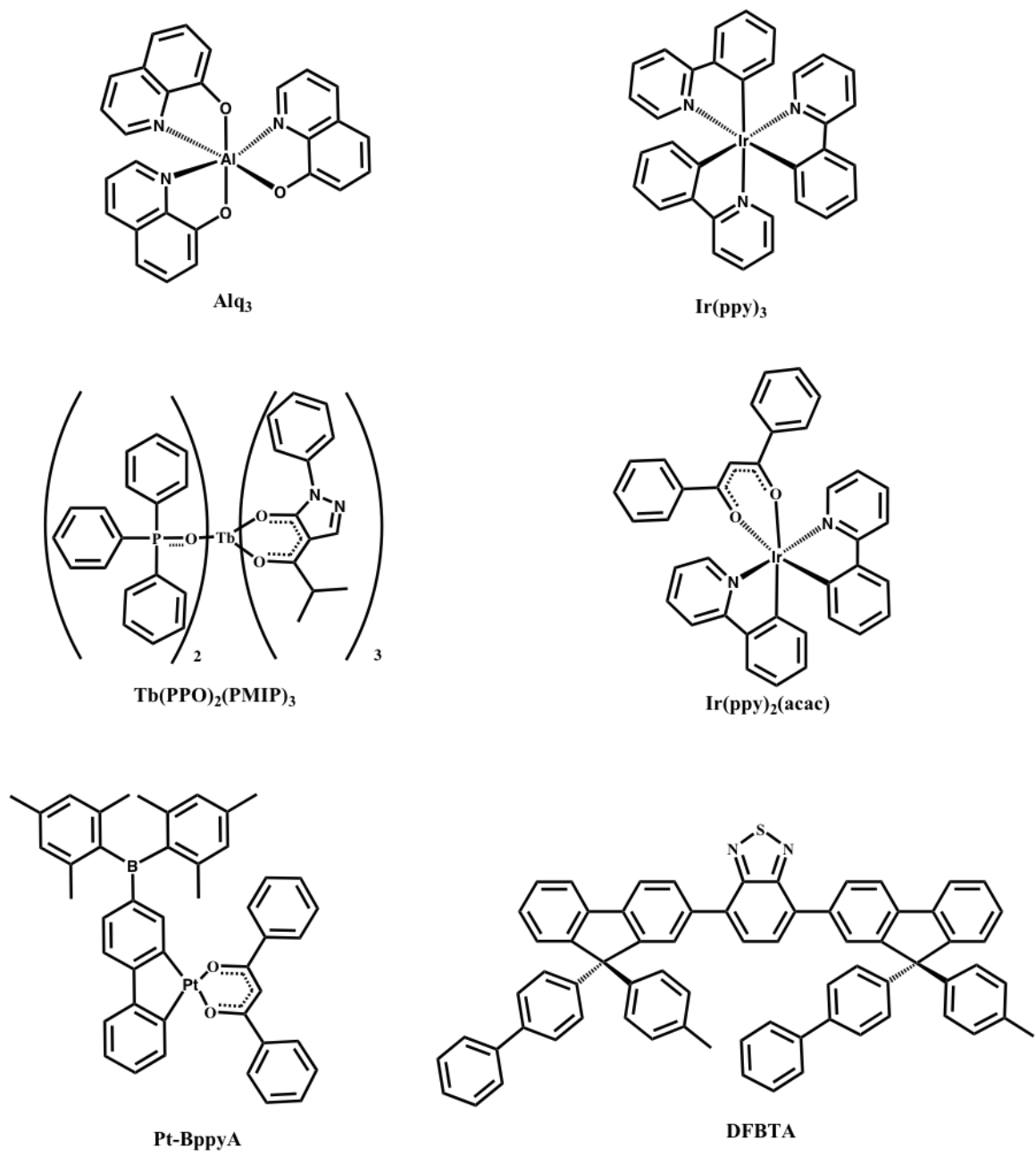
Figure 1.5 Examples of green emitters.

1.2.1.3 Blue Emitters

All blue emitters that are discussed are shown in **Figure 1.6**. The development of more efficient blue EL devices has been more challenging than its red and green counterparts due to the intrinsically large band-gap required for efficient blue emissions, often leading to issues with charge injection into the blue emitters. Consequently there has been interest in the development of host materials with both a high electron affinity as well as a triplet state that is sufficiently higher than the guest blue emitter.[42, 43] Nevertheless, the development of efficient blue emitting complexes is still of paramount importance. There are a number of interesting non-metal blue emitters, such as MQAB and 4P-NPD, which have been used primarily for WOLEDs.[44] The Wang group has designed a variety of fluorescent blue emitters that have demonstrated favorable characteristics in OLED devices. For example, tris[p-(2,2'-dipyridylamino)phenylduryl)borane] (DAPB) and tris[p-(2,2'-dipyridylamino)biphenylduryl)borane] (DABPB) were both efficient systems that had quantum yields of 0.59 and 0.46, respectively.[45] Another more well known system was mes$_2$B(p-4,4'-biphenyl-NPh(1-naphthyl)) (BNaph) which had solution based and solid state quantum yields of 0.95 and 0.31, respectively.[46] Another class of molecules that have demonstrated promise are the dipyrenylbenxene derivatives. In particular, 1-(4-(1-pyrenyl)phenyl)pyrene (PPP), 1-(2,5-dimethoxy-4-(1-pyrenyl)phenyl)pyrene (DOPP) and 1-(2,5-dimethyl-4-(1-pyrenyl)phenyl)pyrene (DMPPP), which had quantum yields ranging from 63-75% and yielding devices with external quantum efficiencies of 4.3-5.2%.[47] Furthermore, the devices using DMPPP demonstrated deep blue emissions that coincided with the coordinates outlined by the Commission Internationale de L'Eclairage (CIE) for blue emitters. The use of rare-earth and transition metals has also been developed considerably. For example, Ir(III)-based phosphors, such as the sky-blue emitter FIrpic, became a standard for guest-host optimization in blue EL

15

devices.[48, 49] Recently a device using FIrpic achieved an unprecedented EQE of 22.0%.[50] Furthermore, Jeon *et al* were not only able to fabricate a device using FCNIr that achieved the target deep blue color coordinates outlined by the Commission Internationale de L'Eclairage (CIE) for true blue emitters but it also had an EQE of 18.4%.[51] Another area that has gained tremendous interest is the use of N-heterocyclic carbenes as ancillary ligands on metal centers of blue phosphors. When coordinated to a metal center they increase the triplet state, which helps to inhibit thermal accessibility to non-emissive pathways.[52, 53] It is particularly promising in bringing transition metals back into the picture as a competitive blue emitter. For example, there has been some considerable interest in the development of Pt(II)-based blue emitters using the NHC carbene as a ligand.[54] Although not very efficient, one promising system is Pt(pmi)(acac) with a photoluminescent quantum yield of 90% and a device EQE of 6.2%.[55]
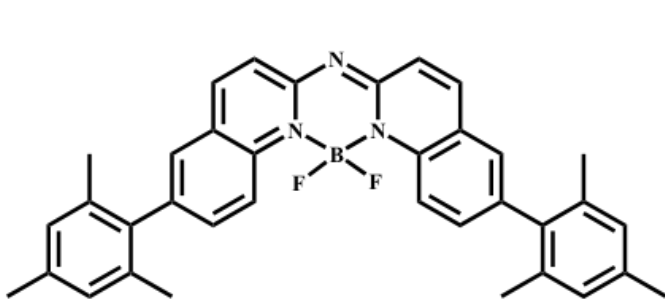
MQAB
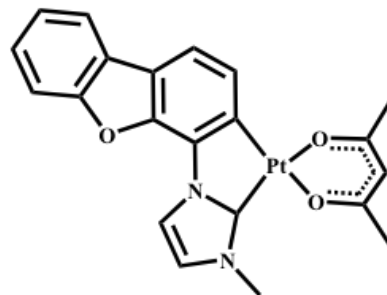
Pt(pmi)(acac)
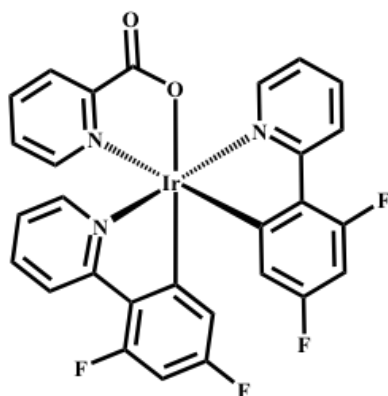
FIrpic
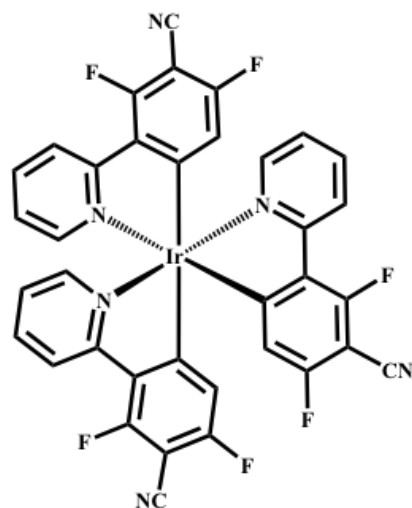
FCNIr
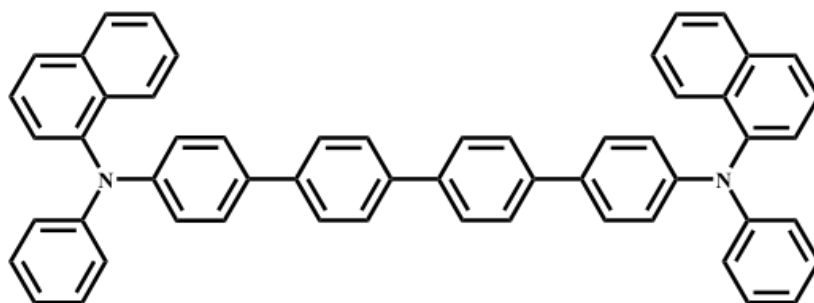
4P-NPD

Figure 1.6 Examples of blue emitters.

1.2.2 Hole Transport Materials (HTMs)

The hole-transport layer has two important tasks in an OLED: it must facilitate hole injection from the anode into the EL device with subsequent migration into the EML, as well as block electrons from escaping the EML. Therefore, successful hole-transporting materials typically have low electron affinities and ionization potentials to promote electron removal, as well as a reversible anodic oxidation that yields a stable cationic radical.[56] Furthermore, it is crucial that potential HTMs have a high glass transition temperature (T_g) in order to ensure morphological stability of the amorphous material at the high operating temperatures of an OLED.[57] It has been demonstrated that either introducing a structurally rigid moiety or increasing the overall molecular weight and size of the material can elevate the T_g. Unfortunately such modifications often lead to compromises in the solubility and processability of these materials. The three most commonly used HTMs used to be N-N'-diphenyl-N,N'-bis(3-methylphenyl)-(1,1'-biphenyl)-4,4'-diamine (TPD), 4,4'-bis(N-(1-naphthyl)-N-phenylamino)-biphenyl (αNPD) and 4,4',4''-tris(N,-3(3-methylphenyl)-N-phenylamino)triphenylamine (*m*-MTDATA).[57] TPD was the least favorable due to its low T_g of 65 ℃ and high ionization potential of 5.5 eV.[56] On the other hand, NPD and *m*-MTDATA were more preferred due to their higher T_gs of 75 ℃ and 95 ℃, respectively, and lower ionization potential of 5.1 eV.[56] Nevertheless, there was still concern over structural integrity at higher operating temperatures, which intensified efforts to design novel HTMs with higher T_gs. Modifications were made to both the TPD/NPD and *m*-MTDATA classes in order to make them more effective. There has also been a lot of interest in systems involving a truxene core, a moiety that substantially increases the overall rigidity of the molecule.

A wide-range of systems consist of the biphenyl diamine core, including both TPD and NPD, which have shown promise as HTMs. The primary drawback of this class of molecules is the low T_g, which could be elevated by introducing more rigidity to the material with moieties such as carbazoles and fluorenyl as in the case of OFC-G2.[58] An alternate solution is to simply increase the size of the system as in the case of TPTE, which is an oligomer of TPD.[59] The structures are illustrated in **Figure 1.7** with their respective T_g.
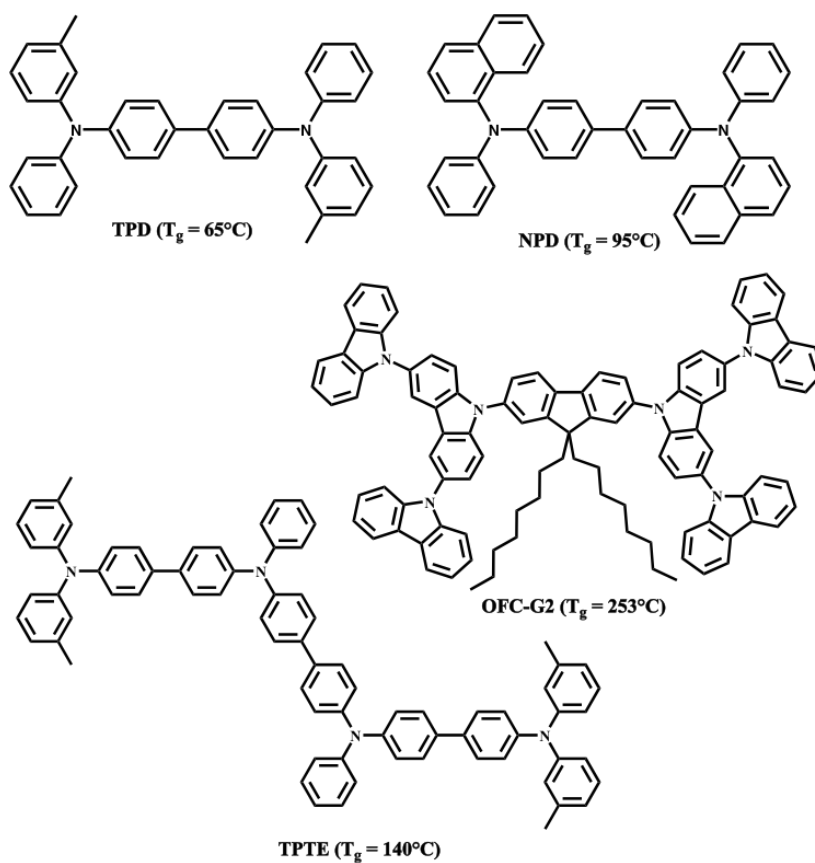
Figure 1.7 Examples of HTMs with diphenyl diamine cores.

Another category includes molecules with a triphenylamine core, such as *m*-MTDATA. Not only do these materials readily form stable amorphous glasses but they also have low ionization potentials that are typically around 5.1 eV.[56, 60-62] Additionally, these materials have demonstrated greater thermal stability than many of the other systems available and relatively high glass transition temperatures. A few examples are shown in **figure 1.8**.

m-MTDATA (T$_g$ = 95°C)

p-PMDATA (T$_g$ = 110°C)

1-TNATA (T$_g$ = 113°C)

TFATA (T$_g$ = 131°C)
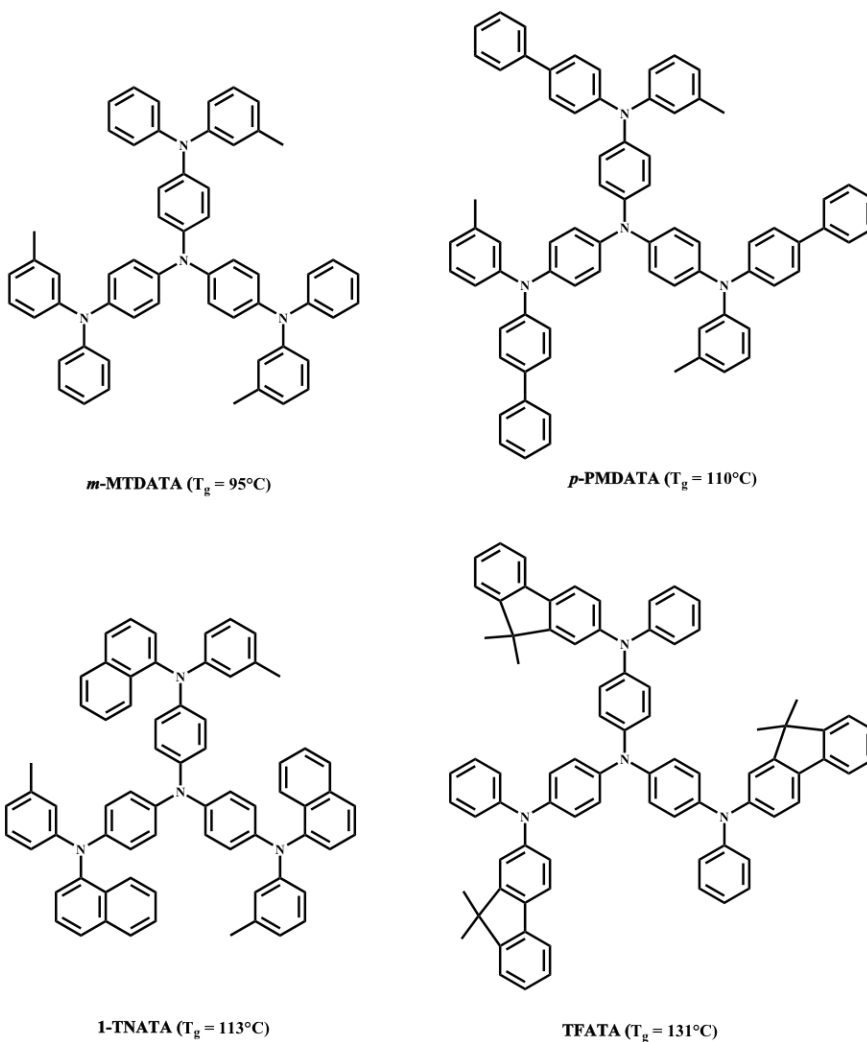
Figure 1.8 Examples of HTMs with a triphenylamine core.

Most impressive are the HTMs with a rigid truxene core, which is a moiety that consists of three fluorenyl moieties fused together. While both TTrTr and TFATr have T_gs higher than 200 ℃, TTrTr has one of the highest values to date at 358 ℃ without any compromise to solubility or processability (**Figure 1.9**).[56, 57, 63] This is supported by dendrimer-like truxenes that have been synthesized more recently exhibiting decomposition at temperatures exceeding 400 ℃. [64]

TTrTr (T_g = 358°C)
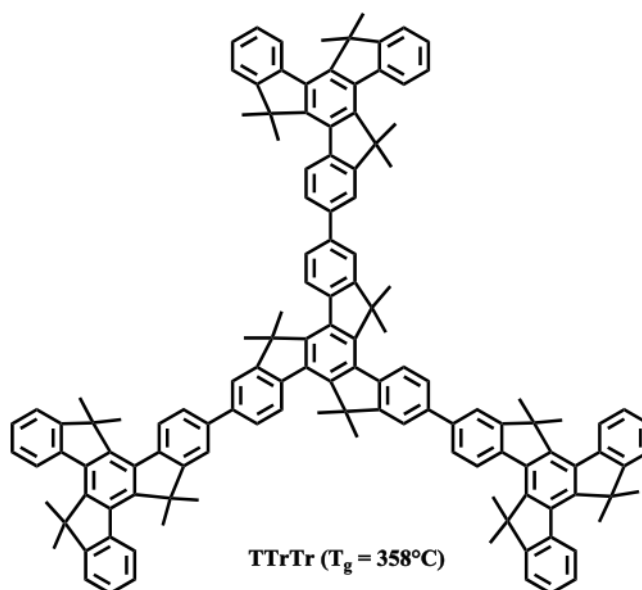
Figure 1.9 Example of an HTM with a truxene core.

1.2.3 Electron Transport Material (ETM)

The function of the electron transport layer (ETL) is to facilitate electron injection from the cathode into the OLED, followed by facile migration of the electron to the EML. Therefore, successful ETMs must demonstrate reversible cathodic reduction forming stable anionic radicals, have a high electron affinity and enable facile electron mobility. Initially EL devices were designed with a hole-blocking layer (HBL) and exciton-blocking layer (EBL) placed in between the ETL and EML, limiting both the leakage of holes from the EML and quenching of either the singlet or triplet excitons.[65] Unfortunately, this resulted in complex OLEDs that were not only more costly but also less efficient due to their thicker nature. As a result, new ETMs were designed to encompass all three roles (ETL, EBL, and HBL).[66] In order to design a successful modern ETM there are three important properties to keep in mind: (1) a low-lying LUMO that matches the cathode to facilitate charge injection, (2) a low-lying HOMO that prevents hole leakage from the EML, and (3) a high triplet state that will limit exciton quenching.[66] Additionally, similar to HTMs, there is a preference for amorphous ETMs with high glass transition temperatures.

Research and development into new ETMs has been less prolific than HTMs. Alq_3 is one of the earliest and most successful systems used as an ETM. The use of Alq_3 and its derivatives as both an ETM and an EML will be discussed in more detail in a later section. Many of the most successful ETMs consist of one of the following groups (**Figure 1.10**): (1) oxadiazole derivatives such as *t*-Bu-PBD, OXD-7, DPOXD-10a-c, and OXDPh-7-10, (2) boron containing materials such as BMB-*n*T (n=2,3), TMB-TB and 3TPYMB, and (3) triphenylbenzene derivatives such as Tm*n*pyPB (n=2-4), T*p*PyPB and T*m*PyPB.

22

One of the well known oxadiazole-based ETMs was *t*-Bu-PBD, which was demonstrated to increase the emission efficiency of a two-layered device by a factor of 10^4.[30] Unfortunately, it had a low T_g (=60 °C) and it was prone to crystallization at the higher device operating temperatures. Another drawback was its high LUMO (~2.16 eV) compared to Alq_3 with a LUMO at 3.3 eV. OXD-7 was another system that had demonstrated promise as an ETL as well as having hole-blocking properties. Similar to *t*-Bu-PBD, the LUMO was quite high (~2.80 eV) resulting in difficulties with electron injection.[67] There have been some recent systems that have shown tremendous promise. Reddy *et al* designed 2,5-diphenyl-1,3,4-oxadiazole (DPOXD-10a-c) derivatives that had HOMOs ~ 6.7 eV and LUMOs ~3.7 eV, and band gaps typically larger than the conventional Alq_3 ($\Delta E = 2.7$ eV).[68] These values demonstrate the ability of this series of molecules to function as both an ETL and HBL, which was supported by device testing. Additionally, these molecules did not have a T_g at temperatures as high as 300 °C. Yang *et al* designed the multi(5-phenyl-1,3,4-oxadiazo-2-yl) (OXDPh-*n*, *n*=7-10) series, which had HOMOs ranging from 6.47-6.65 eV and LUMOs from 3.00-3.46 eV showing great potential as ETMs.[69]

There was considerable interest in the dimesitylboron-containing oligothiophene series BMB-*n*T (*n*=1,2,3). These systems demonstrated sequential, and reversible, cathodic and anodic waves indicating the formation of an anionic and dianionic species, believed to be from the two-dimesitylboron moieties.[70-72] Also BMB-1T, BMB-2T and BMB-3T yielded amorphous materials with T_gs of 71 °C, 107 °C and 113 °C, respectively.[70-72] Most importantly, device luminance and quantum efficiency were increased by 10-20% when either of these molecules was used as the ETL. The effects of a starburst architecture of this type of system was explored with the development of TMB-TB.[73] As expected the T_g (=160 °C) was much higher than the BMB-*n*T series, as well there were three sequential cathodic and anodic waves resulting from the three

23

dimesitylboron moieties.[73] Also the band gap was 3.2 eV, far larger than Alq_3. The usefulness of TMB-TB as both an ETL and HBL compared to Alq_3 was demonstrated when devices with the former showed emission from the EML while devices with the latter showed emission from the ETL—resulting from hole-leakage. A more recent structure that was investigated was 3TPYMB, which had an energy gap of 3.45 eV (HOMO~6.77 eV and LUMO~3.22 eV) and a T_g of 106 °C.[74] Furthermore, crystallization in the solid state was suppressed due to the twisted nature of the system. Not only was the electron mobility of 3TPYMB 10 times greater than Alq_3, the driving voltage was lowered due to the low-lying LUMO.

ETMs with a triphenylbenzene core and pyridyl moieties on the periphery have exhibited some favorable characteristics. Su *et al* designed a series where the periphery pyridyl moieties were attached either para- or meta- to the benzene rings.[75] They found that when they used the newly designed ETMs, TmPyPB and TpPyPB, the driving voltage of the EL device was reduced substantially as a result of the low-lying LUMOs (= 2.73 and 3.04 eV, respectively). Su *et al* then expanded on this series by developing new systems with the attachment of the terminal pyridyl moiety to the meta-position of the benzene ring being rotated from the 2-position through to the 4-position (Tm2PyPB, Tm3PyPB, and Tm4PyPB).[76] These systems demonstrated electron mobilities that were several hundred times larger than Alq_3. Although their LUMOs (~2.7-3.0 eV) were higher in energy compared to Alq_3 the HOMOs were significantly lower (~6.4-6.7 eV) making them very effective hole-blocking materials.

OXD-7 (LUMO = -2.8 eV)

t-**Bu-PBD (LUMO = -2.16 eV)**

BMB-*n*T (*n* = 2, LUMO = -3.45 eV;
***n* = 3, LUMO = -3.25 eV)**

Alq₃ (LUMO ~ 3.0 eV)

OXDPh-10 (LUMO = -3.46 eV)

TMB-TB (LUMO = N/A)

3TPYMB (LUMO = -3.22 eV)

meta- **TmPyPB (LUMO = -2.73 eV)**
para- **TpPyPB (LUMO = -3.04eV)**

x = N; Tm2PyPB (LUMO = -2.74 eV)
y = N; Tm3PyPB (LUMO = -2.90 eV)
z = N; Tm3PyPB (LUMO = -2.94 eV)
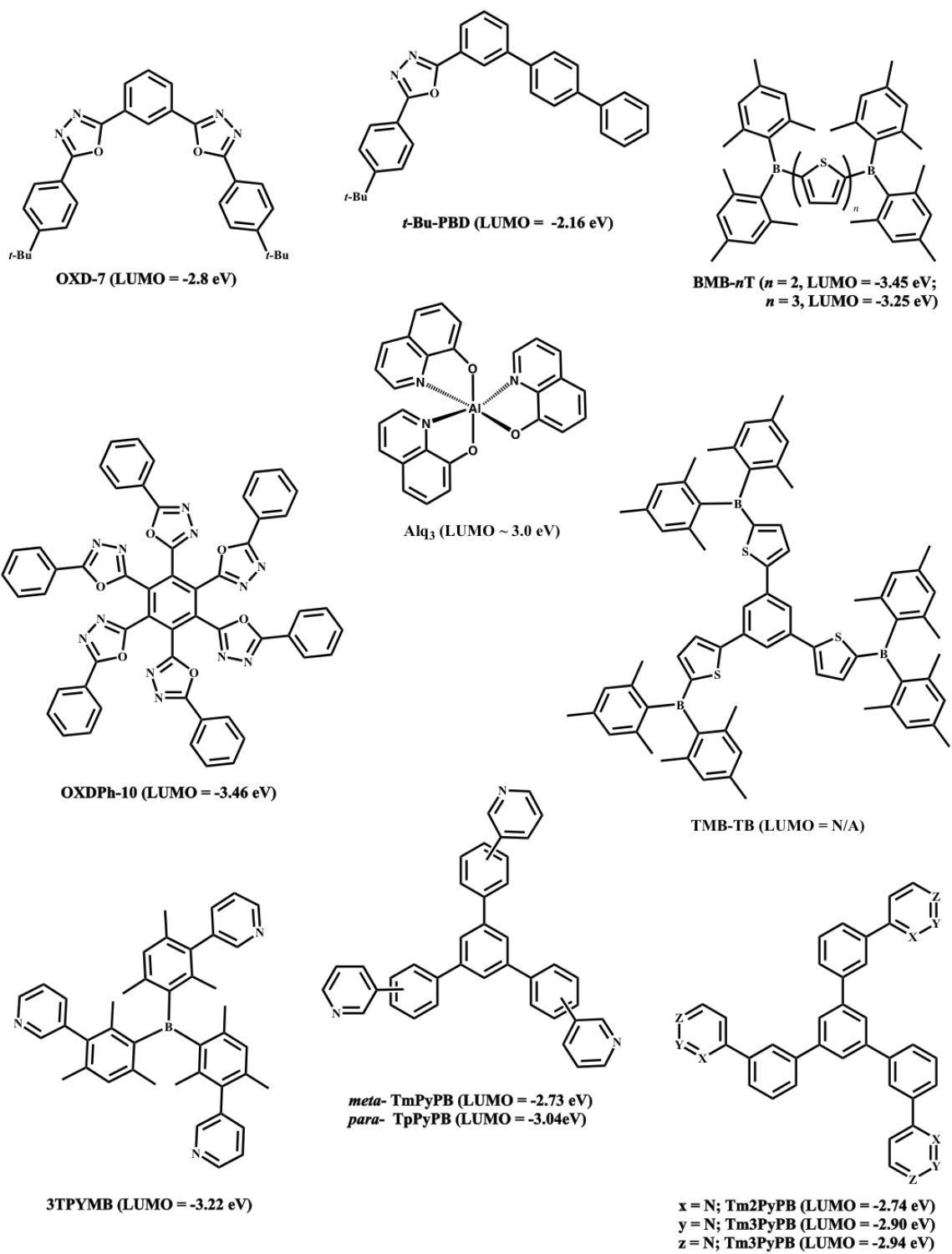
Figure 1.10 Selected examples of ETMs.

1.3 Tris(8-Hydroxyquinoline)Aluminum in OLEDs

Since the discovery of thin-film electroluminescence from Alq_3 in 1987, research and development of this small organic molecule has been prolific. It was critical in the establishment of OLEDs as a viable alternative to other display technologies due to its role as both an efficient green emitter and ETL in EL devices, and thus enabling single-layered devices. Alq_3 is a neutral system that consists of three 8-hydroxyquinoline (q) ligands chelated to an Al^{+3} center in an octahedral geometry. Although this molecule can assume either the *fac-* or *mer-* isomers, the latter is more thermodynamically stable (~4kcal/mol) as well as having a higher electron affinity (~2kcal/mol).[77]

There are many reasons behind the success of Alq_3 in EL devices. This small organic molecule has a T_g of 172 ℃, and it has demonstrated remarkable thermal stability with signs of degradations appearing at temperatures exceeding 350 ℃.[78] These properties have enabled manufacturers to use vacuum deposition during OLED fabrication, a far superior approach to spin-coated devices which are often less efficient. In addition to its glassy amorphous properties, Alq_3 has served as a model for new ETMs due to its low-lying LUMO (~3.0 eV), facilitating electron injection and electron mobility, as well as a low HOMO (~ 5.7 eV), which assists in blocking holes.[57] Though what made this molecule so successful was its ability to act as both an EML and ETL, allowing for the fabrication of thin-film EL devices.

Unfortunately, Alq_3 has not been without its weaknesses. It was discovered that at elevated temperatures and in the presence of moisture, Alq_3 has a tendency to hydrolyze releasing q; a luminescent quenching molecule.[78] Interestingly, the solution to this problem was found to be the use of annealed Alq_3, which showed greater stability towards hydrolysis at the cost of PL

efficiency. More importantly, the unstable nature of the Alq$_3$ cation, formed during hole-migration into the EML, was linked to device degradation and thus reduced device lifetimes.[79]
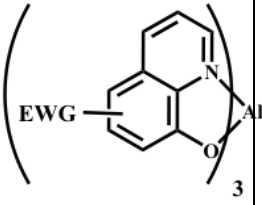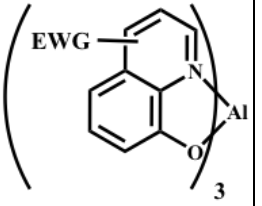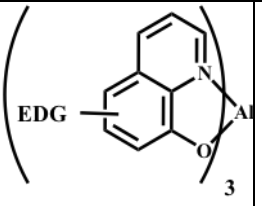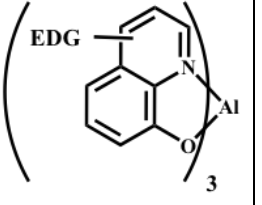
The drawbacks outlined above have sparked interest in gaining a better understanding of Alq$_3$ in an attempt to increase its quantum efficiency, modulate its emission properties, alter the packing order (α,β, or γ) of the *mer-* isomer and widen the bandgap in hopes of enhancing electron mobility and its hole-blocking ability. The remainder of this section will focus on the manipulation of the small molecule's emission properties, beginning with the elucidation of its electronic properties (1.3.1) and examples of various functionalized Alq$_3$ systems (1.3.2).

1.3.1 Electronic Properties

Through density functional theory (DFT) studies the electronic properties of Alq$_3$ have been elucidated allowing for controlled manipulation of its photophysical properties. Studies have indicated that the ground and excited states are ligand localized, with the HOMO and LUMO found on the phenoxide and pyridyl side, respectively. Therefore, the lowest electronic transition comes from a $\pi^* \rightarrow \pi$ transition from the pyridyl to phenoxide part of the ligand.[80, 81] Using this information the emission of Alq$_3$ can be easily manipulated by attaching an electron donating group (EDG) or electron withdrawing group (EDG) to either the phenoxide or pyridyl ring in order to change the energy level of either the HOMO or LUMO and subsequently the bandgap.[82-84] The effects caused by the attachment of either an EDG or EWG to the quinolate ligand are summarized in **Table 1.1**. Also the numbering of the positions on Alq$_3$ is illustrated in **Figure 1.11**.

27

Table 1.1. Summary of the electronic and photophysical changes from substitutions on the quinolate ligand of Alq3.

	Location of Substitution	Energy Level Affected/Direction	Effects on the Band Gap	Absorption and Emission
EWG[a]		HOMO/Lowered	Widened	Blue-shifted
		LUMO/Lowered	Narrowed	Red-shifted
EDG[b]		HOMO/Raised	Narrowed	Red-Shifted
		LUMO/Raised	Widened	Blue-Shifted

[a]EWG- electron-withdrawing group

[b]EDG- electron-donating group
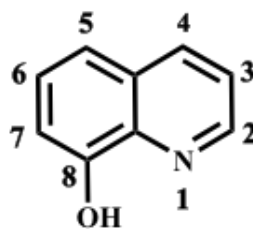
Figure 1.11 The numbering scheme for 8-hydroxyquinoline.

It's important to note that there are some exceptions to the rule. For example, when a fluoride was attached to the C-5 position, the resulting emission was unexpectedly red-shifted. While on the C-6 position the emission was blue-shifted, as expected. It was proposed that since a large proportion of the HOMO is found on the C-5, C-7 and C-8 positions of the phenoxide ring, the lone pairs on the fluoride atom were conjugated with the HOMO on C-5 and thus acted as an EDG. While on the C-6 position, through the inductive effect the fluoride was in fact acting as intended, an EWG.[82] This example demonstrates the complexity of the effects observed from substituents directly attached to q, resulting in considerable research interest over the past decade.

1.3.2 Modifications to 8-Hydroxyquinoline

Anzenbacher and his group have made significant contributions in expanding our understanding of how various modifications of Alq$_3$ affect its electronic and photophysical effects.[85-88] In particular, they helped de-convolute the competing inductive and resonance effects seen from directly attached substituents. In the experiment they attached various aryl substituents

either through an ethynyl linker (series 1) (**Figure 1.12**) or directly (series 2) to 8-hydroxyquinoline (**Figure 1.13**). This enabled the conjugated system of Alq_3 to be extended while eliminating the mesomeric effects of the substituents' π-electrons. It should also be noted that modifications were made on the C-5 position due to its large contribution to the HOMO, and its distance from the chelate position—reducing steric hindrance. While both series showed slight red shifting due to the extension of the conjugated system, there was predictable modulation of the emission characteristics depending on whether an EWG or EDG was used. In addition, the effects were amplified in series 2 since the aryl group was directly attached to q; this is supported by the fact that the emission range of series 1 was 520-600 nm while for series 2 it was 490-620 nm. Devices made from these systems were not very promising. Unfortunately, the triplet bond in series 1 was not stable under the conditions required for vacuum deposition, while the EL devices made from the systems in series 2 were not as efficient as Alq_3.
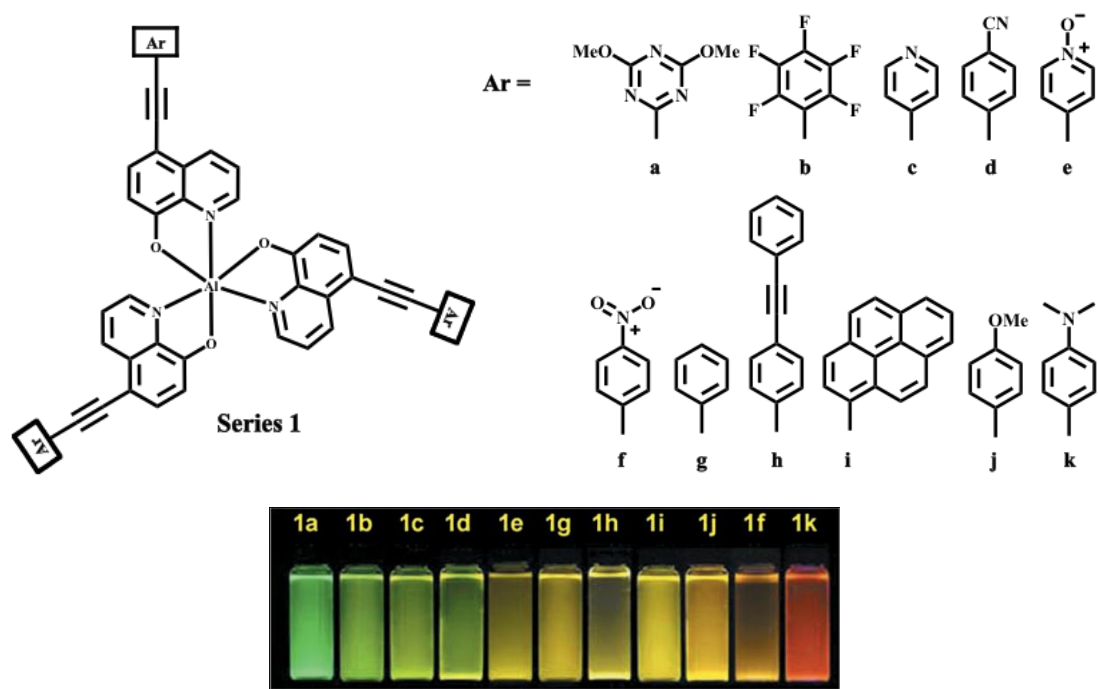
Figure 1.12. Structures of complexes 1a-k and the emission in solution under UV light.[86]
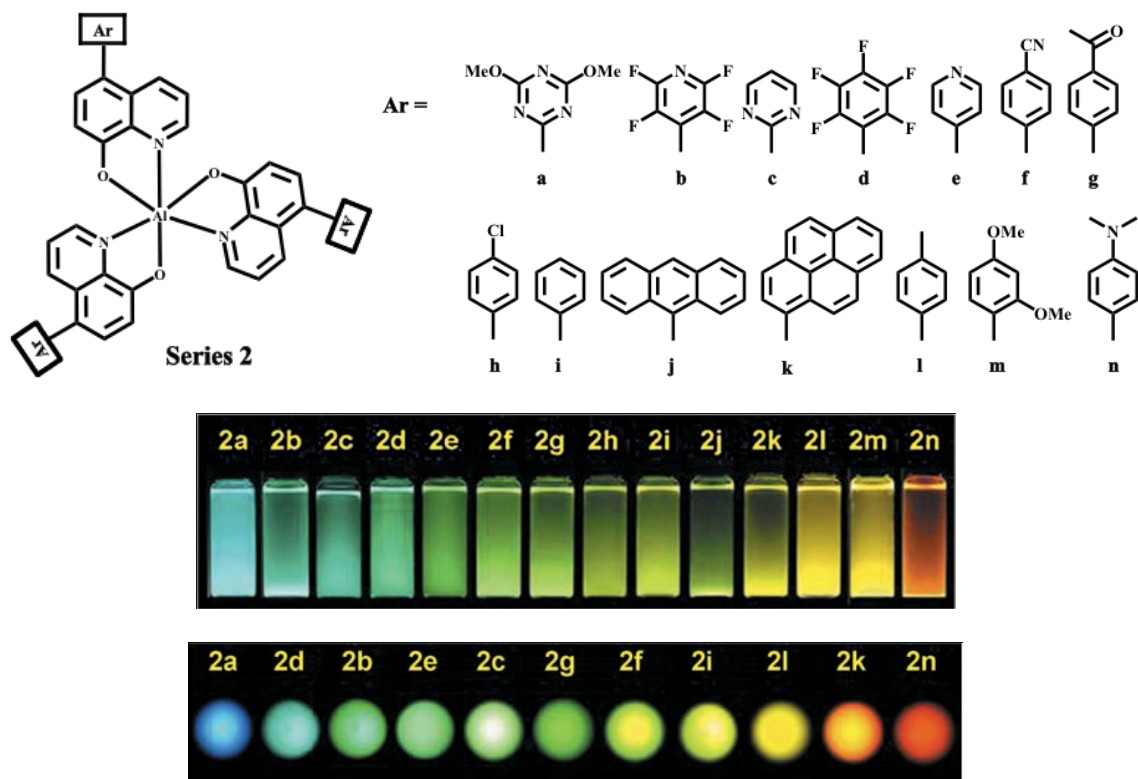
Figure 1.13. Structures of complexes 2a-n and their emissions in solution and solid state under UV light.[86]

There are a number of other variations of Alq$_3$ that have been investigated (**Figure 1.14**). For example, Cheng *et al* developed tris-(5-N-ethylanilinesulfonamide-8-quinolato)aluminum, Al(Saq)$_3$, a system with bulky sulfonamide substituents that inhibit intermolecular stacking, lending it its amorphous characteristics.[89] As predicted, due to the electron withdrawing nature of the sulfonamide moiety the luminescence was blue-shifted ($\lambda_{em} = 483$ nm) compared to Alq$_3$ ($\lambda_{em} = 514$ nm). When it was used as a blue emitter in an EL device, the resulting luminance was quite

weak. The explanation for this was that the HOMO (-6.04 eV) was quite low making it difficult for holes to get into the EML from the ITO and form an exciton.

Another example is $Al(Cq)_3$, which was designed with synergetic intentions. Carbazole, an HTM, was attached to the 5-position of Alq_3, an ETM, in hopes of making it a bifunctional complex. As predicted the carbazole moiety succeeded in raising the HOMO energy level of Alq_3 from -5.90 eV to -5.51 eV, which could be observed by the red-shifting of the emission peak from 514 nm to 555 nm.[90]

Recently, Jiang *et al* had synthesized CP-B8QBA-A1, an ethanol-soluble Alq_3-based coordination polymer that demonstrated ETL characteristics.[91] Devices using CP-B8QBA-A1 had a low turn-on voltage due to the low-lying LUMO (-4.02 eV), while the low HOMO (-6.38 eV) contributed to the hole-blocking characteristics of the polymer. Additionally, craters on the surface of CP-B8QBA-A1 increased the contact area between the ETL and the cathode enabling more effective electron injection into the EL device. More importantly, the polymer showed thermal stability up to temperatures of 300 °C, after which point cracks began to form.
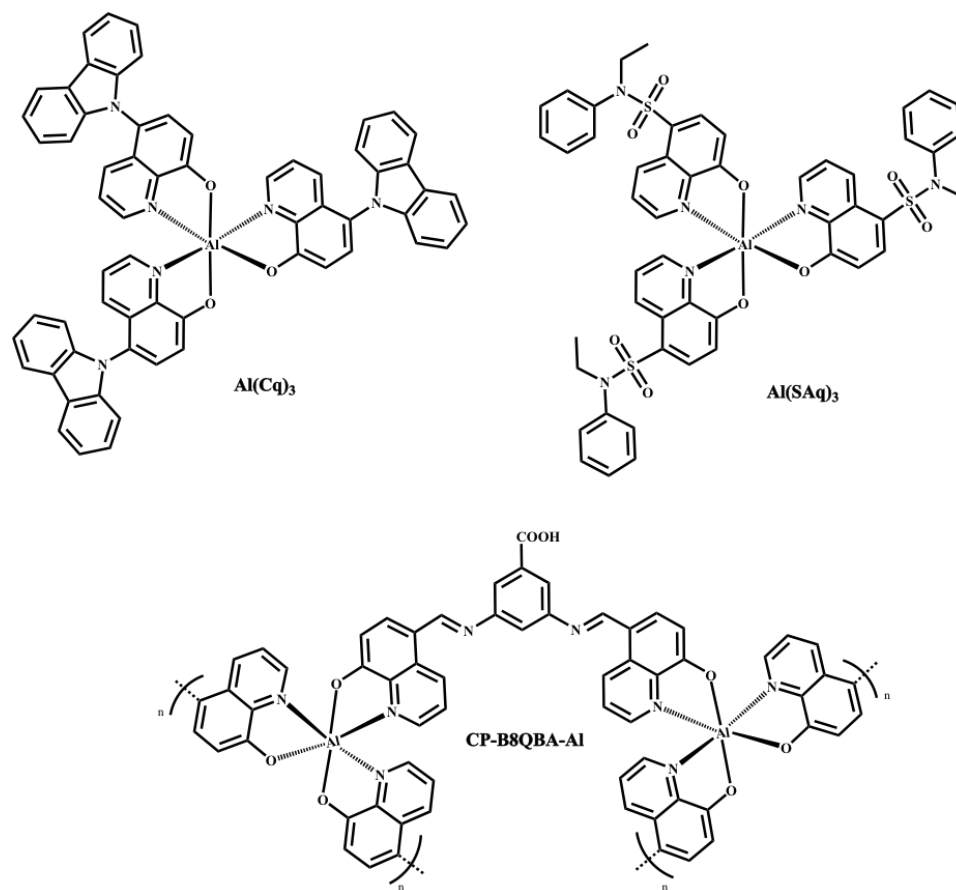
Figure 1.14. Selected examples of Alq$_3$ derivatives.

1.4 Organoboron Compounds

Over the past couple of decades boron chemistry has gained tremendous research interest in materials chemistry due to its wide range of applications, including anion sensors, emitters and ETMs in OLEDs, and photoresponsive materials. It is important to note that the applications of a particular boron-containing material depends on which of the two classes the system falls into, namely three-coordinate (**1.4.1**) or four-coordinate boron (**1.4.2**).

34

1.4.1 Three-Coordinate Boron

In a three-coordinate boron moiety the boron center is sp^2-hybridized. This class of molecules, with its trigonal planar geometry, is inherently electron deficient due to its empty p$_z$ orbital making it an excellent electron acceptor.[92-96] This property enables this moiety to either take part in charge transfer with a donor group leading to fluorescence or to overlap with an aromatic system effectively extending its π-conjugation (**1.4.1.1**). Unfortunately, the boron center is susceptible to attack by water, oxygen and other lewis bases. As a result bulkier substituents, such as mesityl, have been used to increase the steric hindrance around the vacant p$_z$ orbital allowing the synthesis of moisture stable compounds. Even with the increased steric hindrance, small anions such as CN$^-$ and F$^-$ are still able to bind to the boron center changing the photophysical properties of the material. This occurrence has led to the use of triarylboron systems as anion sensors, with particular focus on fluoride (**1.4.1.2**).

1.4.1.1 Luminescence of Triarylboron Systems

Emissions from intramolecular charge transfer (ICT) between an electron deficient boron center and a donor-group, as illustrated in **Figure 1.15**, has led to interest in using these systems in EL devices. In accordance to this phenomenon, DFT calculations place the HOMO and LUMO orbitals predominantly on the donor and acceptor groups, respectively. In order to achieve high quantum yields it is important to use electron rich groups, such as triarylamine derivatives, as

donors. Following charge transfer, the excited-state is highly polarized making the emission dependant on the polarity of the solvent.
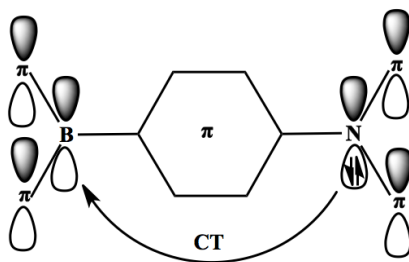
Figure 1.15. Charge transfer in a three-coordinate boron system.

Doi *et al* first reported the ICT phenomenon between a triarylboron acceptor and a triarylamine donor.[97] They discovered that increasing the distance between the donor and acceptor resulted in both a red-shift of the emission as well as a decreased PL quantum yield. This work was than expanded to include systems with U- and V-shaped geometries, which demonstrated weak through-space charge transfer.[98, 99] As expected the shorter the side-arms the stronger the through-space CT and subsequently the higher the quantum yield.

Wang and co-workers have discovered a unique synergic relationship between $BMes_2$ and metal chelates. It started with the discovery that by attaching it to either a pyridyl or bipyridyl linker the electron accepting ability of $BMes_2$ could be increased as a consequence of the electronegativity of the N atom(s). When a metal center was then chelated to the linker the electron accepting ability of the boron moiety was further enhanced, strengthening its ETM properties.[100,101] Even more interesting was the unique luminescent properties of these systems.

The phosphorescence quantum yield is improved by the synergic relationship between the [1]MLCT and [3]LC charge transfer on the BMes$_2$.[96, 102] Hudson *et al* showed the importance of this discovery by synthesizing a series of Pt(II) N,C-chelates that had impressive phosphorescence quantum yields, the highest being 0.98 (**Figure 1.16**).[103] Furthermore, a device using Pt-BppyA had an EQE of 8.9%, one of the highest for a Pt(II) complex, as well as strong electron transporting properties.
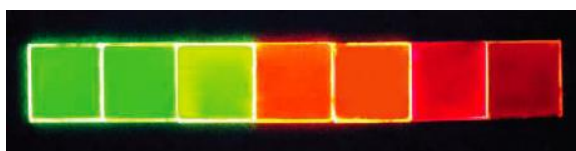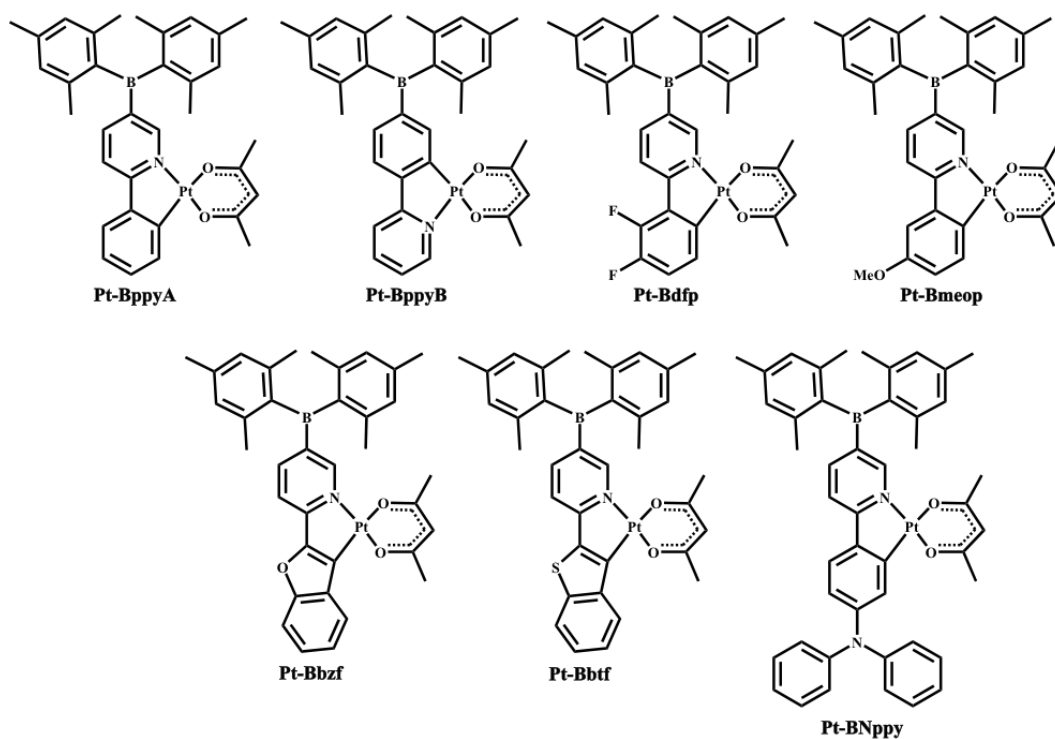
Figure 1.16. Pt(II) structures (top) and emissions from 10wt% in PMMA on quartz substrates under UV light. From left to right: Pt-BppyA, Pt-Bdfp, Pt-BppyB, Pt-Bmeop, Pt-Bnppy, Pt-Bbfp, Pt-Bbzf.[102]

1.4.1.2 Triarylboron Compounds as Fluoride Sensors

Fluoride is typically added to drinking water, toothpaste and other health products due to its benefits to dental health and the prevention of osteoporosis. However, excess can be quite harmful leading to bone and skeletal damage known as fluorosis. According to the Environmental Protection Agency (EPA) the maximum concentration of fluoride advisable is 4ppm (210 μmol), though it is recommended that the concentration be no greater than 2ppm.[104] Also fluoride anions are released upon hydrolysis of phosphorofluoridate nerve agents, such as sarin gas.[105] It is for these reasons that there has been tremendous interest in the development of fluoride sensors that can detect concentrations on the ppm level. During the course of the past decade the use of triarylborons as fluoride sensors has gained momentum.[105-107]

Beginning with the discovery by Yamaguchi *et al* that derivatives featuring a tridurylborane could complex fluoride with a binding constant of 10^5-10^6 M^{-1} in organic solvents, focus was placed on the use of triarylboron systems as potential fluoride sensors.[108] The most attractive aspect of this approach was the photophysical changes that accompanied the binding of the fluoride ion. In triarylboron derivatives, the vacant p_z orbital is conjugated with the π-system contributing to the overall LUMO level of the complex. When a fluoride ion occupies the p_z-orbital the conjugation is disrupted, effectively altering the frontier orbitals of the system, causing changes to the emission pathways.[106]

This phenomenon is demonstrated by the diborylphenylene-containing bis(phenylethynyl)benzenes synthesized by Zhao *et al*.[109] This system has two boron sites making it a bimodal colorimetric fluoride sensor. Fluoride titrations were conducted on $(BMes_2)_2$-NPh_2 in THF (**Figure 1.17a**). As the fluoride source, TBAF, was added to the solution there was a blue-shift in the emission spectra, with the peak at 601 nm disappearing and a new peak emerging at

477 nm. This was associated to one boron site being filled by a fluoride ion (**Figure 1.17b**). Further blue-shifting occurred as the concentration of fluoride was increased, with the peak at 477 nm disappearing and a new peak emerging at 412 nm (**Figure 1.17c**). At this point both boron sites were bound to a fluoride ion and the emission peak was believed to originate from a π^*-π CT within the aryl group. Unfortunately, this type of colorimetric fluoride sensor is constrained to organic solvents. Furthermore, with the binding constants of $(BMes_2)_2$-NPh_2 upon the first and second fluoride complexation being $1.25 \times 10^5 \text{ M}^{-1}$ and $1.79 \times 10^4 \text{ M}^{-1}$, respectively, and the high hydration enthalpy towards fluoride ($\Delta H \simeq -504$ kJ/mol),[105] the presence of water typically dissociates these systems fairly quickly. As a result there has been considerable interest in designing new triarylboron derivatives that can be used as colorimetric fluoride sensors in water.
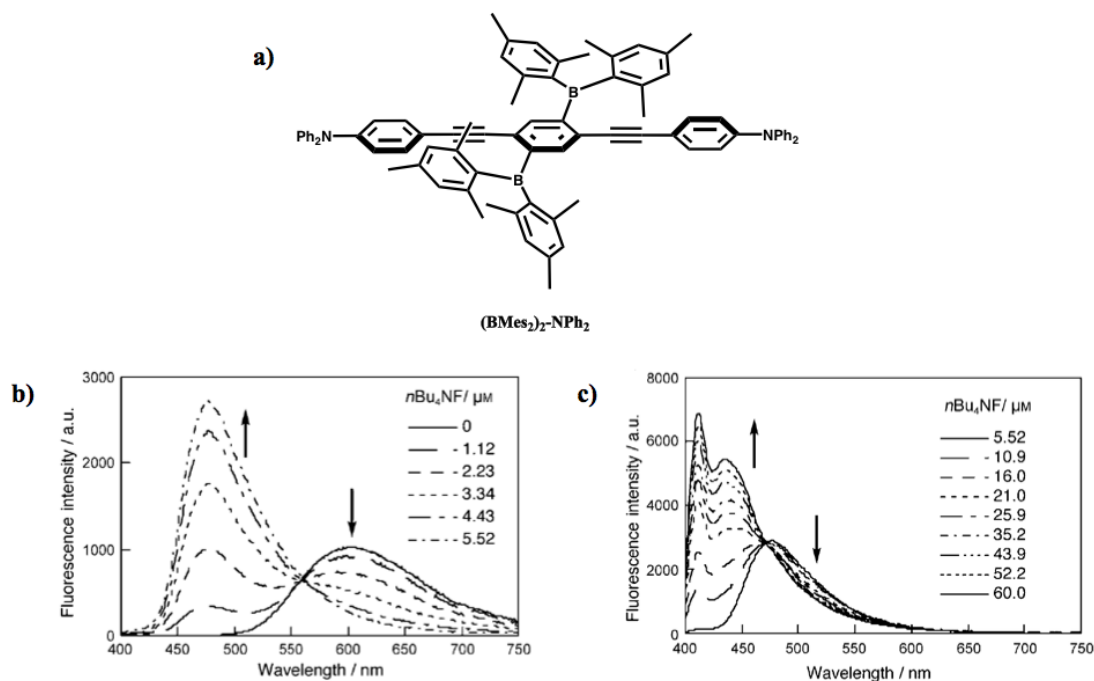
Figure 1.17. Illustrates (a) the structure of (BMes$_2$)$_2$-NPh$_2$, and its fluorescence titration spectra in THF by TBAF from the range of (a) 0 to 5.52x10^{-6} M and (b) 5.52x10-6 to 6.0x10^{-6} M (λ_{ex} = 390 nm).[109]

Solé and Gabbaï explored the concept of using cooperative fluoride complexation in order to increase the binding constant, and perhaps compete with the favorable hydration process.[110] They synthesized 1-(dimesitylboryl)-8-(10'-bora-9'-thiaanthryl)-naphthalene (BMes$_2$BS) to test this idea. Based on fluoride titrations the binding constant of BMes$_2$BS was found to be 5x10^9 M^{-1}, a value that is at least 3 orders of magnitude greater than any monofunctional borane. Furthermore, the presence of water did not lead to dissociation of the [BMes$_2$BS-μ_2-F$^-$] complex, leading the way for a new class of triarylboron-based anionic sensors.

1.4.2 Four-Coordinate Boron Systems for OLEDs

The four-coordinate boron, which is typically synthesized using a monoanion chelate ligand, is sp^3-hybridized giving it a tetrahedral geometry. Interest in these systems intensified with the discovery that the covalent bond to the anion on the chelate group was typically stronger than its Al counterpart, leading to the potential for more stable OLED materials.[111] Four-coordinate boron derivatives are typically classified based on the nature of the chromophore chelate, which includes N,N'-, or N,C-, or N,O-. Some examples are shown in **Figure 1.18**. Bodipy (**1a**) and its analogues are popularly known as dyes,[112] **1b** emits at 445 nm in solution with a quantum yield of 0.46,[113] and **1c** shows promise as an ETM for OLEDs.[114]
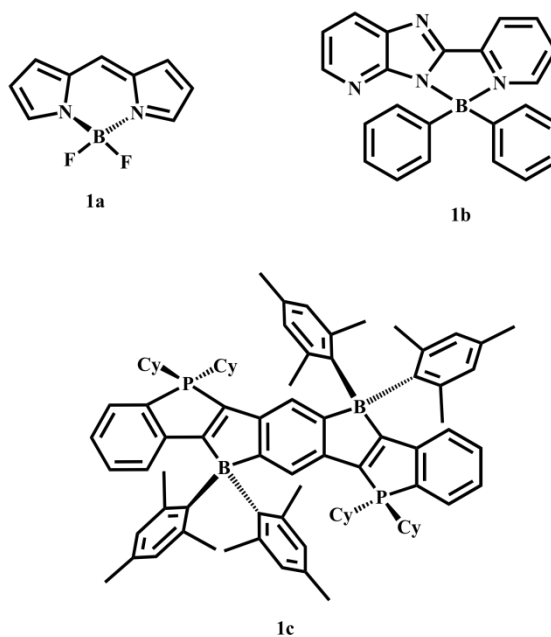
Figure 1.18. Examples of four-coordinate boron with N,N'-, C,C'- and N,C- chelates.

Motivated by the potential applications as emitters and/or electron transport materials, there has been considerable interest in boron chelate compounds with 8-hydroxyquinoline (q), all presented at the end in **Figure 1.19**. Wang and co-workers have made significant contributions to this area of four-coordinate boron chemistry. The first group of systems that was investigated was a set of three compounds that varied in the R groups attached to boron, which were: $B(C_2H_5)_2q$, BPh_2q and $B(2\text{-naph})_2q$.[115] All three compounds exhibited bright green-blue emissions, which is blue-shifted compared to Alq_3. EL device tests were conducted on BPh_2q and $B(2\text{-naph})_2q$, due to their higher melting points. It was found that while both proved to be possible emitters, they were very promising ETMs.

Substituent effects on the emission properties of structures with the general formula BAr_2q' was further explored by the group. The following structures were investigated: $BPh_2(5\text{-}(1\text{-naphthyl})\text{-}q)$ **(1)**, $BPh_2(5\text{-}(2\text{-benzothienyl})\text{-}q)$ **(2)**, $B(2\text{-benzothienyl})_2q$ **(3)**, and $B(2\text{-benzothienyl})_2\text{-}(2\text{-Me-q})$ **(4)**.[116] Interestingly, the emission spectra of **3** and **4** were very similar to $B(C_2H_5)_2q$, BPh_2q and $B(2\text{-naph})_2q$, indicating that changing the R group has little effect on the emission properties of BAr_2q'. The weaker emission efficiencies of **1** and **2** were attributed to the substituent being attached to the 5-positions of q, a phenomenon that has been previously reported.[84] Also the low quantum yield of **2** was believed to be a result of the "heavy atom" effect from S. As a result of the less than spectacular photoluminescent properties of some of these systems, an EL device was only made using **3**. Unfortunately, the results were not promising due to a tendency for **3** to form an exciplex with the HTM, NPB.

Interested by the concept of cooperative electronic effects between multiple boron centers, a series of linear and starburst systems with 2 or 3 four-coordinate boron centers was explored.[117] The three systems were: two BPh_2 centers on a biphenyl linker (**B1** and **B2**), three BPh_2 centers

on a triazine (**B3**) or benzene core (**B4**) and two BPh₂ centers on a thienyl linker (**B5**). While the HOMO energy levels of **B1**-**B4** were all about the same (~ -5.75 eV), **B5** had a HOMO that was much higher in energy (-5.40 eV). The LUMOs on the other hand varied a little more, with B5 having the highest LUMO (-3.02 eV) and B3 having the lowest LUMO (-3.28 eV). In all cases, the addition of the boron center significantly decreased the LUMO of the corresponding free ligands making the boron compounds favorable candidates as ETMs. Contrary to the predicted outcome, the introduction of multiple boron centers did not have the intended cooperative effects on the electronic nature of the compounds.
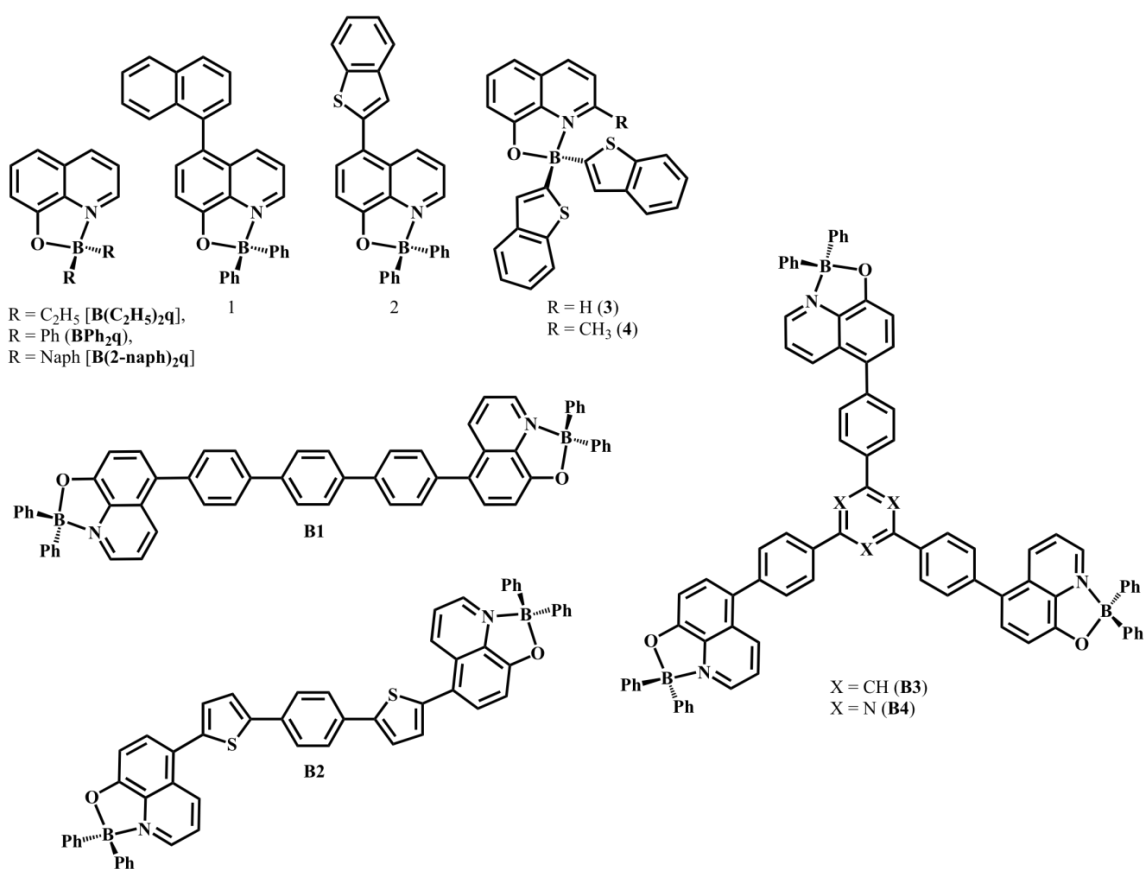
Figure 1.19. Examples of quinolate boron compounds.

Another series of BPh_2q' compounds that was synthesized and characterized by Qin *et al* focused on the color tunability that could be achieved through functionalizations on the 5-position of q with EWGs and EDGs.[118] This group discovered that although the emission shifts were consistent with the predicted effects of an EWG or EDG on the phenoxide ring, there was an overall blue-shift in comparison to the Alq_3 analogues, believed to be a result of the four-coordinate boron center. This was an important discovery in that blue emitters, which are in high demand, could be more easily developed using the boron quinolate moiety.

1.5 Motivation and Scope of the Thesis

At the moment hole mobiliy in organic materials is 1-2 orders of magnitude greater than electron mobility,[119] leading to charge imbalances that have been linked to reduced device efficiency and lifetime.[79] This highlights the importance of developing more efficient electron transport materials. As discussed above, there are two classes of molecules that have demonstrated promise as efficient ETMs: (1) modified Alq_3 derivatives and (2) boron-containing molecules. More importantly, the addition of a boron center has been shown to lower a system's LUMO energy level, an important property for good ETMs. To date there are no examples of Alq_3 or BPh_2q systems that incorporate the triarylboron moiety. Therefore, the aim of my research was to explore the luminescent and electronic properties of the first triarylboron modified Alq_3 and BPh_2q derivatives.

In Chapter 2, the synthesis and investigation of two different triarylboron-functionalized Alq_3 systems, one with an ethynyl linker and the other with a bisthiophene linker, will be presented.

Chapter 3 will focus on the investigation of three BPh_2q complexes that contain a triarylboron moiety. Comparisons will be made to other BPh_2q systems synthesized by our group in order to ascertain the effects of the additional three-coordinate boron moiety.

1.6 References

1) C. W. Tang and S. A. Van Slyke, *Appl. Phys. Lett.*, **1987**, 51, 913.

2) Z. H. Kafafi, *Organic Electroluminescence*, **2005**, Taylor and Francis Group, Boca Raton.

3) J. Shinar, *Organic Light-Emitting Devices: A Survey*, **2004**, Springer-Verlag, New York.

4) C. D. Entwistle and T. B. Marder, *Chem. Mater.*, **2004**, 16, 4574.

5) H. Hoppe and N. S. Sariciftci, *J. Mater. Res.*, **2004**, 19, 1924.

6) H. Spanggaard and F. C. Krebs, *Sol. Energ. Mat. Sol. Cells*, **2004**, 83, 125.

7) R. Schuepper, K. Schmidt, C. Uhrich, K. Schulze, D. Wynands, J. L. Brédas, E. Brier, E. Reinold, H.-B. Bu, P. Baeuerle, B. Maennig, M. Pfeiffer and K. Leo, *Phys. Rev. B*, **2008**, 77, 085311.

8) K. Parab, K. Venkatasubbaiah and F. Jäkle, *J. Am. Chem. Soc.*, **2006**, 128, 12879.

9) R. M. Duke, E. B. Vaele, F. M. Pfeffer, P. E. Kruger and T. Gunnlaugsson, *Chem. Soc. Rev.*, **2010**, 39, 3936.

10) E. Kim and S. B. Park, *Chem. –Asian J.*, **2009**, 4, 1646.

11) P.-T. Chou and Y. Chi, *Chem. –Eur. J.*, **2007**, 13, 380.

12) Z. H. Li, M. S. Wang, H. Fukutani and Y. Tao, *Chem. Mater.*, **2005**, 17, 5035.

13) K.-R. Wee, H.-C. Ahn, H.-J. Son, W.-S. Han, J.-E. Kim, D. W. Cho and S. O. Kang, *J. Org. Chem.*, **2009**, 74, 8472.

14) N. C. Eddingsaas and K. S. Suslick, *J. Am. Chem. Soc.*, **2007**, 129, 6718.

15) N. Terasaki, H. Zhang, H. Yamada and C.–N. Xu, *Chem. Commun.*, **2011**, 47, 8034.

16) J. L. Adcock, P. S. Francis and N. W. Barnett, *Anal. Chim. Acta*, **2007**, 601, 36.

17) A. Roda, *Chemiluminescence and Bioluminescence*, **2011**, RSC Publiching, Cambridge, UK.

18) C. Furetta, *Handbook of Thermoluminescence*, 2nd Ed., **2010**, World Scientific Publishing Co. Pte. Ltd., Toh Tuck Link, Singapore.

19) H. Namai, H. Ikeda, Y. Hoshi, N. Kato, Y. Morishita and K. Mizuno, *J. Am. Chem. Soc.*, **2007**, 129, 9032.

20) J. R. Lakowicz, *Principles of Fluorescence Spectroscopy*, 2nd Ed., **1999**, Kluwer Academic/Plenum Publishers, New York.

21) H. Yersin, *Highly Efficient OLEDs with Phosphorescent Materials*, **2008**, Whiley-VCH Verlag GmbH & Co. KGaA, Weinheim, Germany.

22) D. F. Eaton, *Pure & Appl. Chem.*, **1988**, 60, 1107.

23) J. Shinar and R. Shinar, *J. Phys. D: Appl. Phys.*, **2008**, 41, 133001.

24) C. Adachi, M. A. Baldo, M. E. Thompson and S. R. Forrest, *J. Appl. Phys.*, **2001**, 90, 5048.

25) N. C. Greenham, R. H. Friend and D. D. C. Bradley, *Adv. Mater.*, **1994**, 6, 491.

26) C. W. Tang, S. A. Van Slyke and S. A. C. H. Chen, *J. Appl. Phys.*, **1989**, 65, 3610.

27) C.-T. Chen, *Chem. Mater.*, **2004**, 16, 4389.

28) J. Kido and Y. Okamoto, *Chem. Rev.*, **2002**, 102, 2357.

29) J. Kido, H. Hayase, K. Hongawa, K. Nagai, and K. Okuyama, *Appl. Phys. Lett.*, **1994**, 65, 2124.

30) C. Adachi, T. Tsutsui and S. Saito, *Appl. Phys. Lett.*, **1989**, 55, 1489.

31) H. C. Yeh, S. J. Yeh and C.-T. Chen, *Chem. Commun.*, **2003**, 2632.

32) Y.-T. Lee, C.-L. Chiang and C.-T. Chen, *Chem. Commun.*, **2008**, 217.

33) S. E. Shaheen, B. Kippelen, N. Peyghambarian, J.-F. Wang, J. D. Anderson, E. A. Mash, P. A. Lee, N. R. Armstrong and Y. Kawabe, *J. Appl. Phys.*, **1999**, 85, 7939.

34) Y. T. Tao, E. Balasubramaniam, A. Daniels, B. Jarosz and P. Tomasik, *Appl. Phys. Lett.*, **2000**, 77, 1575.

35) X. Xu, G. Yu, S. Chen, C. Di and Y. Liu, *J. Mater. Chem.*, **2008**, 18, 299.

36) K. R. J. Thomas, M. Velusamy, J. T. Lin, Y.-T. Tao and C.-H. Chuen, *Adv. Funct. Mater.*, **2004**, 14, 387.

37) S.-Y. Ku, L.-C. Chi, W.-Y. Hung, S.-W. Yang, T.-C. Tsai, K.-T. Wang, Y.-H. Chen and C.-I. Wu, *J. Mater. Chem.*, **2009**, 19, 773.

38) M. Ikai, S. Tokito, Y. Sakamoto, T. Suzuki and Y. Taga, *Appl. Phys. Lett.*, **2001**, 79, 156.

39) R. C. Evans, P. Douglas and C. J. Winscom, *Coord. Chem. Rev.*, **2006**, 250, 2093.

40) J. A. G. Williams, S. Develay, D. C. Rochester and L. Murphy, *Coord. Chem. Rev.*, **2008**, 252, 2596.

41) Z. M. Hudson, C. Sun, M. G. Helander, H. Armane, Z.-H. Lu and S. Wang, *Adv. Funct. Mater.*, **2010**, 20, 3426.

42) S.-O. Jeon, Y.-M. Jeon, J.-W. Kim, C. W. Lee and M. –S. Gong, *Org. Electronics*, **2008**, 9, 522.

43) I. Tanaka, Y. Tabata and S. Tokito, *Chem. Phys. Lett.*, **2004**, 400, 86.

44) H. Sasabe and J. Kido, *Chem. Mater.*, **2011**, 23, 621.

45) W.-L. Jia, D. Song and S. Wang, *J. Org. Chem.*, **2003**, 68, 701.

46) W.-L. Jia, X. D. Feng, D. R. Bai, Z. H. Lu, S. Wang and G. Vamvounis, *Chem. Mater.*, **2005**, 17, 164.

47) K.-C. Wu, P.-J. Ku, C.-S. Lin, H.-T. Shih, F.-I. Wu, M.-J. Huang, J.-J. Lin, I.-C. Chen and C.-H. Cheng, *Adv. Funct. Mater.*, **2008**, 18, 67.

48) S. Tokito, T. Tsuzuki, F. Sato and T. Iijima, *Curr. Appl. Phys.*, **2005**, 5, 331.

49) C. Adachi, R. C. Kwong, P. Djurovich, V. Adamovich, M. A. Baldo, M. E. Thompson, S. R. Forrest, *Appl. Phys. Lett.*, **2001**, 79, 2082.

50) L. Xiao, S.-J. Su, Y. Agata, H. Lan and J. Kido, *Adv. Mater.*, **2009**, 21, 1271.

51) S. O. Jeon, K. S. Yook, C. W. Joo and J. Y. Lee, *Adv. Funct. Mater.*, **2009**, 19, 3644.

52) L. Mercs and M. Albrecht, *Chem. Soc. Rev.*, **2010**, 39, 1903.

53) Y. Chi and P.-T. Chou, *Chem. Soc. Rev.*, **2010**, 39, 638.

54) Y. Wu, S.-X. Wu, H.-B. Li, Y. Geng and Z.-M. Su, *Dalton Trans.*, **2011**, 40, 4480.

55) Y. Unger, D. Meyer, O. Molt, C. Schildknecht, I. Münster, G. Wagenblast and T. Strassner, *Agnew. Chem: Int. Ed.*, **2010**, 49, 10214.

56) Y. Shirota and H. Kagayema, *Chem. Rev.*, **2007**, 107, 953.

57) Y. Shirota, *J. Mater. Chem.*, **2005**, 15, 75.

58) O. Usler, S. Demic, D. A. M. Egbe, E. Birckner, C. Tozlu, A. Pivrikas, A. M. Ramil and N. S. Sariciftci, *Adv. Funct. Mater.*, **2010**, 20, 4152.

59) H. Tanaka, S. Tokito, Y. Taga and A. Okada, *Chem, Commun.*, **1996**, 2175.

60) Y. Shirota, K. Okumoto and H. Inada, *Synth. Met.*, **2000**, 111-112, 387.

61) H. Murata, C. D. Merritt, H. Inada, Y. Shirota and Z. H. Kafafi, *Appl. Phys. Lett.*, **1999**, 75, 3252.

62) K. Okumoto and Y. Shirota, *Chem. Lett.*, **2000**, 1034.

63) K. Okumoto and Y. Shirota, *Jpn. Kokai Tokkyo Koho*, **2003**, 261473.

64) Z. Yang, B. Xu, J. He, L. Xue, Q. Guo, H. Xia and W. Tian, *Org. Electron.*, **2009**, 10, 954.

65) S. Watanabe, N. Ide and J. Kido, *Jpn. J. Appl. Phys.*, **2007**, 46, 1186.

66) S.-J. Su, D. Tanaka, Y.–J. Li, H. Sasabe, T. Takeda and J. Kido, *Org. Lett.*, **2008**, 10, 941.

67) D. O'Brien, A. Bleyer, D. G. Lidzey, D. D. C. Bradley and T. Tsutsui, *J. Appl. Phys.*, **1997**, 82, 2662.

68) M. A. Reddy, G. Mallesham, A. Thomas, K. Srinivas, V. J. Rao, K. Bhanuprakash, L. Giribabu, R. Grover, A. Kumar, M. N. Kamalasanan and R. Srivastava, *Synth. Met.*, **2011**, 161, 869.

69) C.-C. Yang, C.–J. Hsu, P.–T, Chou, H. C. Cheng, Y. O. Su and M. K. Leung, *J. Phys. Chem. B*, **2010**, 114, 756.

70) T. Noda and Y. Shirota, *J. Am. Chem. Soc.*, **1998**, 120, 9714.

71) A. J. Mäkinen, I. G. Hill, T. Noda, Y. Shirota and Z. H. Kafafi, *Appl. Phys. Lett.*, **2001**, 78, 670.

72) A. J. Mäkinen, I. G. Hill, M. Kinoshita, T. Noda, Y. Shirota and Z. H. Kafafi, *J. Appl. Phys.*, **2002**, 91, 5436.

73) M. Kinoshita and Y. Shirota, *Chem. Lett.*, **2001**, 614.

74) D. Tanaka, T. Takeda, T.Chiba, S. Watanabe and J. Kido, *Chem. Lett.*, **2007**, 36, 262.

75) S.-J. Su, T. Chiba, T. Takeda and J. Kido, *Adv. Mater.*, **2008**, 20, 2125.

76) S.-J. Su, Y. Takahashi, T. Chiba, T. Takeda and J. Kido, *Adv. Funct. Mater.*, **2009**, 19, 1260.

77) A. Curioni and W. Andreoni, *J. Am. Chem. Soc.*, **1999**, 121, 8216.

78) K. A. Higginson, X.-M. Zhang and F. Papadimitrakopoulos, *Chem. Mater.*, **1998**, 10, 1017.

79) H. Aziz, Z. D. Popovic, N.-X. Hu, A.-M. Hor, and G. Xu, *Science*, **1999**, 283, 1900.

80) A. Curioni, M. Boero and W. Andreoni, *Chem. Phys. Lett.*, **1998**, 294, 263.

81) M. D. Halls and H .B. Schlegel, *Chem. Mater.*, **2001**, 13, 2632.

82) Y.-W. Shi, M.-M. Shi, J.-C. Huang, H.-Z. Chen, M. Wang, X.-D. Liu, Y.-G. Ma, H. Xu and B. Yang, *Chem Commun.*, **2006**, 1941.

83) A. Irfan, R. Cui, J. Zhang and L. Hao, *Chem. Phys.*, **2009**, 364, 39.

84) L. S. Sapochak, A. Padmaperuma, N. Washton, F. Endrino, G. T. Schmett, J. Marshall, D. Fogarty, P. E. Burrows and S. R. Forrest, *J. Am. Chem. Soc.*, **2001**, 123, 6300.

85) C. Pérez-Bolívar, V. A. Montes and P. Anzenbacher Jr., *Inorg. Chem.*, **2006**, 45, 9610.

86) V. A. Montes, R. Pohl, J. Shinar and P. Anzenbacher Jr., *Chem. Eur. J.*, **2006**, 12, 4523.

87) V. A. Montes, G. Li, R. Pohl, J. Shinar and P. Anzenbacher Jr., *Adv. Mater.*, **2004**, 16, 2001

88) R. Pohl, V. A. Montes, J. Shinar and P. Anzenbacher Jr., *J. Org. Chem.*, **2004**, 69, 1723.

89) J.-A. Cheng, C. H. Chen and C. H. Liao, *Chem. Mater.*, **2004**, 16, 2862.

90) J. Xie, Z. Ning and H. Tian, *Tetrahedron Lett.*, **2005**, 46, 8559.

91) P. Jiang, W. Zhu, Z. Gan, W. Huang, J. Li, H. Zeng and J. Shi, *J. Mater. Chem.*, **2009**, 19, 4551.

92) C. D. Entwistle and T. B. Marder, *Angew. Chem. Int. Ed.*, **2002**, 41, 2927.

93) F. Jäkle, *Coord. Chem. Rev.*, **2006**, 250, 1107.

94) S. Yamaguchi and A. Wakamiya, *Pure Appl. Chem.*, **2006**, 78, 1413.

95) Z. M. Hudson and S. Wang, *Dalton Trans.*, **2011**, 40, 7805.

96) Z. M. Hudson and S. Wang, *Acc. Chem. Res.*, **2009**, 42, 1584.

97) H. Doi, M. Kinoshita, K. Okumoto and Y. Shirota, *Chem. Mater.*, **2003**, 15, 1080.

98) X.-Y. Liu, D.-R. Bai and S. Wang, *Chem. Int. Ed.*, **2006**, 45, 5475.

99) D.-R. Bai, X.-Y. Liu and S. Wang, *Chem. –Eur. J.*, **2007**, 13, 5713.

100) Y. Sun, N. Ross, S. –B. Zhao, K. Huszarik, W.-L. Jia, R.-Y. Wang, D. Macartney and S. Wang, *J. Am. Chem. Soc.*, **2007**, 129, 7510.

101) Y. Sun and S. Wang, *Inorg. Chem.*, **2010**, 49, 4394.

102) Y.-L. Rao and S. Wang, *Inorg. Chem.*, **2009**, 48, 7698.

103) Z. M. Hudson, C. Sun, M. G. Helander, H. Armane, Z.-H. Lu and S. Wang, *Adv. Funct. Mater.*, **2010**, 20, 3426.

104) Y. Kim and F. P. Gabbaï *J. Am. Chem. Soc.*, **2009**, 131, 3363.

105) T. W. Hudnall, C.-W. Chiu and F. P. Gabbaï *Acc. Chem. Res.*, **2009**, 42, 388.

106) E. Galbraith and T. D. James, *Chem. Soc. Rev.*, **2010**, 39, 3831.

107) C. R. Wade, A. E. J. Broomsgrove, S. Aldridge and F. P. Gabbai, *Chem. Rev.*, **2010**, 110, 3958.

108) S. Yamaguchi, S. Akiyama and K. Tamao, *J. Am. Chem. Soc.*, **2001**, 123, 11372.

109) C.-H. Zhao, E. Sakuda, A. Wakamiya and S. Yamaguchi, *Chem. Eur. J.*, **2009**, 15, 10603.

110) S. Solé and F. P. Gabbaï, *Chem. Commun.*, **2004**, 12, 84.

111) Y.-L. Rao and S. Wang, *Inorg. Chem.*, **2011**, As soon as publishable.

112) I. J. Arroyo, R. Hu, G. Merino, B. Z. Tang and E. Peña-Cabrera, *J. Org. Chem.*, **2009**, 74, 5719.

113) Q.-D. Liu, M. S. Mudadu, R. Thummel, Y. Tao and S. Wang, *Adv. Funct. Mater.*, **2005**, 15, 143.

114) A. Fukazawa, H. Yamada and S. Yamaguchi, *Angew. Chem. Int. Ed.*, **2008**, 47, 5582.

115) Q. Wu, M. Esteghamatian, N.-X. Hu, Z. Popovic, G. Enright, Y. Tao, M. D'Iorio and S. Wang, *Chem. Mater.*, **2000**, 12, 79.

116) Y. Cui, Q.-D. Liu, D.-R. Bai, W.-L. Jia, Y. Tao and S. Wang, *Inorg. Chem.* **2005**, 44, 601.

117) Y. Cui and S. Wang, *J. Org. Chem.*, **2006**, 71, 6485.

118) Y. Qin, I. Kiburu, S. Shah and F. Jäkle, *Org. Lett.*, **2006**, 8, 5227.

119) T. H. Lee, K. M. Lai and L. M. Leung, *Polymer*, **2009**, 50, 4602.

Chapter 2

Triarylboron-Functionalized 8-Hydroxyquinoline and their Al(III) Complexes

2.1 Introduction

As discussed in chapter 1, the importance of Alq_3 lies in its ability to be used as either an emissive or electron transport layer in EL devices. Due to a large body of research and a better understanding of the electronic properties of this material, a wide-range of derivatives with well-controlled photophysical properties have been synthesized, which were discussed in some detail in the first chapter. Though with the emergence of triplet emitters over the past decade, Alq_3 has become better known for its electron transport properties, a role that has been investigated extensively.[1]

There has also been considerable interest in the use of triarylboron compounds as electron transport materials due to the low-lying empty p_z orbital on the boron center, which has demonstrated strong electron accepting properties. Furthermore, this attribute contributes to the intense luminescence charge-transfer observed from this class of molecules, a property that can be exploited for anion sensing—which was also discussed in the first chapter.

The concept of combining these two systems, both of which exhibit strong electron transport characteristics, is quite promising. Attaching a dimesitylboron moiety to Alq_3 would result in a multifunctional material that could be used as an emissive or electron-transport material in OLEDs as well as a sensor for small anions.

55

Herein the synthesis and characterization of the first triarylboron-functionlized 8-hydroxyquinoline ligands (**1** and **2**) and their aluminum (III) complexes (Al(**1**)$_3$ and Al(**2**)$_3$) will be reported (**Figure 2.1**). It should be noted that while both **2** and Al(**2**)$_3$ were synthesized by Dr. Yi Sun, I undertook the task of characterizing these two systems. A rigid and flexible linker had been incorporated into **1** and **2**, respectively. Both linkers were expected to enhance the electronic communication between the boron center and the Alq$_3$ unit, with **1** possessing a highly planar π-conjugated acetylene system and **2** a hexylthiophene linker that has been demonstrated to provide good electron mobility in optoelectronic devices.[2,3]
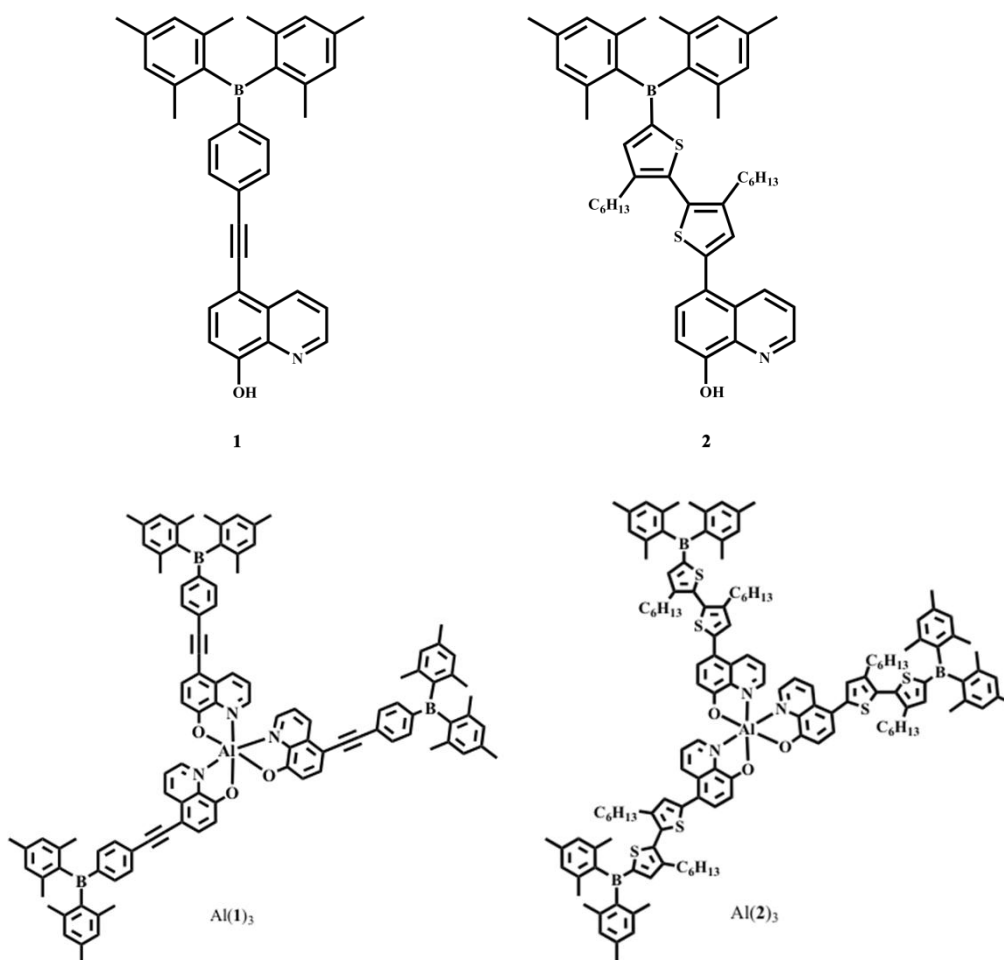
Figure 2.1. Structure of the ligands and their Al(III) complexes.

2.2 Experimental Section

Dry solvents were obtained from a solvent purification system (Innovative Technologies, Inc.). Reactions that required oxygen-free environments were conducted under an inert nitrogen atmosphere in oven-dried glassware using standard Schlenk techniques unless otherwise stated. ^{1}H and ^{13}C NMR spectra were recorded using Bruker Avance 300, 400 or 500 MHz

spectrometers. UV-Vis measurements were acquired using a Varian Cary 50 Bio Spectrometer. Excitation and emission spectra were recorded using a Photon Technologies International Quanta Master model C-60 spectrometer. High-resolution mass spectra were obtained using a Water/Micromass GC-TOF EI-MS spectrometer. Elemental analyses were conducted by Canadian Microanalytical Service Ltd. Cyclic voltammetry measurements were acquired using a BAS CV-50W analyzer with a typical sample concentration of 4 mg of sample and 50 mg of NBu_4PF_6 (TBAP) as supporting electrolyte in 3 mL of DMF using a standard Ag/AgCl reference electrode, Pt working electrode, and Pt auxiliary. The ferrocenium/ferrocene couple was used as an internal standard (E_o = 0.55 V). Aside from 8-hydroxyquinoline, ordered from TCI, all reagents were obtained from the Sigma-Aldrich chemical company. 8-tert-butoxycarbonyloxy-5-ethynylquinoline[4], 5,5'-dibromo-3,3'-dihexyl-2,2'-bithiophene[5] and 5-bromo-8-(methylmethoxy)quinoline[6] were synthesized as outlined in literature.

2.2.1 Synthesis of Ligand 1

(p-Iodophenyl)dimesitylborane: Diiodobenzene (3 g, 9.09 mmol) was dissolved in 60 mL of dry THF at room temperature. The temperature of the reaction flask was reduced to -78°C to which a hexane solution of nBuLi (1.6 M, 5.2 mL, 8.18 mmol) was added and the contents of the flask reacted for 2 hrs. A solution of dimesitylboron fluoride (2.20 g, 8.18 mmol) in 20 mL of THF was added to the reaction flask and allowed to react for 2 hours at -78°C and then at room temperature overnight. The solvent was removed under vacuum and the product purified using column chromatography on silica gel (hexane) and then recrystallized in hexane to give white

crystalline product in 50% yield. ^{1}H NMR (CDCl$_3$, 25°C): δ (ppm) = 7.70 (d, J = 8.0 Hz, 2H), 7.21 (d, J = 8.0 Hz, 2H), 6.81 (s, 4H), 2.30 (s, 6H), 1.98 (s, 12H). This data matches literature spectral data.[7]

1: A mixture of (p-iodophenyl)dimesitylborane (604 mg, 1.34 mmol), 8-tert-butoxycarbonyloxy-5-ethynylquinoline (300 mg, 1.11 mmol), Pd(PPh$_3$)$_4$ (64 mg, 0.056 mmol), CuI (21 mg, 0.11 mmol) and DIPEA (5 mL) was stirred in THF (40 mL) overnight at room temperature. The THF was removed *in vacuo*. Water was added to the mixture and the product was extracted with CHCl$_3$. **1-Boc** was purified by column chromatography on silica gel (hexane/acetone = 9:1) and then recrystallized using hexane in 67% yield. Then to a stirred solution of **1-Boc** (100 mg, 0.17 mmol) in 1 mL of dry CHCl$_3$, piperidine (50 μL, 0.50 mmol) was added and allowed to stir for approximately 10 minutes at room temperature. The CHCl$_3$ was removed *in vacuo* and the product was recrystallized in acetone resulting in quantitative yield of **1**. ^{1}H NMR (CD$_2$Cl$_2$, 25°C): 8.89 (d, J = 3.0 Hz, 1H), 8.75 (d, J = 7.6 Hz, 1H), 7.80 (d, J = 8.0 Hz, 1H), 7.64 (m, 1H), 7.64 (d, J = 8.1 Hz, 2H), 7.55 (d, J = 8.1 Hz, 2H), 7.20 (d, J = 8.0 Hz, 1H), 6.89 (s, 4H), 2.35 (s, 6H), 2.05 (s, 12H). ^{13}C {^{1}H} NMR (CD$_2$Cl$_2$, 25°C): δ (ppm) = 153.7, 149.0, 141.2, 139.3, 138.4, 136.6, 135.3, 133.0, 131.2, 129.3, 128.6, 127.0, 123.1, 111.5, 110.2, 93.5, 88.9, 23.5, 21.3. HRMS of C$_{35}$H$_{32}$BNO: calcd [M+H$^+$] m/z = 494.2655, found [M+H$^+$] m/z = 494.2661.

2.2.2 Synthesis of Ligand 2

5-bromo-5'-dimesitylboryl-3,3'-dihexyl-2,2'-bithiophene: 5,5'-dibromo-3,3'-dihexyl-2,2'-bithiophene (1.92 g, 3.89 mmol) was dissolved in 20 mL of dry THF at room temperature. The temperature of the reaction flask was reduced to -78°C to which a hexane solution of nBuLi (1.6 M, 2.55 mL, 4.08 mmol) was added and the contents of the flask reacted for ~2 hrs. A solution of dimesitylboron fluoride (1.28 g, 4.28 mmol) in 15 mL of THF was added to the reaction flask and allowed to react for 2 hours at -78 ^{o}C and then at room temperature overnight. The solvent was removed *in vacuo* and the product was purified using column chromatography on silica gel using hexanes as eluent (80% yield). ^{1}H NMR (CDCl$_3$, 25°C): δ (ppm) = 7.30 (s, 1H), 6.91 (s, 1H), 6.84 (s, 4H), 2.49 (m, 4H), 1.48 (m, 4H), 1.22 (m, 12H), 0.86 (m, 6H). ^{13}C {^{1}H} NMR (CD$_2$Cl$_2$, 25 ^{o}C): δ (ppm) 145.3, 143.2, 142.7, 142.0, 141.2, 139.6, 138.8, 131.9, 128.4, 31.9, 31.8, 31.1, 30.8, 29.3, 29.0, 23.8, 22.8, 21.5, 14.3. HRMS of C$_{38}$H$_{50}$BBrS$_2$: calcd *m/z* = 660.2630, found *m/z* = 660.2645.

2: To a solution of 5-bromo-5'-dimesitylboryl-3,3'-dihexyl-2,2'-bithiophene (1.10 g, 1.66 mmol) in THF (15 mL) at -78 ^{o}C, was added nBuLi (1.6 M, 1.14 mL, 1.82 mmol). The mixture was allowed to react for 2 hrs. Then 2-isopropoxy-4,4,5,5-tetramethyl-1,3,2-dioxaborolane (0.42 mL, 2.08 mmol) was added slowly at -78°C. The reaction mixture was allowed to react for 2 hours at -78°C before it was warmed to room temperature and allowed to react overnight. The product was purified using column chromatography on silica gel using hexane and ethyl acetate sequentially, resulting in a yield of 69% of **5-pinacolboryl-5'-dimesitylboryl-3,3'-dihexyl-2,2'-bithiophene**. In a 20 mL Schlenk flask was added the above boronic ester (750 mg, 1.06 mmol), 5-bromo-8-(methoxymethoxy)quinoline (190 mg, 0.71 mmol), K$_3$PO$_4$ (567 mg, 2.13 mmol),

Pd(CH$_3$COO)$_2$ (8.00 mg, 0.035 mmol), and 2-dicyclohexylphosphino-2',6'-dimethoxybiphenyl (29 mg, 0.07 mmol) in toluene (3 mL). The reaction proceeded overnight under reflux. The product was purified using column chromatography on silica gel (ethyl acetate/hexane = 1:2) to give **2-MOM** in 95% yield, which was then deprotected according to literature methods[6][1] to produce compound **2** in 90%. H NMR (CDCl$_3$, 25°C): δ (ppm) = 8.83 (d, J = 4.0 Hz, 1H), 8.66 (d, J = 8.5 Hz, 1H), 7.61 (d, J = 8.0 Hz, 1H), 7.50 (dd, J = 8.5 Hz, 4.0 Hz, 1H), 7.467,374 (s, 1H), 7.25 (d, J = 8.0 Hz, 1H), 7.03 (s, 1H), 6.86 (s, 4H), 2.63 (m, 4H), 2.33 (s, 6H), 2.20 (s, 12H), 1.58 (m, 4H), 1.27 (m, 12H), 0.90 (m, 6H). ^{13}C {^{1}H} NMR (CD$_2$Cl$_2$, 25°C): δ (ppm) = 152.4, 149.6, 147.9, 144.6, 142.8, 142.7, 142.1, 141.0, 140.6, 138.6, 138.4, 134.7, 129.4, 129.3, 129.0, 128.3, 127.0, 123.0, 122.2, 109.7, 31.7, 31.7, 31.0, 30.9, 29.4, 29.2, 29.1, 28.9, 23.6, 22.7, 21.3, 14.2. HRMS of C$_{47}$H$_{56}$BNOS$_2$: calcd m/z = 725.3896, found m/z = 725.3905.

2.2.3 Synthesis of Al(1)$_3$

To a solution of 1 (100 mg, 0.203 mmol) in toluene (30 mL) at 25°C, Al(Me)$_3$ (34 μL, 0.068 mmol) was added. The reaction was allowed to proceed for 15 minutes at which point the toluene was removed *in vacuo* and the product was recrystallized using hexanes in 80% yield. ^{1}H NMR (CDCl$_3$, 25°C): δ (ppm) 8.82 (m, 5H), 7.82 (d, J = 8.14 Hz, 3H), 7.63 (m, 1H), 7.56 (m, 1H), 7.56 (d, J = 8.0 Hz, 2H), 7.48 (d, J = 8.0 Hz, 2H), 7.40 (m, 1H), 7.33 (d, J = 5.1 Hz, 1H), 7.05 (d, J = 8.15 Hz, 1H), 7.02 (d, J = 8.15 Hz, 1H), 6.93 (d, J = 8.15 Hz, 1H), 6.83 (s, 4H), 2.30 (s, 18H), 2.00 (s, 36H). ^{13}C {^{1}H} NMR (CD$_2$Cl$_2$, 25°C): δ (ppm) = 160.8, 160.5, 160.1, 146.2, 145.5, 143.7, 141.9, 141.2, 140.0, 139.6, 139.5, 139.3, 139.3, 139.1, 139.0, 136.6, 136.4, 136.2, 131.1, 130.4,

130.3, 129.4, 128.6, 127.6, 127.4, 127.3, 125.6, 123.2, 123.1, 122.6, 113.4, 113.2, 113.0, 105.7, 105.6, 105.2, 93.2, 93.1, 93.0, 89.7, 89.4, 89.1, 66.1, 23.6, 21.3, 15.5, 1.2. HRMS of $C_{105}H_{93}B_3N_3O_3Al$: calcd $[M+Na^+]$ m/z = 1526.7209, found $[M+Na^+]$ m/z = 1526.9110.

2.2.4 Synthesis of Al(2)₃

To a solution of 2 (100 mg, 0.138 mmol) in toluene (30 mL) at 25°C, Al(Me)₃ (23 μL, 0.0460 mmol) was added. The reaction was allowed to proceed for 15 minutes at which point the toluene was removed *in vacuo* and the product purified by centrifugation in hexanes in quantitative yield. ^1H NMR (CDCl₃, 25°C): δ (ppm) = 8.80 (m, 5H), 7.65 (m, 3H), 7.51 (m, 1H), 7.42 (m, 1H), 7.34 (s, 3H), 7.22 (m, 1H), 7.16 (m, 4H), 6.93 (m, 3H), 6.83 (s, 12H), 2.59 (m, 12H), 2.30 (s, 18H), 2.17 (s, 38H), 1.56 (m, 12H), 1.24 (m, 36H), 0.84 (m, 18H). ^{13}C {^1H} NMR (CD₂Cl₂, 25°C): δ (ppm) = 159.7, 159.5, 159.1, 149.9, 149.8, 145.7, 145.2, 144.9, 144.8, 144.8, 143.5, 143.3, 143.1, 143.1, 143.0, 142.5, 141.7, 141.3, 141.2, 140.5, 139.9, 139.8, 138.9, 138.9, 138.8, 138.7, 138.3, 133.3, 133.1, 132.8, 129.5, 129.2, 129.1, 129.0, 128.7, 128.6, 128.4, 128.1, 125.8, 122.5, 121.9, 118.0, 117.8, 117.6, 113.9, 113.4, 112.9, 32.1, 32.0, 31.4, 31.3, 31.3, 31.2, 29.7, 29.6, 29.5, 29.3, 24.0, 23.1, 23.1, 21.9, 21.7, 21.2, 14.6, 14.5. HRMS of $C_{141}H_{165}B_3N_3O_3S_6Al$: calcd $[M+H^+]$ m/z = 2021.1343, found $[M+H^+]$ m/z = 2201.1396.

2.2.5 Molecular Orbital Calculations

DFT calculations were conducted on ligands **1** and **2** as well as their aluminum complexes, Al(**1**)$_3$ and Al(**2**)$_3$. The calculations were done using the Gaussian03 program and the results were obtained at the B3LYP/6-31G* level of theory.

2.3 Results and Discussion

2.3.1 Synthesis

2.3.1.1 Synthesis of Ligand 1

As shown in **Figure 2.2** the synthetic scheme pertaining to **1** had two different components that were attached on the final step. The synthesis of the boc-protected 8-hydroxyquinolne and the subsequent attachment of trimethylsilane (TMS) protected acetylene was followed according to literature.[4] There were several steps that deviated from the literature procedure. Although triethylamine (TEA) was used as the base during the Sonogashira coupling step, it was found that using bulkier bases, such as diisopropylethylamine (DIPEA) is more favorable as it prevents the removal of the boc-protecting group that enables chelation to the catalyst. The TMS protecting group was removed using KF in a solution of methanol (11 vol%), water (22 vol%) and THF (67 vol%).

63

The synthesis of (p-iodophenyl)dimesitylborane was achieved by lithiating diiodobenzene at -78 °C. After FBMes$_2$ was added to the solution at -78 °C the solution was allowed to return to room temperature and react overnight.

In the final step, linking (p-iodophenyl)dimesitylborane and the modified 8-hydroxyquinoline could only be accomplished using diisopropylamine as the base. If TEA was used the reaction yield was typically below 10%, while the use of DIPEA provided yields greater than 60%, due to the aforementioned reasons.
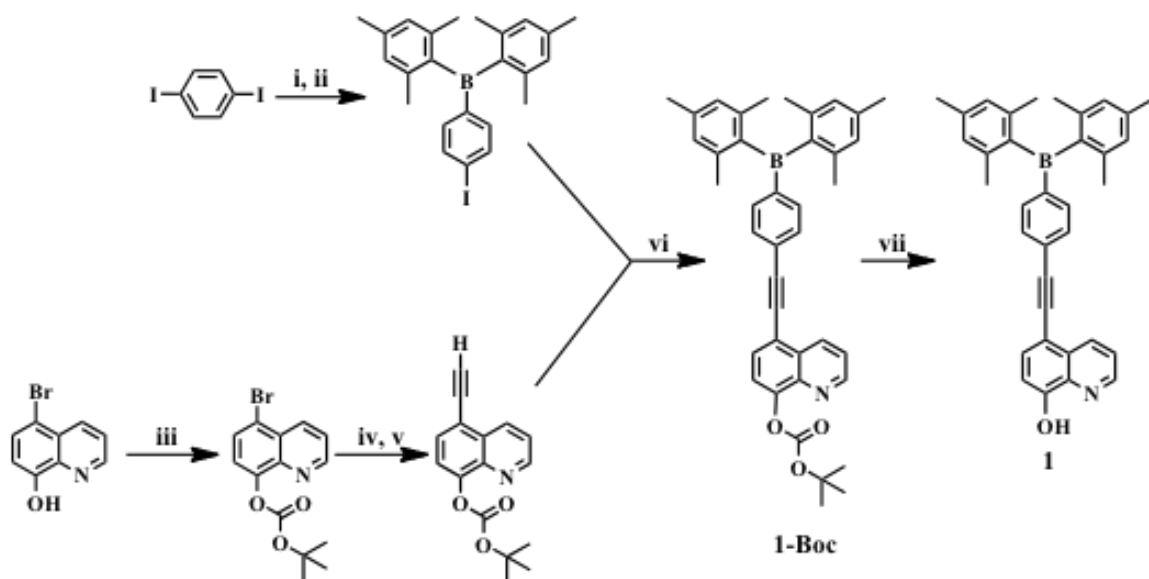
Reagents and conditions: (i) *n*-BuLi, THF, -78 °C; (ii) FBMes$_2$, THF, -78-25 °C, overnight; (iii) di-*t*-butyl carbonate, dimethylaminopyridine, hexane, R.T., 5hrs; (iv) [PdCl$_2$(PPh$_3$)$_2$], CuI, trimethylsilylacetylene, THF, triethylamine, 60 °C, overnight; (v) KF, MeOH, water, THF, R.T., 5 hrs; (vi) [Pd(PPh$_3$)$_4$], CuI, THF, DIPEA, r.t., overnight; (vii) piperidine, dry CH$_2$Cl$_2$, r.t., overnight.

Figure 2.2. Synthetic scheme for 1.

2.3.1.2 Synthesis of 2

As outlined in the introduction to this chapter, ligand **2** was synthesized entirely by Dr. Yi Sun. Similar to **1**, the synthetic procedure for this ligand was divided into two components, as illustrated in **Figure 2.3**. In this particular case the protecting group used was chloromethoxymethane. Also, in order to ensure that the catalyst would not become chelated by the hydroxyquinoline ligand in the final Sonogashira coupling step the bulky SPhos ligand was used. Furthermore, the hexyl groups on the bisthiophene linker were added to increase the system's solubility properties.
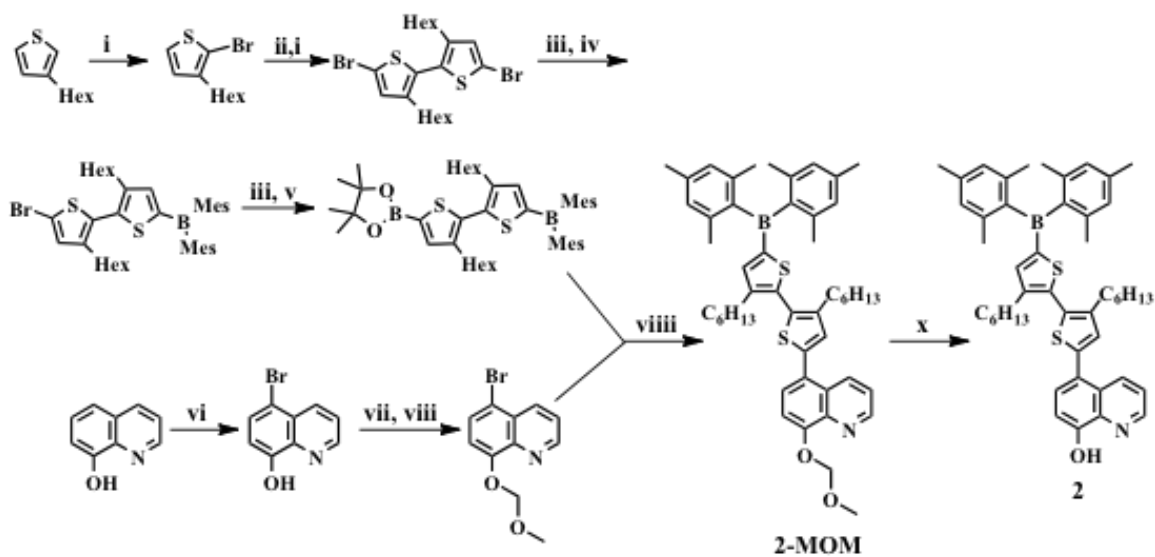
Reagents and conditions: (i) NBS, CHCl$_3$, AcOH, 0 ℃ to 25 ℃, 3 hrs; (ii) NiCl$_2$(PPh$_3$)$_2$, PPh$_3$, Zn, KI, THF, reflux, overnight; (iii) NBS, THF, 0 ℃ to 25 ℃; (iv) *n*-BuLi, THF, -78 ℃; (v) FBMes$_2$, THF, -78 ℃ to 25 ℃; (vi) B(pin)(O^{i}Pr), THF, -78 ℃ to 25 ℃; (vii) Br$_2$, H$_2$SO$_4$, -10 ℃; (viii) NaH, THF, 0 ℃; (viiii) CH$_3$OCH$_2$Cl, THF, 0 ℃ to 25 ℃; (x) Pd(OAc)$_2$, SPhos, K$_3$PO$_4$, toluene, reflux; (xi) HCl, CH$_3$OH, reflux.

Figure 2.3. Synthetic scheme for 2.

65

2.3.1.3 Synthesis of Al(1)$_3$ and Al(2)$_3$

Since the syntheses of both of these complexes were identical, they will be grouped together in this section. Again, a special note will be made that the synthesis of Al(**2**)$_3$ was also conducted entirely by Dr. Yi Sun. The synthetic schemes are presented in **Figure 2.4**. The source of aluminum came from Al(Me)$_3$, which was reacted with **1** and **2**, respectively, under room temperature. While Al(**1**)$_3$ precipitated out of toluene during the course of the reaction, the same was not true for Al(**2**)$_3$ due to the hexyl-chains on the bisthiophene chain. Due to limited solubility in hexanes, both compounds were isolated via centrifugation in hexanes.
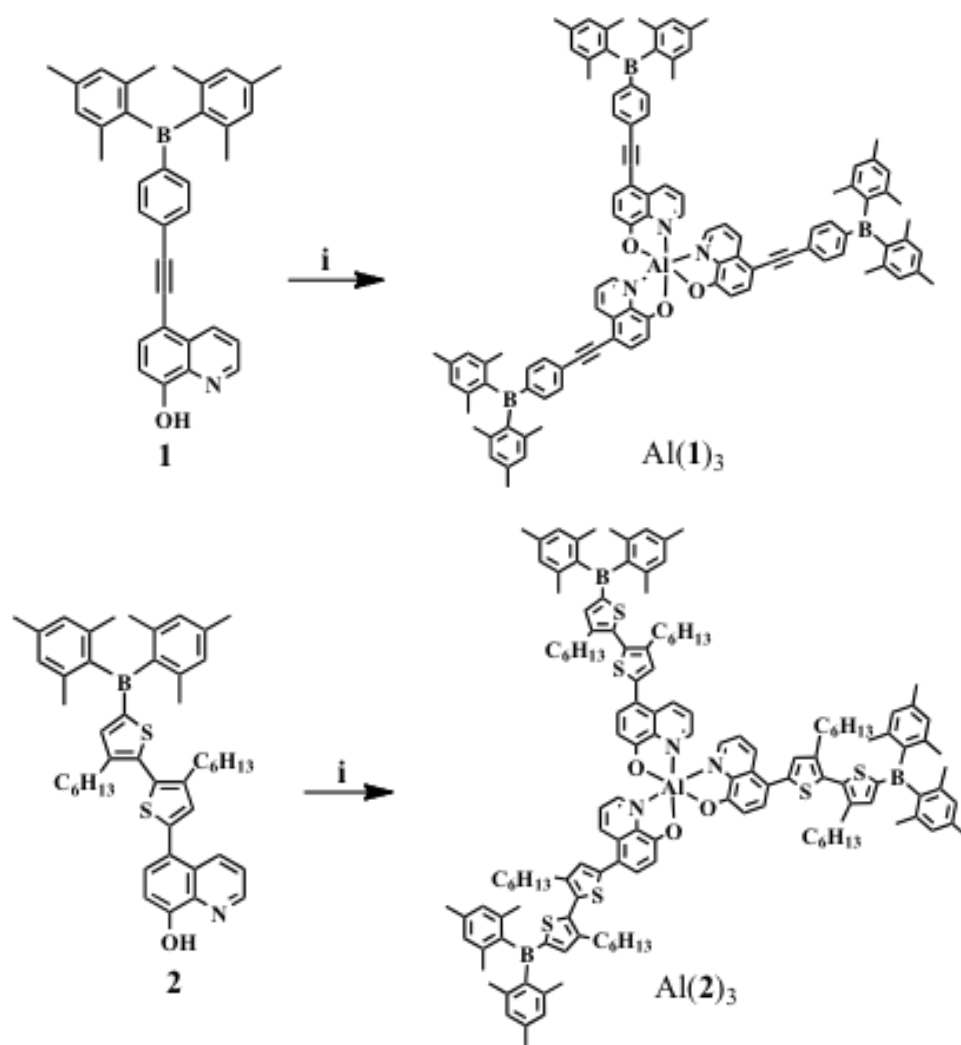
Reactions and conditions: (i) Al(Me)$_3$, THF, r.t., 1hr.

Figure 2.4. The synthetic scheme for Al(1)$_3$ and Al(2)$_3$.

2.3.2 . Structural and Isomeric Elucidation of Free Ligands and Their Aluminum Complexes

Alq$_3$ is made up of three ligands that are bound to the metal center through nitrogen and oxygen donors, giving the system an octahedral geometry. Aluminum(III) complexes can be

found in two possible isomeric forms: (1) a meridional isomer with C_1 symmetry or (2) the facial isomer with a C_3 symmetry. It has been reported that *mer*-Alq$_3$ is common due to its more thermodynamically stable nature compared to the facial isomer.[8] Nevertheless, it was crucial to determine the isomeric form of the two new aluminum compounds using NMR spectra. In the case of a facial isomer all three ligands on Al(III) complex would share the same chemical environment leading to one set of ^{1}H NMR peaks that would integrate to three times the number of protons on one ligand. Compared to a meridional system, where each ligand would have a distinct chemical environment leading to three sets of ^{1}H NMR peaks that would be representative of each individual ligand. As a result of the potentially complicated nature of the ^{1}H NMR spectra of Al(**1**)$_3$ and Al(**2**)$_3$, the spectra of **1** and **2** along with their proton assignments are presented in **Figure 2.5** and **Figure 2.7**, respectively.

Based on the three distinct peaks present in the ^{1}H NMR of Al(**1**)$_3$ and Al(**2**)$_3$, as well as structural elucidation from the COSY NMR spectra (**Figure 2.6** and **Figure 2.8**, respectively), it was determined that both complexes were in fact *mer*-isomers. Furthermore, the protons on positions 2-, 3-, and 6- experienced the greatest chemical shifts due to their proximity to the metal center, which is consistent with literature.[9] It should be noted that the structures accompanying the COSY NMR spectrum in **Figure 2.6** and **Figure 2.8** were obtained from DFT calculations, which will be discussed in further detail later in this chapter. The numbering scheme for the ligands in the Al(III) compounds in the peak assignments of the COSY NMR spectra are the same as that used in the peak assignments of the respective free ligands.
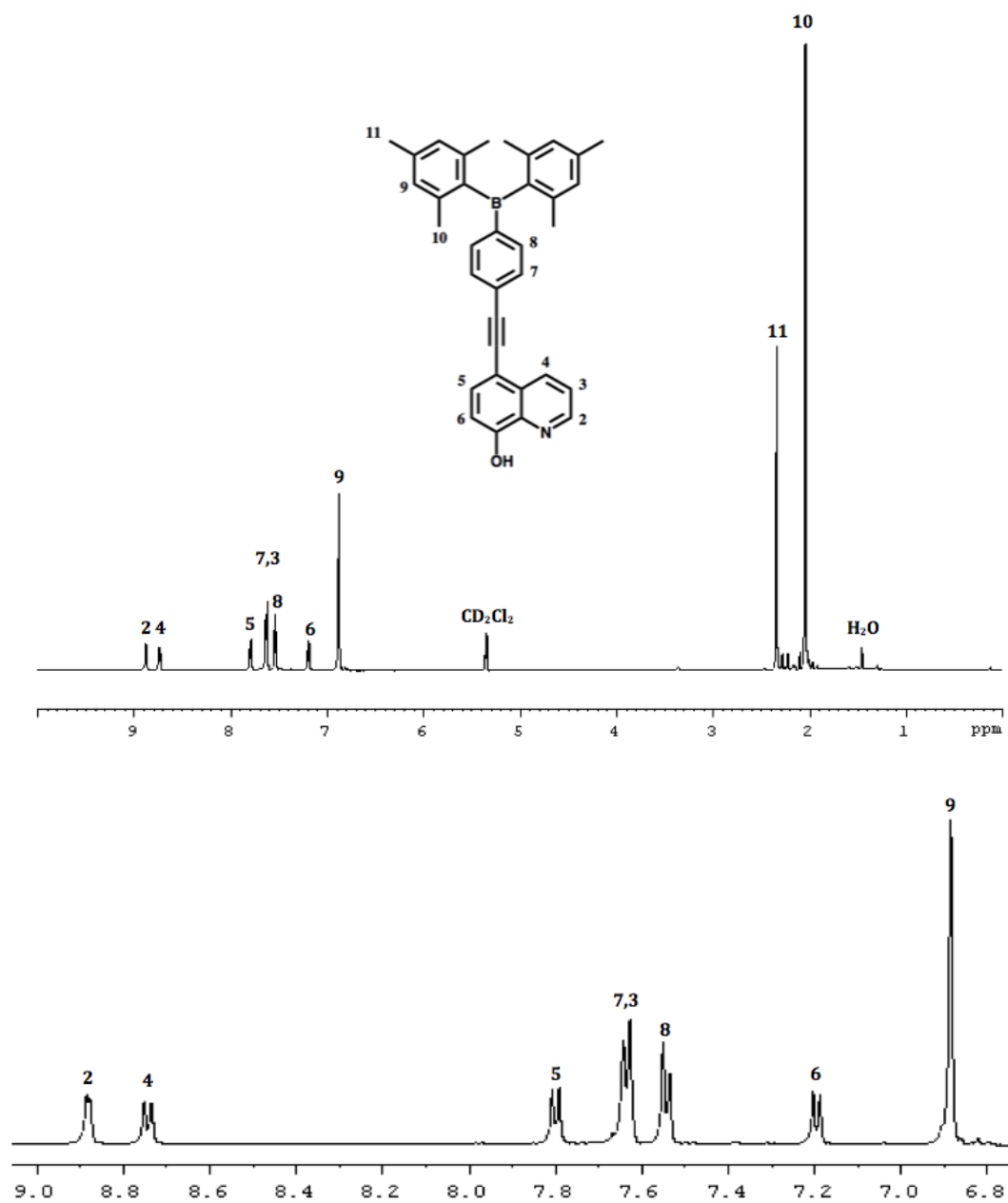
Figure 2.5. The ¹H NMR spectrum of 1 (top) and the aromatic region of the spectrum has been enlarged for clarity (bottom) (CD₂Cl₂, 25 ℃). Inset: The structure of 1 with numbering schemes.
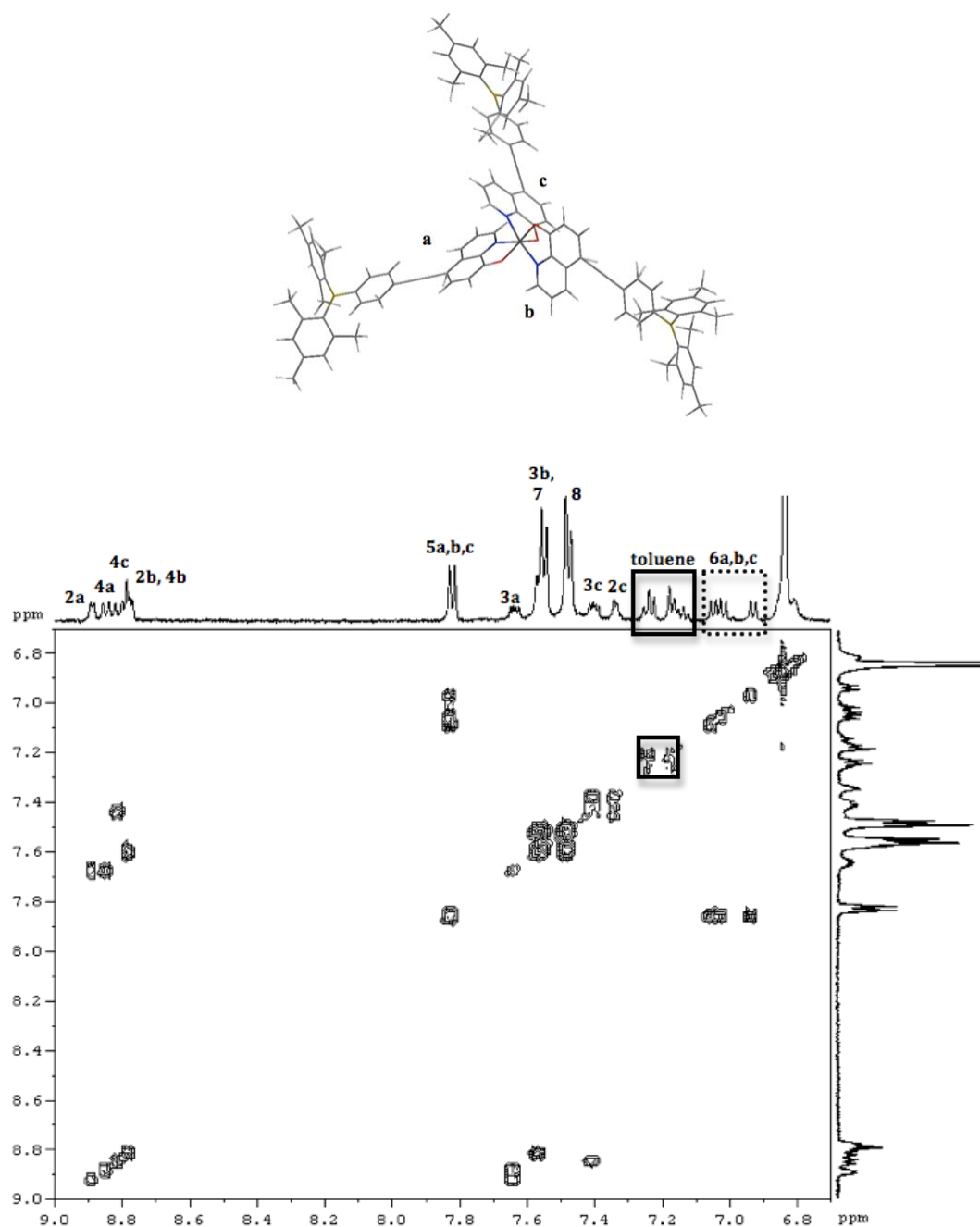
Figure 2.6. The structure of *mer*-Al(1)₃ with its three distinct ligands labeled as a-c (top) and the COSY NMR spectrum of *mer*-Al(1)₃ with peak assignments using the same numbering scheme as shown in figure 2.5 (bottom). For clarity, only the aromatic region (5.0-9.0 ppm) is presented.
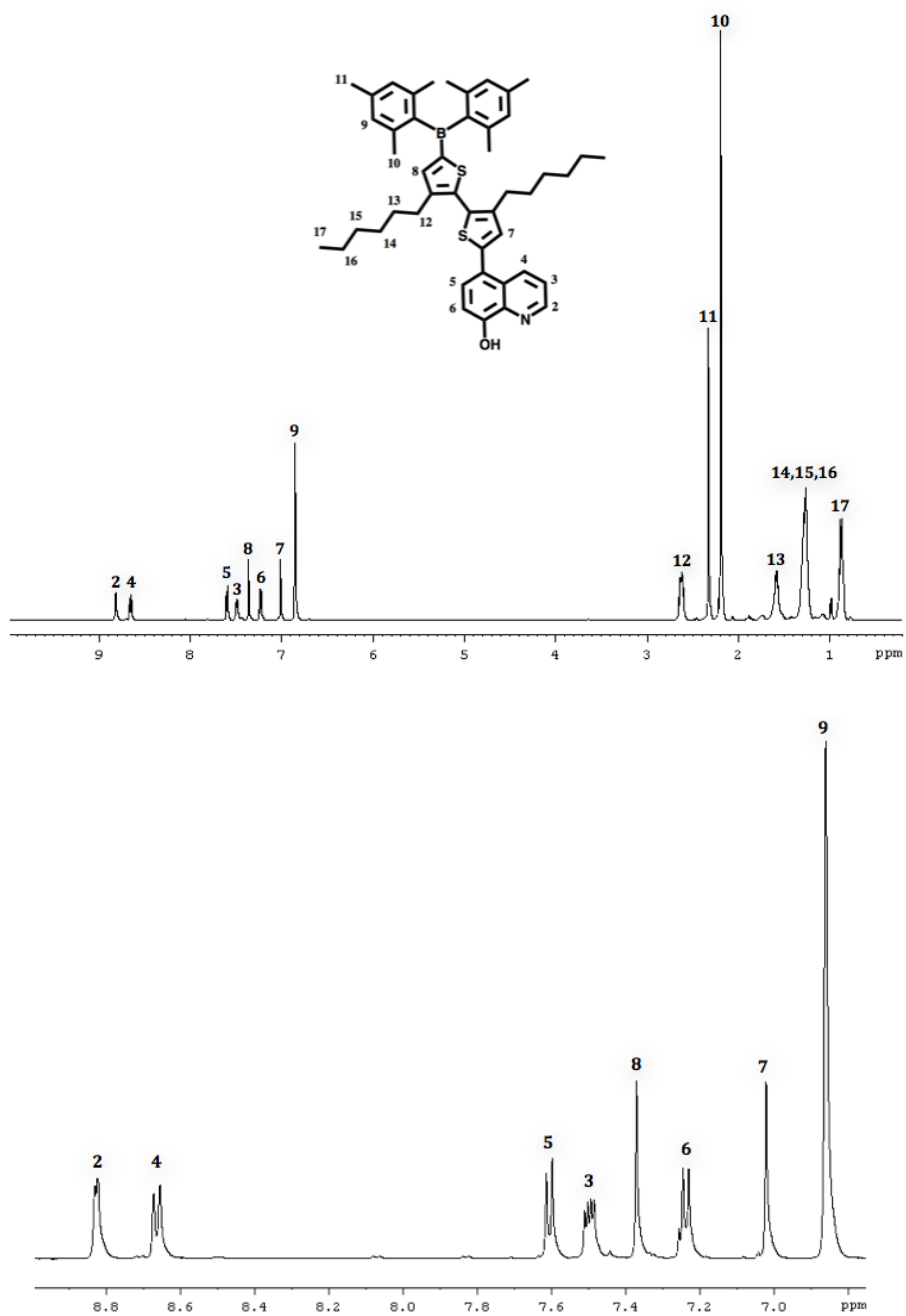
Figure 2.7. The ¹H NMR spectrum of 2 (top) and the aromatic region of the spectrum has been enlarged for clarity (bottom) (CD₂Cl₂, 25 °C). Inset: the structure of 2 with numbering schemes.
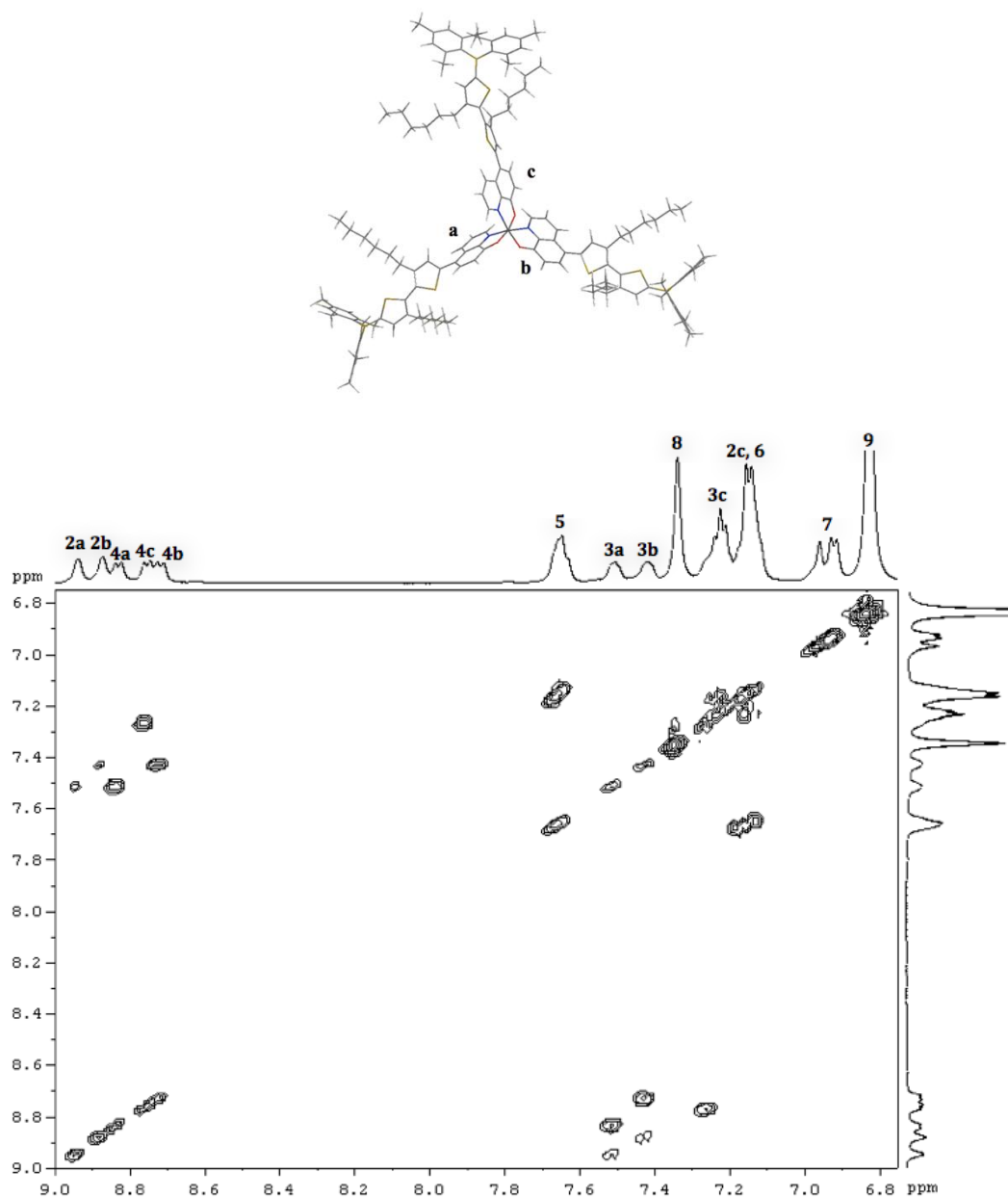
Figure 2.8. The structure of *mer*-Al(2)$_3$ with its three distinct ligands labeled a-c (top) and the COSY spectrum of *mer*-Al(2)$_3$ and peak assignments with the same numbering schemes as shown in Figure 2.7 (bottom). For clarity, only the aromatic region (6.75-9.0 ppm) is presented.

2.3.3 UV-Vis Absorption Spectra

The electronic properties of the free ligands and their respective Al(III) complexes were elucidated by UV-Vis absorption spectra. The absorption spectra of the free ligands are presented in **Figure 2.9**. There is considerable overlap in the absorption range between the two free ligands. The free ligands both exhibit an absorption band at ~250 nm from a π-π* transition within the 8-hydroxyquinoline ligand. On the other hand the absorption band at ~360 nm is attributed to a π-π* transition that involves the triarylboron center. It should be noted that the absorption of **2** is both stronger and slightly red-shifted, compared to **1,** due to its extended π-system.

The UV-Vis absorption spectra of Al(**1**)$_3$ and Al(**2**)$_3$ are plotted alongside Alq$_3$ for comparison (**Figure 2.10**). Due to the extended π-skeleton of the two new systems and the presence of the boron center, the absorption profiles of Al(**1**)$_3$ and Al(**2**)$_3$ are much stronger and extend over a wider absorption range than Alq$_3$. As was discussed in the previous section, the ligands bound to the aluminum center are non-degenerate, which leads to three non-degenerate highest HOMOs and lowest LUMOs. More importantly, two of the ligands, bound weakly to the aluminum center, have HOMO and LUMO energy levels that are quite similar compared to the third ligand which is more strongly bound to the Al(III) center (a concept that will elaborated later in the chapter). Therefore, it would be anticipated that there would be one strong absorption peak that is a combination of a π-π* transition from the two 8-hydroxyquinoline ligands with the weaker covalent bond to the aluminum center and small absorption band from the π-π* transition originating on the third ligand. This was supported by the UV-Vis spectra obtained for the aluminum complexes. The absorption band at ~260 nm is a result of a combined π-π* transition from two of the 8-hydroxyquinoline ligands while the peak at ~370 nm is a result of π-π* transition within the third ligand. Similarly, the peaks at ~266 nm for the two new complexes

were also a result of LC transitions within two of the 8-hydroxyquinoline ligands. The stronger absorption profile of Al($\textbf{1}$)$_3$ and Al($\textbf{2}$)$_3$ in the 280-460 nm region compared to Alq$_3$ is a result of the new chromophores attached to the 5-position of 8-hydroxyquinoline. The absorption properties of these attachments mask the weaker absorption band attributed to the LC π-π* transition from the third 8-hydroxyquinoline ligand. Similar to the free ligands, the absorption profile of Al($\textbf{2}$)$_3$ is slightly red-shifted compared to the other two aluminum complexes. Furthermore, it is evident that the Al($\textbf{1}$)$_3$ exhibits more intense absorption properties than either of the other two systems. The order of decreasing efficiency in absorption of photons is as follows: Al($\textbf{1}$)$_3$>Al($\textbf{2}$)$_3$>Alq$_3$.
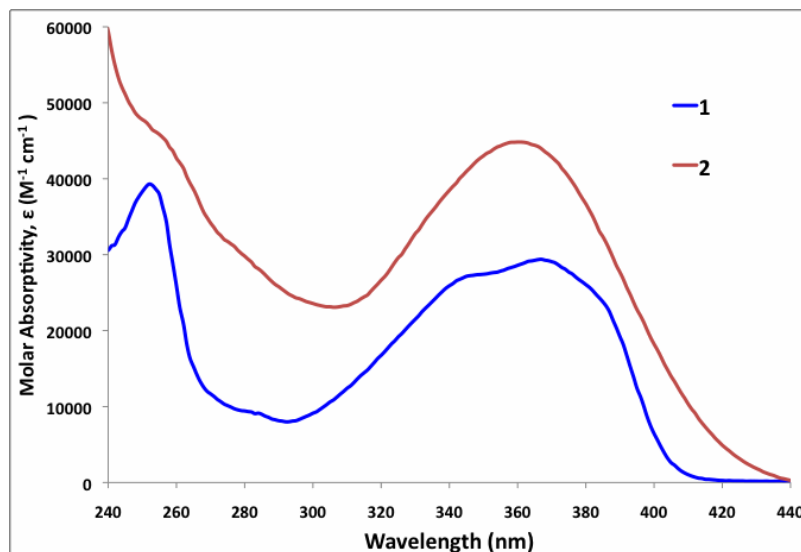
Figure 2.9. UV-Vis absorption spectra of ligands 1 and 2, recorded in CH$_2$Cl$_2$.

74
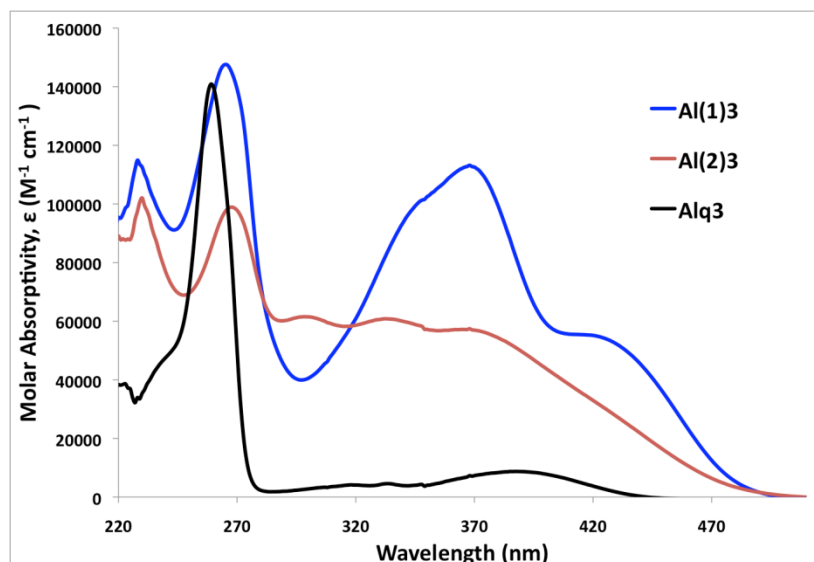
Figure 2.10. UV-Vis absorption spectra of Al(1)$_3$, Al(2)$_3$ and Alq$_3$, recorded in CH$_2$Cl$_2$.

2.3.4 Luminescence

The luminescent properties of the free ligands were studied using fluorescent spectroscopy. For the purpose of illustrating the difference in Stokes' shifts between the two free ligands, both the excitation and emission peaks will be displayed in **Figure 2.11**. A smaller Stokes' Shift for **1** can be attributed to the molecule's rigidity, which reduces the number of vibrational states available, compared to **2** with its two flexible hexyl-chains on the bisthiophene linker. Under UV irradiation the luminescence of the free ligands in solid state and in solution (CH$_2$Cl$_2$) for both **1** (λ_{max} = 413 nm and $\Phi_{solution/solid}$ = <0.1%/0.3%) and **2** (λ_{max} = 480 nm and $\Phi_{solution/solid}$ = 0.56%/<0.1%) were barely visible due to the phenolic proton, which has been demonstrated to quench fluorescence via excited-state proton transfer.[10]

75
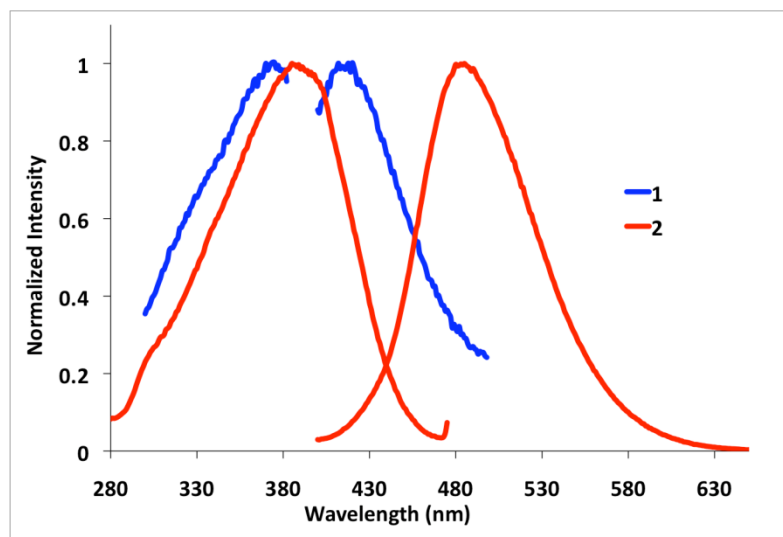
Figure 2.11. The normalized excitation and emission spectra of 1 and 2 (1.0 x 10^{-5} M) in CH$_2$Cl$_2$ at room temperature.

Under UV irradiation the colors of Alq$_3$, Al(**1**)$_3$ and Al(**2**)$_3$ were green, yellow and orange, respectively, in solution (CH$_2$Cl$_2$) and solid state (**Figure 2.12**). The red-shifting of the emission peaks for the two new complexes compared to Alq$_3$ is consistent with the effects of adding an EDG on the 5-position of the quinoline ligand, which was discussed in the first chapter. Furthermore, the empty p$_z$ orbital on boron center will lower the LUMO level contributing further to the narrowing of the bandgap.[11] The larger π-system of Al(**2**)$_3$ elevates its HOMO energy level more significantly than the other two aluminum complexes resulting in both a smaller band gap and thus the most red-shifted emission. Unfortunately, the quantum yield of Alq$_3$ (Φ_{solid} = 0.14) was substantially higher than both Al(**1**)$_3$ (Φ_{solid} = 0.06) and Al(**2**)$_3$ (Φ_{solid} = 0.02). A lower quantum yield for Al(**2**)$_3$ can be attributed to the presence of the hexyl chains which reduce the

rigidity of the complex and thus contribute to an increased number of pathways for non-radiative decay. A summary of the absorption and luminescent properties are presented in **Table 2.1**.
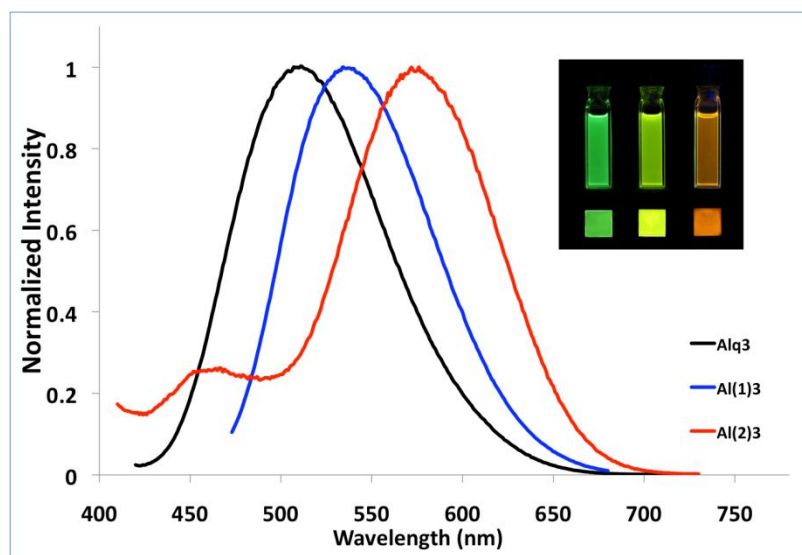
Figure 2.12. The normalized emission spectra of the aluminum complexes. Inset: A photograph of the fluorescence of Alq$_3$, Al(1)$_3$ and Al(2)$_3$ in CH$_2$Cl$_2$ (1.0 x 10^{-5} M) and as a film.

Table 2.1. Absorption and luminescent properties of the free ligands and their respective aluminum complexes.

Compound	λ_{abs}/nm (log ε/M^{-1} cm^{-1})	$\lambda_{em}{}^a$/nm	Φ Soln^b/Solid^c
1	254 (4.59), 368 (4.47)	413	<0.001/0.003
2	363 (4.65)	480	0.0056/<0.0001
Alq$_3$	260 (5.15), 393 (3.93)	507	0.12/0.14
Al(**1**)$_3$	266 (5.17), 370 (5.05), 427 (4.73)	533	0.10/0.06
Al(**2**)$_3$	270 (4.99), 337 (4.78), 373 (4.75), 430 (4.44)	570	0.01/0.02

^{a} In CH$_2$Cl$_2$ at 1.0 x 10^{-5} M. ^{b} Relative to Alq$_3$ = 0.12[12]. ^{c} Measured using an integration sphere.

Interestingly, Alq$_3$ and Al(**2**)$_3$ have a strong quantum yields in the solid state, while Al(**1**)$_3$ has a better quantum yield in solution. It is likely that in the solid state there is a higher degree of intermolecular stacking due to the high degree of planarity in **1**, which leads to self-quenching, a drawback that was discussed in greater detail in the first chapter.

2.3.5 Electrochemical Properties

Cyclic voltammetry measurements were all done in dry DMF with NBu$_4$PF$_6$ as the electrolyte, using scan rates of 200-500 mV/s.

The reduction peaks of the free ligands are presented in **Figure 2.13** and summarized in **Table 2.2**. The first reduction potential of **1** is observed at -2.22 V (vs FeCp$_2^{0/+}$), which is believed to be from the quinoline moiety. While the reduction peak from the quinoline moiety on **2** was slightly more negative at -2.27 V (vs FeCp$_2^{0/+}$). Ligand **2** had a second peak at ~2.42 V likely from the boron center, an observation that is similar to other triarylboron systems.[13] A possible explanation for the more positive reduction potential of **1** is that the electron-accepting properties of the boron center have a larger effect on the system due its shorter and highly conjugated π-skeleton. In the case of **2**, the extended length as well as the fact that the two-hexyl chains force the thiophene rings to take a staggered conformation to ease steric hindrance diminishes the overall π-conjugation of the ligand and thus reducing the effects of the boron moiety on the rest of the system. All of the systems are weakly reversible, with the boron center demonstrating any significant reversibility.
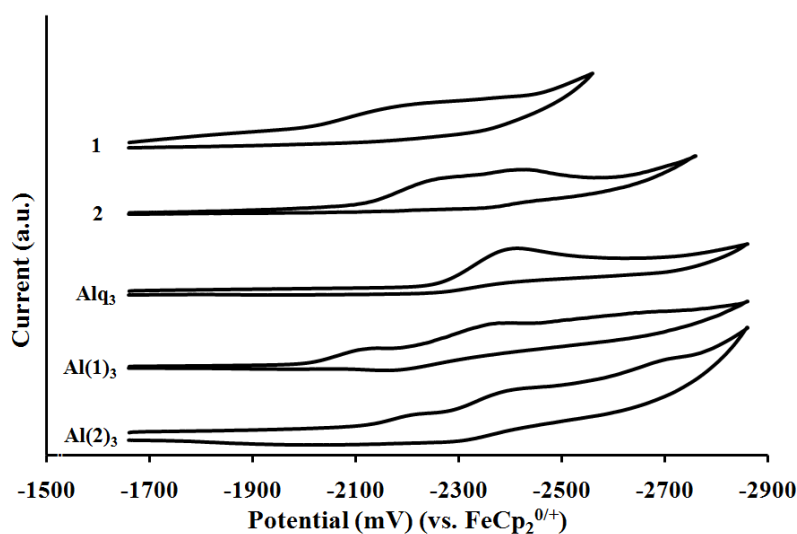
Figure 2.13. The CV diagrams of the Alq3, the free ligands and their respective aluminum complexes recorded in DMF.

Table 2.2. The Reduction Potentials of the Free Ligands and their Respective Aluminum complexes.

Compounds	1	2	Alq$_3$	Al(**1**)$_3$	Al(**2**)$_3$
$E_{1/2}^{red}$/V	-2.22	-2.27	-2.40	-2.11	-2.22

The reduction potential of Al(**1**)$_3$ and Al(**2**)$_3$ were -2.11 mV and -2.22 mV, respectively, which are more positive than Alq$_3$ with its reduction potential of -2.40 mV (vs. FeCp$_2^{0/+}$). This emphasizes the contribution of the triarylboron moiety on the electron accepting abilities of the two new aluminum complexes. The explanation for the more positive reduction potentials of Al(**1**)$_3$ compared to Al(**2**)$_3$ follows the argument made above for the respective free ligands.

As was discussed in the first chapter, promising ETM candidates must have a low-lying LUMO to facilitate charge injection, facilitate charge mobility towards the EML as well as a HOMO that is low enough to block holes from leaking out of the emitting layer. Although Al(**1**)$_3$ and Al(**2**)$_3$ have lower LUMOs than Alq$_3$ making them both promising candidates, Al(**2**)$_3$ has the highest HOMO energy level making it undesirable (**Figure 2.14**). In fact Al(**1**)$_3$ is the most promising ETM candidate to replace Alq$_3$ with its low HOMO and LUMO. It should be noted that the HOMOs and LUMOs were calculated using the UV-Vis data and the CV measurements, respectively. A summary of the HOMOs and LUMOs of the various systems are presented in **Table 2.3**. Comparisons between these experimental values and the DFT calculated values will be made in the following section. It should be noted that the reduction peaks are not reversible likely bringing into question the electro-stability of these materials. Further investigations are required.
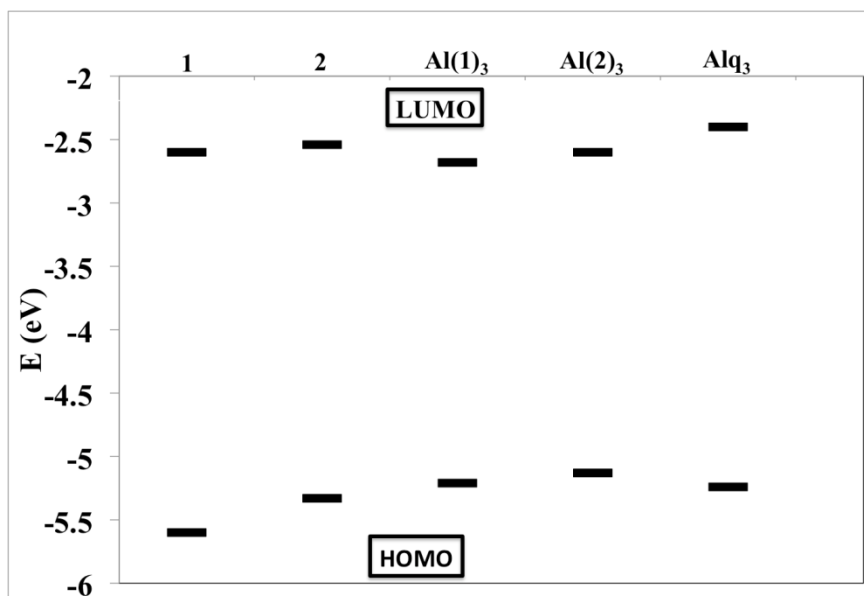
Figure 2.14. The HOMO and LUMO energy levels of Alq3, the free ligands and their respective aluminum complexes, estimated from CV and UV-Vis data.

Table 2.3. Experimentally Determined HOMOs and LUMOs.

Experimental Energy (eV)			
Compound	HOMO^a	LUMO^b	Band Gap^c
1	-5.60	-2.60	3.00
2	-5.33	-2.54	2.79
Alq$_3$	-5.24	-2.40	2.34
Al(1)$_3$	-5.21	-2.68	2.53
Al(2)$_3$	-5.13	-2.60	2.53

^{a}Obtained from the calculated LUMO level and the HOMO-LUMO band gap. ^{b} From reduction values in DMF. ^{c} Using the band edge of the UV-Vis spectra.

2.3.6 Molecular Orbitals

DFT calculations were conducted on the aluminum complexes in order to better understand their electronic transitions. The results of the calculations for Al(**1**)$_3$ and Al(**2**)$_3$ are presented in **Figure 2.15** and **Figure 2.16**, respectively. Similar to Alq$_3$, the HOMOs and LUMOs of the two new complexes were located predominantly on the phenoxide ring and the pyridyl ring, respectively.[14] In addition, due to its low-lying empty p$_z$-orbital, the boron center also made a large contribution to the LUMOs.[11] With the aluminum complexes having a *mer-* octahedral geometry, the three ligands are nondenegerate, resulting in each of the individual ligands making up one of the three highest HOMOs and three lowest LUMOs.[9]

HOMO

LUMO+2

HOMO-1

LUMO+1

HOMO-2
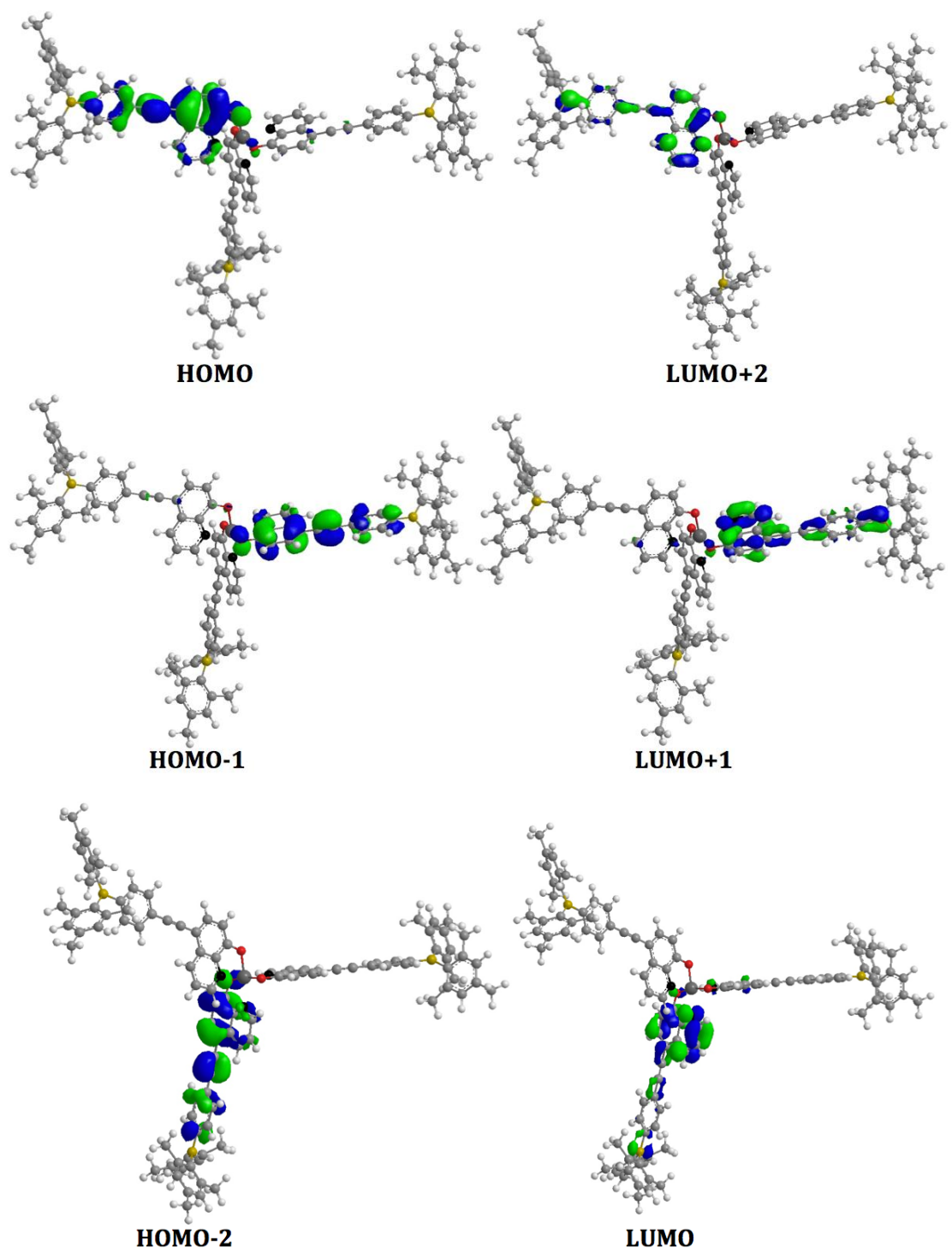
LUMO

Figure 2.15. The molecular orbitals of Al(1)₃.
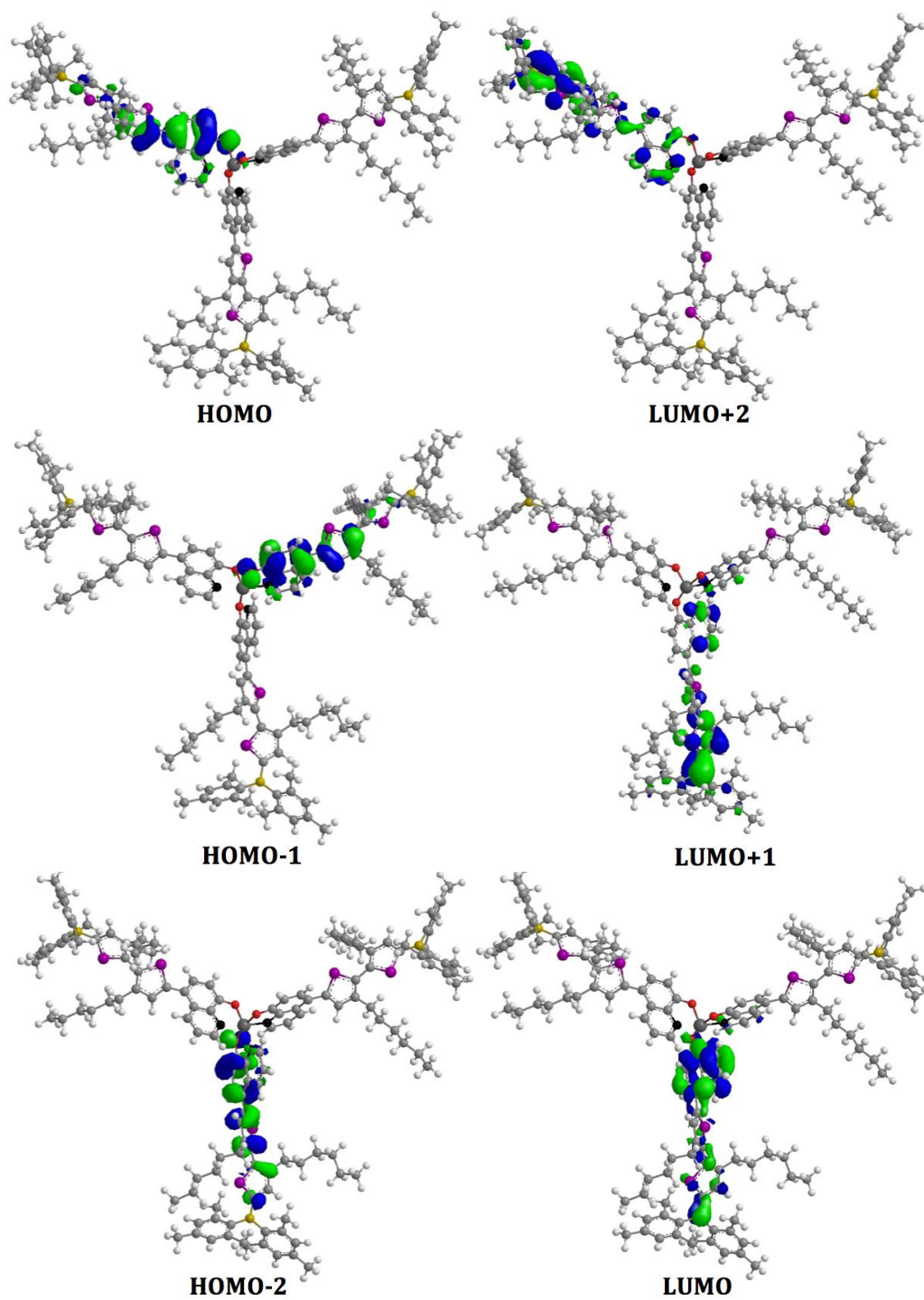
Figure 2.16. The frontier molecular orbitals of Al(2)₃.

The values of the energy levels for the HOMOs and LUMOs of Al($\mathbf{1}$)$_3$ and Al($\mathbf{2}$)$_3$ are presented in **Table 2.4**. Although the ligands are nondegenerate, they are identical leading to the expectation that the difference in energy between the three highest HOMOs, for example, would be equal in magnitude. Interestingly this was not the case, as the differences between the HOMO and HOMO-1 levels and the HOMO-1 and HOMO-2 levels of Alq$_3$ were found to be ~0.30 eV and ~0.15 eV, respectively.[9] A possible explanation for this phenomenon is a result of one of the three ligands having a stronger electrostatic attraction to the metal center.[9] On the other hand the differences between the highest HOMOs of the new complexes were much smaller with the values being 0.15 eV and 0.10 eV for Al($\mathbf{1}$)$_3$ and 0.21 eV and -0.11 eV for Al($\mathbf{2}$)$_3$. This is likely due to the fact that the HOMOs and LUMOs are spread out over an extended π-skeleton limiting the effects from the interaction between the 8-hydroxyquinoline moiety and the metal center. A similar trend applies to the LUMO energy levels.

Table 2.4. The energy levels of the HOMOs and LUMOs of Al($\mathbf{1}$)$_3$ and Al($\mathbf{2}$)$_3$ calculated using DFT.

[a]Calculated Energy Levels (eV)						
Compounds	LUMO+2	LUMO+1	LUMO	HOMO	HOMO-1	HOMO-2
Al($\mathbf{1}$)$_3$	-2.00	-2.09	-2.24	-5.06	-5.21	-5.31
Al($\mathbf{2}$)$_3$	-1.97	-2.04	-2.18	-5.05	-5.26	-5.37

[a] Obtained at the B3LYP/6-31G* level of theory.

2.3.7 Lewis Acidity: Properties

All fluoride and cyanide titrations were conducted in dry methylene chloride using TBAF as the fluoride source and tetraethylammonium cyanide as the cyanide source. Furthermore, the concentration of the free ligands in solution was 1.0×10^{-5} M in each case.

2.3.7.1 Properties of Free Ligands as Anion Sensors

2.3.7.1.1 UV-Vis spectral titration of the Free Ligands by Fluoride ions

Titration of **1** with TBAF yielded a distinct UV-Vis spectral change (**Figure 2.17**). The absorbance peaks at 253 nm, 347 nm and 368 nm showed a general increase in absorbance between 0-1.5 eq of fluoride, followed by a decrease between 1.5-3.0 eq. On the other hand the peak at 290 nm and the broad peak in the 411-490 nm region increased in absorbance intensity. Interestingly, although there was a single boron site on **1**, more than 3 equivalents of fluoride was required to reach saturation. Similarly an excess of TBAF, 9 equivalents, was required for the titration of **2** (**Figure 2.18**). In both systems the peak centered at ~370 nm, attributed to the π-p_π* transition centered on the triarylboron moiety, diminished in intensity. The rise of a low energy band at 400-500 nm region for **1** may be attributed to the hydroxyquinoline anion. The same low energy band is not apparent for **2** due to the presence of a broad shoulder band in the same region. A possible explanation for the unusual spectral changes could be attributed to binding of the fluoride ion to both the boron center and the hydroxyl proton of the hydroxyquinoline ligand (**Figure 2.19).** A qualitative analysis of the binding events will be addressed in the fluorescence section using the Stern-Volmer plot.
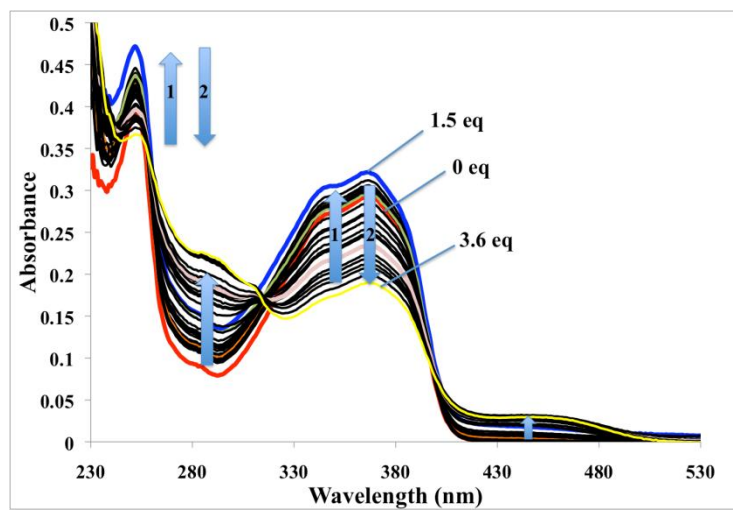
Figure 2.17. UV-Vis titration spectrum of **1** using TBAF (1.0×10^{-5} M in dry CH_2Cl_2).
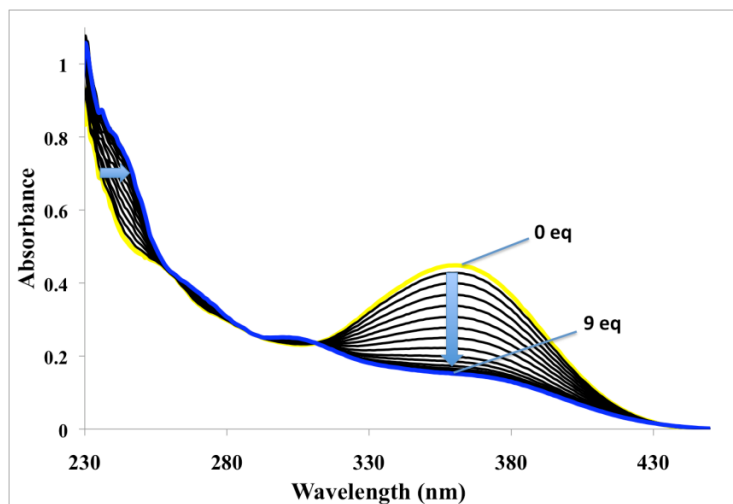
Figure 2.18. UV-Vis titration spectrum of **2** using TBAF in CH_2Cl_2 (1.0×10^{-5} M).
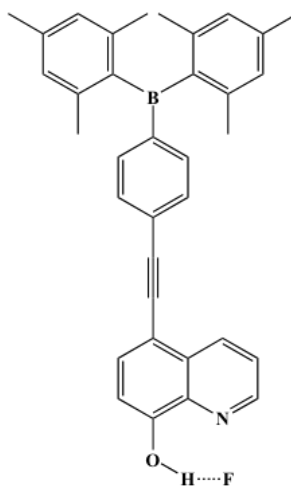
Figure 2.19. Example of H-bonding between 1 and fluoride anion.

2.3.7.1.2 UV-Vis spectral titration of Free Ligands by Cyanide

The UV-Vis absorption titration spectra of **1** and **2** with NEt$_4$CN were less complicating than the TBAF titrations. Approximately 2 equivalents of CN$^-$ was required during the titration of **1** (**Figure 2.20**) and ~7 equivalents of CN$^-$ for **2** (**Figure 2.21**) to reach saturation, likely a result of the fewer binding events. Based on the pK$_a$ of HF (3.14) and HCN (9.22), the cyanide anion is a stronger base and therefore anticipated to have a stronger binding interaction with the boron center.[15] Similar to the fluoride titration, upon saturation of both complexes the peak at ~360 nm diminished as a result of the inhibition of the π to p$_\pi$* transition involving the triarylboron moiety. In the case of compound **1**, a new π-π* transition emerged leading to the peak at ~280 nm. On another note, the UV-Vis titration spectrum of **1** and **2** had an isobestic point at 310 nm and 320 nm, respectively. This indicates that the titration is neat proceeding from the starting material to the final product.
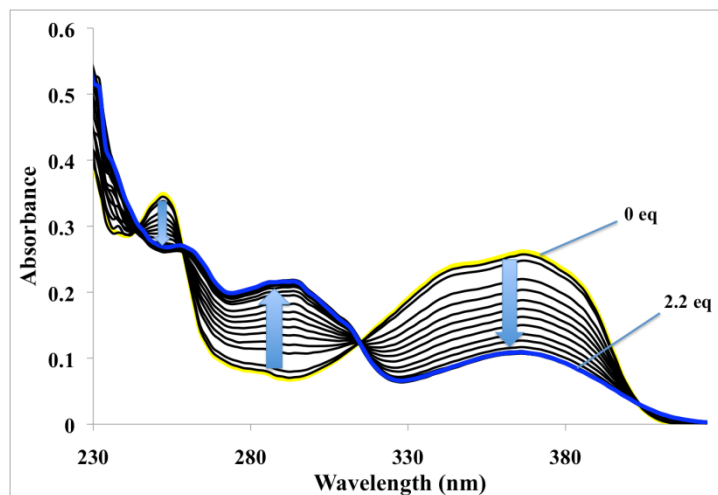
Figure 2.20. UV-Vis titration spectrum of 1 with NEt$_4$CN in CH$_2$Cl$_2$ (1.0 x 10^{-5} M).
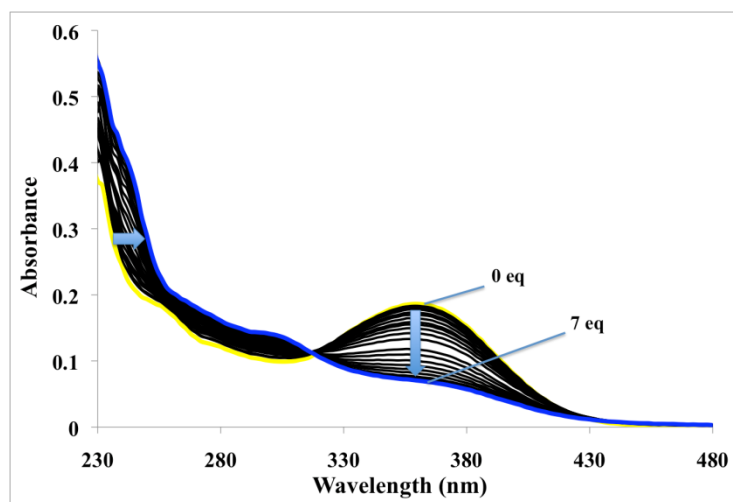
Figure 2.21. UV-Vis titration spectrum of 2 with NEt$_4$CN in CH$_2$Cl$_2$ (1.0 x 10^{-5} M).

2.3.7.1.3 Fluorescence titration of the Free Ligands by Fluoride

A general red-shifting in the emission spectrum of **1** was observed as the concentration of F$^-$ increased and saturation was reached at ~3.5 eq. (**Figure 2.22**). It is also worth noting that although the emission peak at 408 nm fluctuated, there was an overall decrease in its intensity. The new low energy emission peak appeared at ~550 nm with the addition of fluoride, which can be attributed to the hydroxyquinoline anion due to its similarity to the Alq$_3$ emission peak. Based on the Stern-Volmer plot presented in **Figure 2.24** (λ_{max} = 408 nm) it is evident that the binding between the fluoride anion and the boron compound is complex, which can be attributed to binding to both boron and the proton. This would explain the fluctuations observed in the UV-Vis absorption and fluorescence spectra as well as the need for more than 1 equivalent of TBAF to reach saturation. Meanwhile for **2**, upon saturation with ~9 equivalents of the fluoride anion the emission peak at 480 nm was almost completely quenched (**Figure 2.23**). Based on the number of equivalents required to reach saturation it would appear **1** has a stronger affinity to the fluoride anion than **2**, though it is difficult to make this conclusion since there may be other processes going on which are essentially sacrificing some of the fluoride anions. According to the Stern-Volmer plot of **1** it would appear that there are two different binding events, as there is an increase in the I/I$_o$ ratio from 0-1 eq. of fluoride, followed by a decrease onward. This may perhaps be a result of H-bonding with the fluoride, which subsequently reduces the hydrogen proton transfer and thus increase the fluorescence characteristics. On the other hand the Stern-Volmer plot of **2** shows a single binding event represented by a continuous downward slope data line.

90
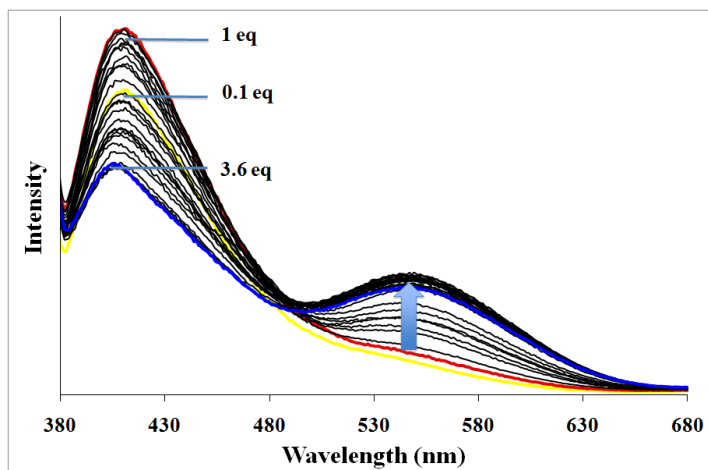
Figure 2.22. Fluorescent titration spectrum of 1 with TBAF in CH_2Cl_2 (1.0 x 10^{-5} M).
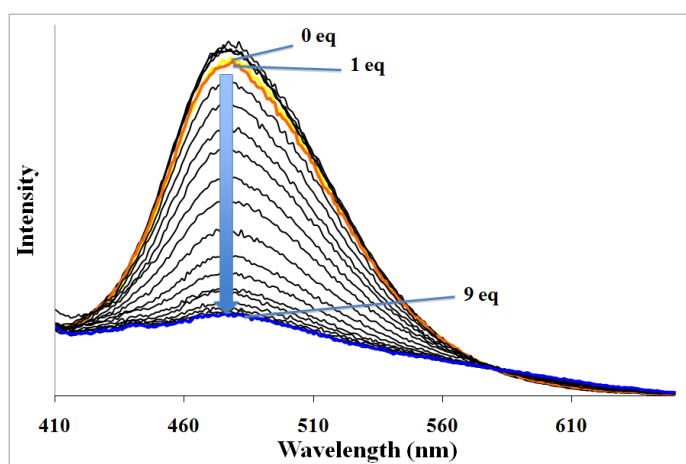
Figure 2.23. Fluorescent titration spectrum of 2 with TBAF in CH_2Cl_2 (1.0 x 10^{-5} M).
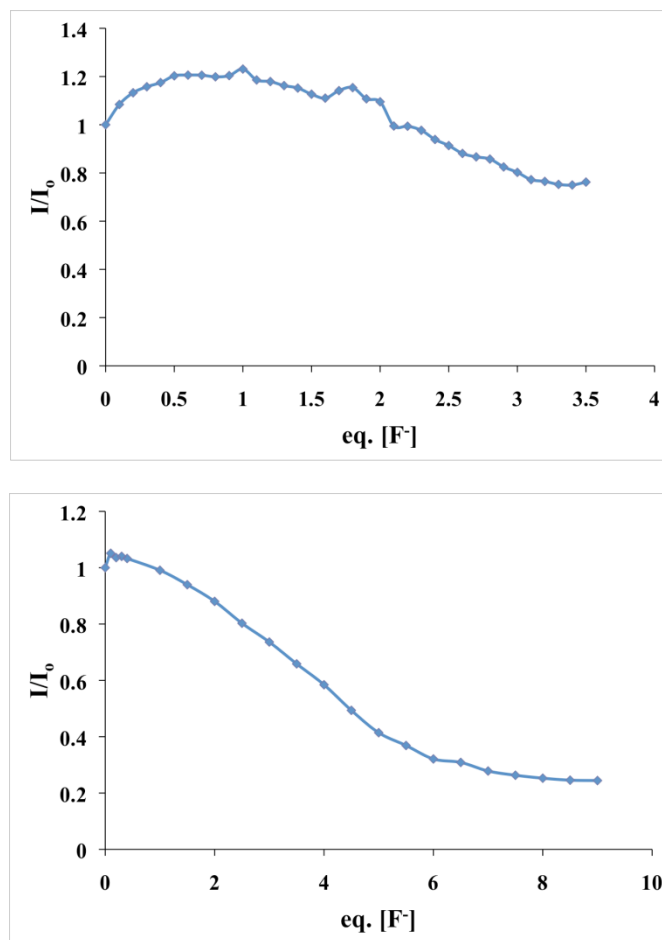
Figure 2.24. The Stern-Volmer plots of 1 using $\lambda_{max} = 408$ nm (top) and of 2 using $\lambda_{max} = 480$ nm (bottom) from fluorescence.

2.3.7.1.4 Fluorescence titration of the Free Ligands by Cyanide

There was a general red-shifting in the emission spectrum of **1** during the course of the CN⁻ titration (**Figure 2.25**). Presumably with CN⁻ binding to the boron center, the high energy CT was inhibited yielding an alternate π^*-π transition. This is evident by the quenching of the emission

peak at 405 nm and the subsequent increase in intensity of the peak at 450 nm. Similar to the titrations using F$^-$ anion, more than 1 equivalent was required to reach saturation (~2.2 eq). As was predicted based on the UV-Vis titration spectra, the Stern-Volmer plot suggests a relatively weak binding constant between the CN$^-$ anion and the boron center (**Figure 2.27**).

On the other hand compound **2** has an emission peak that abruptly blue-shifts by ~10 nm, from 474 nm to 464 nm, between 0.8 and 1.0 equivalents of CN$^-$ (**Figure 2.26**). An explanation for this phenomenon is difficult to address, but may be a result of the interaction between the anion and the proton on the hydroxy group of the quinoline ligand mentioned earlier. Subsequently, upon saturation the peak at 464 nm was quenched.

The spectral change of **1** appears to be two-step, first quenching of the peak at 405 nm with a clear isobestic point, then the rise of the peak at 450 nm, which may be attributed to the two step binding of boron and proton, respectively. This isobestic point is important as it indicates that the titration is neat and proceeds from a starting material to a final product. This is supported by the Stern-Volmer plot of **1** with its direction break in the trendline. There is a downwad slope between 0 to ~1.3 eq. followed by an upward slope between ~1.3 to 2.2 eq, indicating two different binding events. The same may be said for **2**.

There appears to be a fluorescence turn-on phenomenon of **1** by for both fluoride and cyanide. As such, it may be useful for practical sensing.
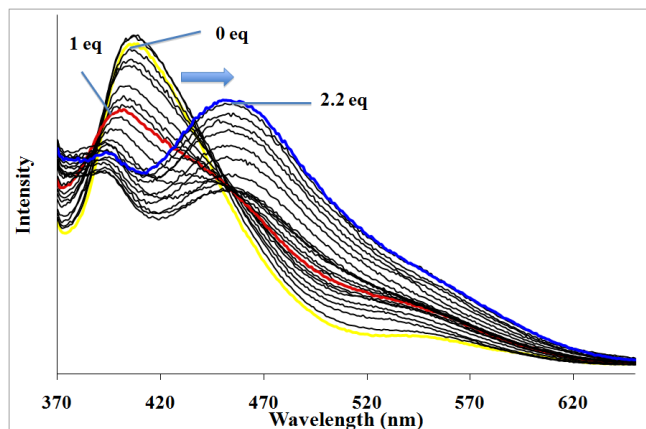
Figure 2.25. The fluorescent titration spectrum of 1 with NEt$_4$CN in CH$_2$Cl$_2$ (1.0 x 10^{-5} M).
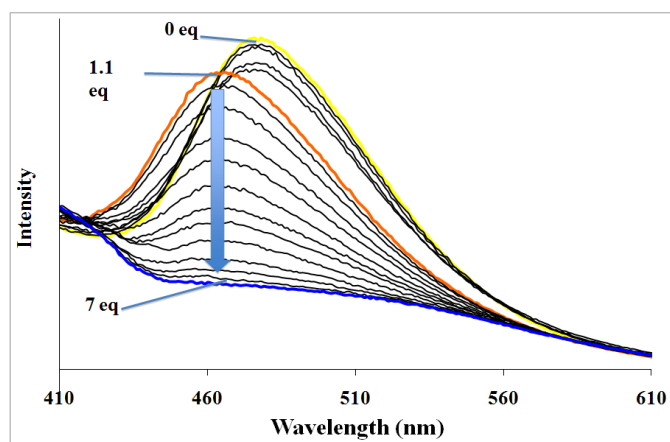
Figure 2.26. The fluorescent titration spectrum of 2 with NEt$_4$CN in CH$_2$Cl$_2$ (1.0 x 10^{-5} M).
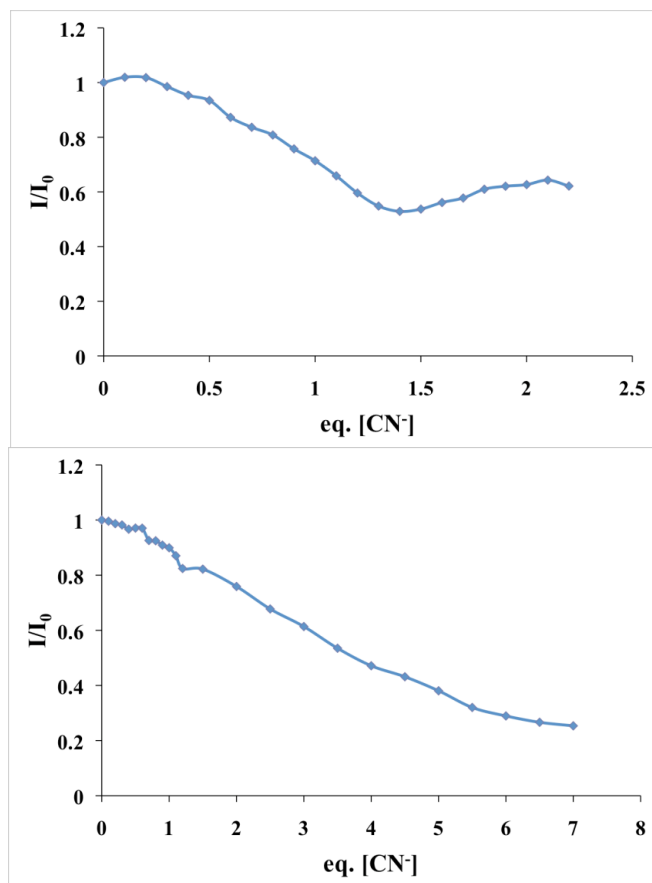
Figure 2.27. The Stern-Volmer plots of 1 using λ_{max} = 405 nm (top) and of 2 using λ_{max} = 474 nm (bottom) from fluorescence.

2.3.7.2 Properties of Al(III) Complexes as Anion Sensors

2.3.7.2.1 UV-Vis spectral titration of Aluminum Complexes by Fluoride

Under the assumption of a relatively strong binding constant between the anion and the ligands it would be expected that due to three ligands around the aluminum center of an Alq$_3$

derivative ~3 eq. of TBAF would be required to reach saturation. This is however not the case with either Al($\mathbf{1}$)$_3$ or Al($\mathbf{2}$)$_3$ which required 6.9 eq. and 18 eq. of TBAF, respectively, indicating either very weak binding interactions or other binding events. The cause of these results will be discussed in greater detail later in the chapter. As illustrated in **Figure 2.28**, the absorbance profile of Al($\mathbf{1}$)$_3$ was blue-shifted during the course of the titration with TBAF. The peak at 370 nm and its shoulder at 425 nm were both quenched as a result of the binding of the fluoride anion to the empty p_π orbital of the boron center. Simultaneously a new peak at 311 nm emerged due to a new π-π* pathway within the system, which excludes the boron center. Similarly, the absorbance characteristics of Al($\mathbf{2}$)$_3$ were blue-shifted with the peaks at 303 nm, 338 nm and 370 nm diminishing while a new peak emerged at 316 nm during the course of the titration (**Figure 2.29**). Interestingly, all three aluminum complexes shared a peak at ~270 nm believed to be from a π-π* transition within the q ligand. Similar to the UV-Vis spectra obtained for the free ligands, the peak at ~370 nm for both compounds is due to a π to p_π* transition involving the triarylboron moiety. It is also of importance to mention that only Al($\mathbf{1}$)$_3$ had an isobestic point which was at ~333 nm. The presence of an isobestic point indicates that upon titration the starting material is converted to a single final product, with the fluoride bound to the three-coordinate boron center.
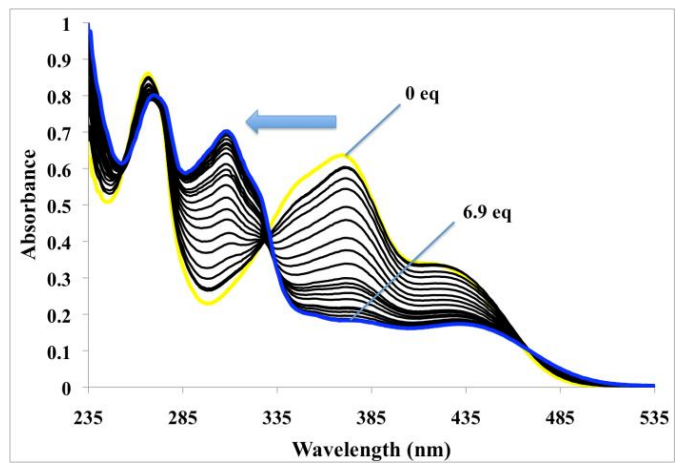
Figure 2.28. UV-Vis titration spectrum of Al(1)$_3$ with TBAF in CH$_2$Cl$_2$ (1.0 x 10^{-5} M).
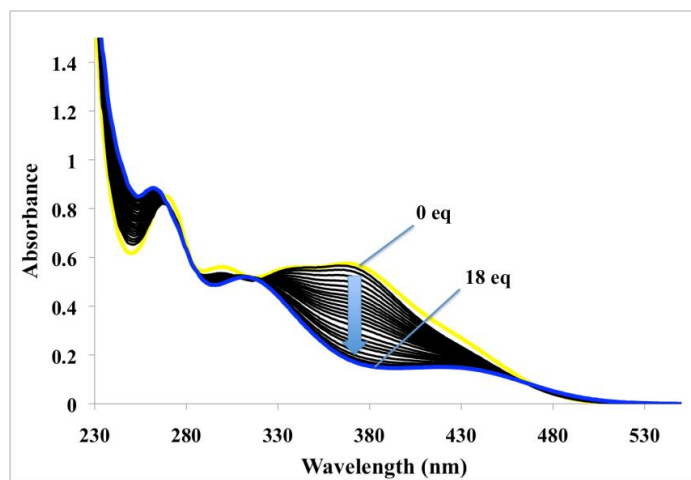
Figure 2.29. UV-Vis titration spectrum of Al(2)$_3$ with TBAF in CH$_2$Cl$_2$ (1.0 x 10^{-5} M).

2.3.7.2.2 UV-Vis spectral titration of Aluminum Complexes by Cyanide

The UV-Vis absorbance spectra of Al($\mathbf{1}$)$_3$ and Al($\mathbf{2}$)$_3$ during the course of the cyanide titrations are presented in **Figure 2.30** and **Figure 2.31**, respectively. In comparison to the fluoride titrations, approximately half the amount of cyanide was needed to reach saturation, 4.5 eq. and 9 eq. for Al($\mathbf{1}$)$_3$ and Al($\mathbf{2}$)$_3$, respectively. In addition, the changes to the absorbance profiles of the two complexes were identical to those observed during the titrations using fluoride, including the isobestic point at ~333 nm for Al($\mathbf{1}$)$_3$, indicating a the progress from a single starting material to a single final product. These results would indicate that there is a stronger interaction between the boron center and cyanide. A discussion of the changes to the π-π* transitions would be similar to those outlined in the previous section.
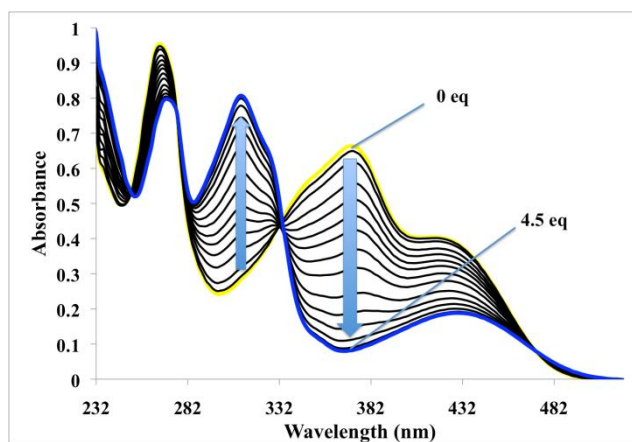
Figure 2.30. UV-Vis titration spectrum of Al(1)$_3$ with NEt$_4$CN in CH$_2$Cl$_2$ (1.0 x 10^{-5} M).
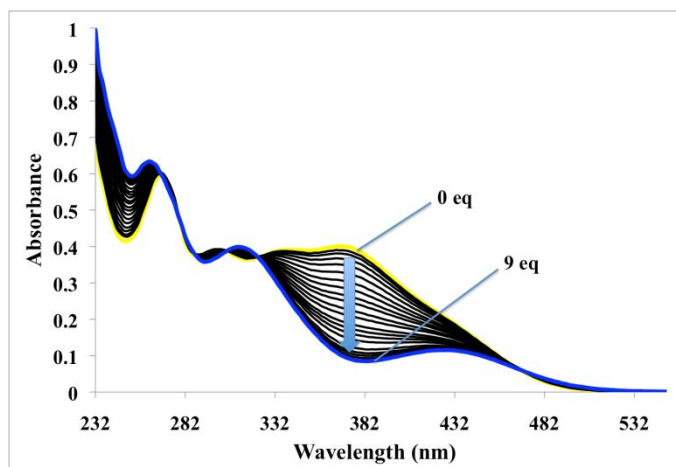
Figure 2.31. UV-Vis titration spectrum of Al(2)$_3$ with NEt$_4$CN in CH$_2$Cl$_2$ (1.0 x 10^{-5} M).

2.3.7.2.3 Fluorescence titration of the Al(III) Complexes by Fluoride

Upon saturation by fluoride the fluorescent properties of Al(**1**)$_3$ and Al(**2**)$_3$ were almost completely quenched, as illustrated in **Figure 2.32** and **Figure 2.33**, respectively. These observations are a result of the fluoride anion binding to the empty p$_z$-orbital on the boron center and subsequently inhibiting the intramolecular CT. It should be noted that during the titration of Al(**2**)$_3$ a smaller emission peak characteristic of **2** emerged at ~470 nm and was subsequently quenched. This is believed to be a result of the ejection of **2** from the metal center followed by quenching via fluoride anions. This subject will be discussed in greater detail at the end of this chapter. Furthermore, based on the Stern-Volmer plot it is evident that the fluorescence of Al(**2**)$_3$ is quenched more rapidly than Al(**1**)$_3$ (**Figure 2.34**).
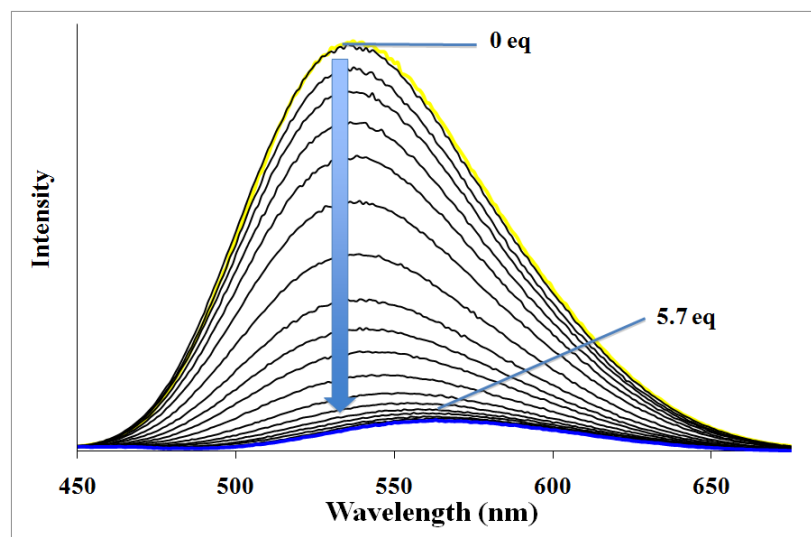
Figure 2.32. The fluorescent titration spectrum of Al(1)$_3$ by TBAF in CH$_2$Cl$_2$ (1.0 x 10^{-5} M).
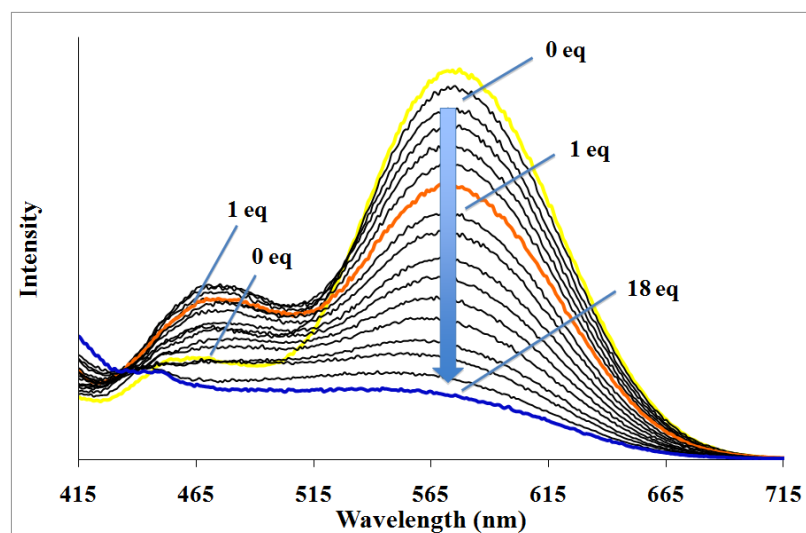
Figure 2.33. The fluorescent titration spectrum of Al(2)$_3$ with TBAF in CH$_2$Cl$_2$ (1.0 x 10^{-5} M).

100
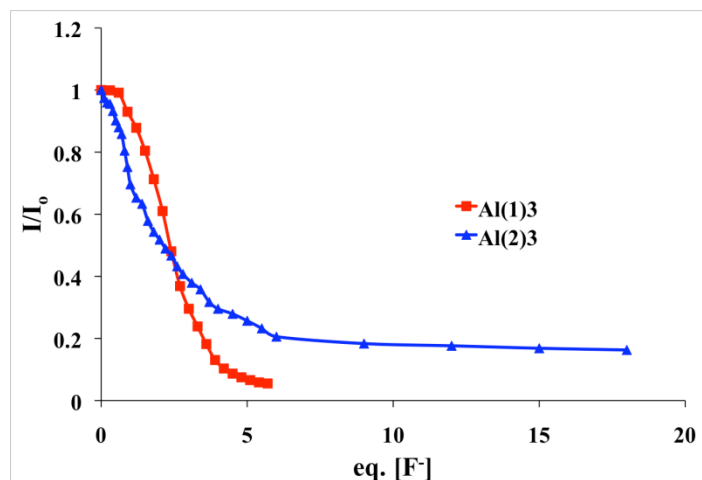
Figure 2.34. The Stern-Volmer plot from fluorescence of Al(1)$_3$ and Al(2)$_3$ at λ_{max} = 536 nm and λ_{max} = 570 nm, respectively, from fluoride titrations.

2.3.7.2.4 Fluorescence titration of the Al(III) Complexes by Cyanide

Cyanide proved to be a better quencher towards Al(**1**)$_3$ having only required 4.5 eq. to reach

saturation, which is much closer to the theoretical 3 eq. expected (**Figure 2.35**). On the other

hand ~9 eq. of cyanide was required to reach saturation for Al(**2**) (**Figure 2.36**), which was 3

times greater than the expected amount but half the amount of fluoride required to achieve the

same outcome. Furthermore as a result of the absence of a peak at ~470 nm, it is believed that the

use of cyanide did not lead to the ejection of the free ligand **2** from the metal center. Based on the

Stern-Volmer plot it would appear that the fluorescence emission of Al(**1**)$_3$ was quenched more

rapidly than Al(**2**)$_3$ (**Figure 2.37**).
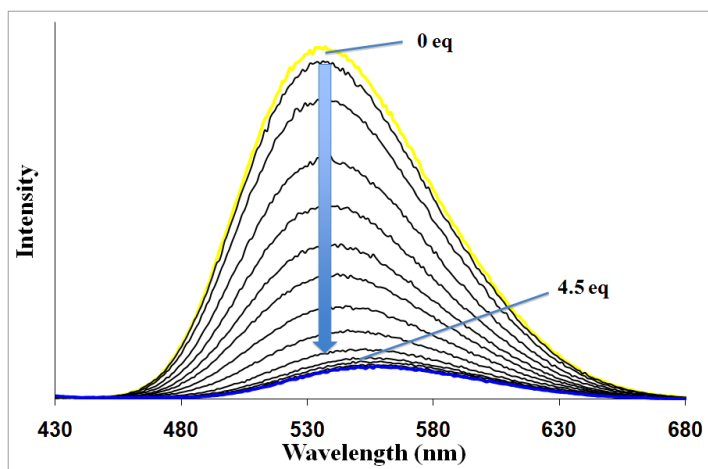
Figure 2.35. The fluorescence titration spectrum of Al(1)$_3$ with NEt$_4$CN in CH$_2$Cl$_2$ (1.0 x 10^{-5} M).
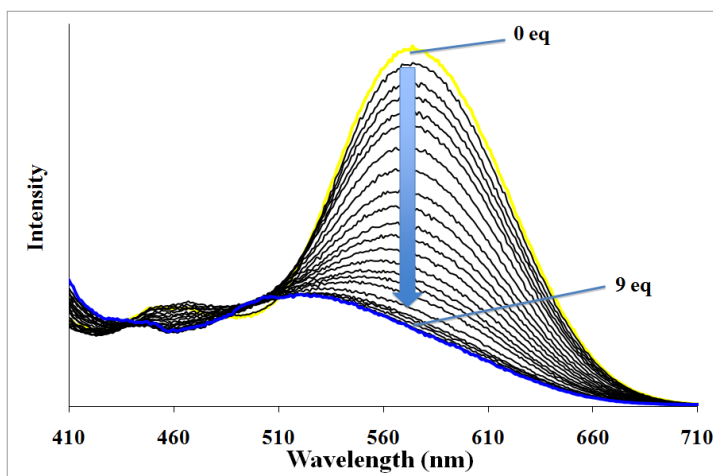
Figure 2.36. The fluorescence titration spectrum of Al(2)$_3$ by NEt4$_C$N in CH$_2$Cl$_2$ (1.0 x 10^{-5} M).
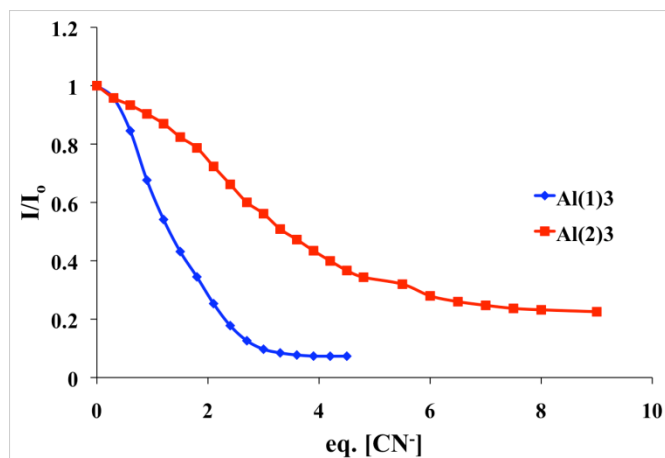
Figure 2.36. The Stern-Volmer plot from fluorescence of Al(**1**)$_3$ and Al(**2**)$_3$ at λ_{max} = 536 nm and λ_{max} = 570 nm, respectively, from cyanide titrations.

2.3.7.2.5 Effects of Hard and Soft Lewis Bases on the Structural Integrity of Alq$_3$

Based on the fluorescence and UV-Vis spectra obtained over the course of the titrations it was evident that fluoride and cyanide behaved differently towards the aluminum complexes. In particular, during the titration of Al(**2**)$_3$ with fluoride a second peak at ~460 nm in the emission spectrum emerged that was similar to the emission spectrum of its free ligand. The most likely explanation for these results was believed to be due to the 'Hard and Soft [Lewis] Acid and Base' (HSAB) principle. According to this theory, as a result of the hard nature of both the aluminum center and the fluoride anion, they should have a high affinity toward each other. Thus it is likely that the fluoride ions not only attack the boron center but also the aluminum center by disrupting the Al-O and Al-N bonds. Furthermore, the Al-F interaction would be more favorable than the Al(III) interaction with a soft Lewis base such as cyanide. Therefore, less cyanide is needed to reach saturation since it is only interacting with the boron center as opposed to the fluoride anion,

103

which is interacting with both the aluminum center and the boron moiety. In order to explore this theory the behavior of Alq_3, which does not have a boron center, was investigated in the presence of an excess of either Lewis base. The importance in using Alq_3 as a control was due to the lack of a boron center, which would make it easier to attribute any spectral changes to an interaction involving the Lewis base and the aluminum center. As expected there were no observable changes between the UV-Vis or fluorescence profiles of Alq_3 and Alq_3/CN^- (**Figure 2.38**). Conversely, an addition of excess TBAF to Alq_3 led to a blue-shift of its UV-Vis and fluorescence spectra indicating the binding of fluoride to the aluminum center. This was further supported by ^{1}H NMR data (**Figure 2.39**). The proton peaks of Alq_3 were unchanged upon addition of excess cyanide while with the addition of excess fluoride new peaks began emerging whose chemical shifts were similar to those of 8-hydroxyquinoline. This supports the theory that there was competition between the fluoride anion ejecting the ligand as a result of its interaction with the aluminum center and binding to the empty p_z-orbital of the boron center.
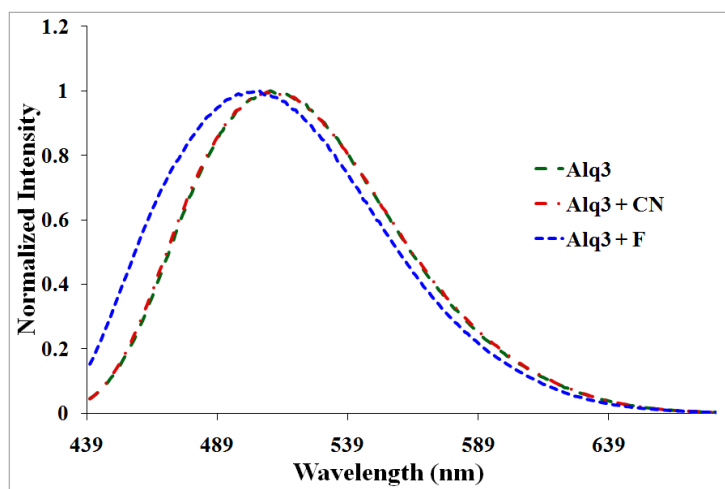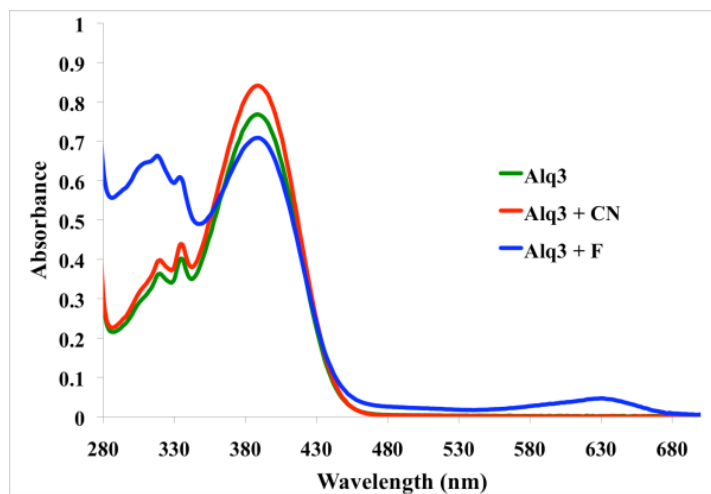
Figure 2.37. The UV-Vis (top) and fluorescence spectra (bottom) of Alq₃ as a control and in the presence of excess cyanide or fluoride in CH₂Cl₂.
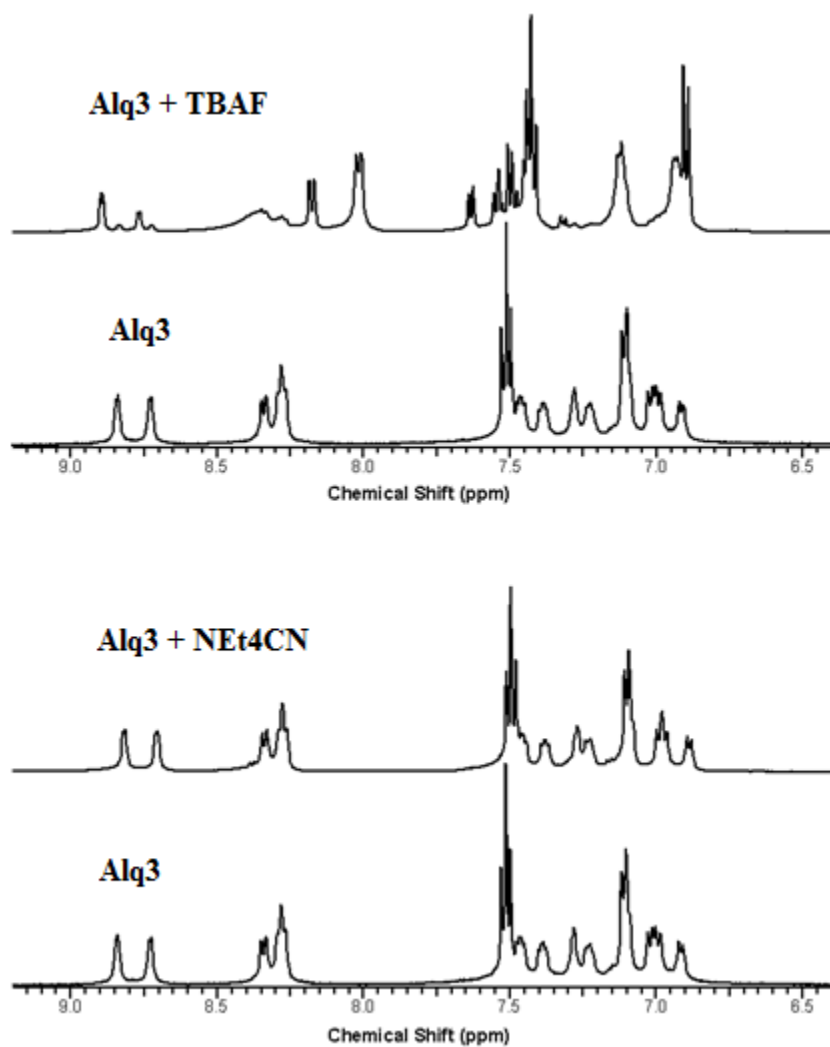
Figure 2.38. ^{1}H NMR spectra of Alq$_3$ titrated with excess tetrabutylammonium fluoride (top) and tetraethylammonium cyanide (bottom) in CD$_2$Cl$_2$.

2.3.8 Conclusion

In conclusion, the first examples of multifunctional tirarylboron-functionalized Alq_3 complexes have been realized. Using COSY NMR it was established that both $Al(\mathbf{1})_3$ and $Al(\mathbf{2})_3$ had C_1 symmetry, which is characteristic of the *mer*-isome. The new ligands were designed with the intent of enhancing the electron transporting properties of their respective aluminum complexes while retaining their luminescent functionality. Based on CV measurements the two new aluminum complexes had better electron accepting abilities than Alq_3, making them promising candidates for use as ETMs, though further investigations on its electron mobility characteristics will need to be investigated. Furthermore, due to the rigidity, shorter length and highly conjugated nature of the π-skeleton of $Al(\mathbf{1})_3$, the electron deficient boron center had a stronger effect on the system leading to the slightly lower reduction potential compared to $Al(\mathbf{2})_3$. The experimentally determined HOMO and LUMO energy levels, determined using CV and absorbance measurements, were consistent with those obtained from DFT calculations. Although the solid state quantum yield of $Al(\mathbf{1})_3$ was considerably higher than that of $Al(\mathbf{2})_3$, Alq_3 had the strongest luminescent properties of all three aluminum complexes investigated. In the case of $Al(\mathbf{2})_3$ the lower quantum yield was attributed to the more flexible nature of the thiophene linker leading to a greater number of pathways for non-radiative decay through vibronic coupling. In addition to the luminescent and electron transporting properties of the two new aluminum complexes they also demonstrated anion sensing abilities, particularly towards soft lewis bases. Unfortunately, hard lewis bases were found to degrade the $Al(\mathbf{1})_3$ and $Al(\mathbf{2})_3$ by interacting with the aluminum center and ejecting the respective ligands in the process. Furthermore, based on the Stern-Volmer plots $Al(\mathbf{1})_3$ had a stronger binding constant towards cyanide than $Al(\mathbf{2})_3$.

107

2.3.9 References

1) B. C. Lin, C. P. Cheng, Z. Q. You and C. P. Hsu, *J. Am. Chem. Soc.*, 2004, **127**, 66.

2) A. J. Mäkinen, I. G. Hill, T. Noda, Y. Shirota and Z. H. Kafafi, *Appl. Phys. Lett.*, **2001**, 78, 670.

3) A. J. Mäkinen, I. G. Hill, M. Kinoshita, T. Noda, Y. Shirota and Z. H. Kafafi, *J. Appl. Phys.*, **2002**, 91, 5456.

4) V. A. Montes, R. Pohl, J. Shinar and P. Anzenbacher, Jr., *Chem. Eur. J.*, 2006, **12**, 4523.

5) M. Takahashi, K. Masui, H. Sekiguchi, N. Kobayashi, A. Mori, M. Funahashi and N. Tmaoki, *J. Am. Chem. Soc.*, 2006, **128**, 10930.

6) Y. Cui and S. Wang, *J. Org. Chem.*, 2006, **71**, 6485.

7) Z. Yuan, C. D. Entwistle, J. C. Collings, D. Albesa-Jové, A. S. Batsanov, J.A.K Howard, N.J. Taylor, H. M. Kaiser, D. E. Kaufmann, S. -Y. Poon, W.-Y. Wong, C. Jardin, S. Fathallah, A. Boucekkine, J. -F. Halet and T.B. Marder, *Chem. Eur. J.*, 2006, **12**, 2758.

8) A. Curioni and W. Andreoni, *J. Am. Chem. Soc.*, **1999**, 121, 8216.

9) G. Gahunga, J. Zhang, V. Ntakarutimana and N. Gahunga, *J. Phys. Chem. A*, **2010**, 114, 652.

10) (a) H. Shizuka, *Acc. Chem. Res.*, **1985**, 18, 141. (b) H. –T. Yu, W. J. Colucci, M. L. McLaughlin and M. D. Barkley, *J. Am. Chem. Soc.*, **1992**, 114, 8449.

11) W. L. Jia, D. R. Bai, T. McCormick, Q. D. Liu, M. Motala, R. Y. Wang, C. Seward, Y. Tao and S. Wang, *Chem. –Eur. J.*, **2004**, 10, 994.

12) R. Ballardini, G. Varani, M. T. Indelli and F. Scandola, *Inorg. Chem.*, **1986**, 25, 3858.

13) T. Noda and Y. Shirota, *J. Am. Chem. Soc.*, **1998**, 120, 9714.

14) (a) J. Zhang and G. Frenking, *J. Phys. Chem. A.*, **2004**, 108, 10296. (b) A. Curioni, M. Boero and W. Andreoni, *Chem. Phys. Lett.*, **1998**, 294, 263. (c) A. Irfan, R. Cui, J. Zhang and C. Hao, *Chem. Phys.*, **2009**, 364, 39.

15) J. N. Spencer, G. M. Bodner and L. H. Rickard, *Chemistry: Structure and Dynamics,* 5th edition, **2010**, John Wiley and Sons Inc., United States of America.

Chapter 3

Diboron-Functionalized 8-Hydroxyquinoline

3.1 Introduction

Over the past decade there has been tremendous research interest towards four-coordinate boron systems that are chelated to a π-conjugated backbone. These types of systems have demonstrated considerable promise as optoelectronic materials in OLEDs.[1-5] In addition, boron chelates have been found to have stronger covalent bonds lending them greater stability compared to their aluminum analogues.[5,6] Although there are a numerous examples of luminescent materials that incorporate a four-coordinate boron moiety,[2-4] investigation of their properties as ETMs is fairly limited.[3,7] Interestingly, it was discovered that upon coordination to a four-coordinate boron moiety the LUMO of the corresponding ligand could be decreased considerably.[8] Therefore, there is a lot of promise in the use of four-coordinate boron systems as ETMs.

In the second chapter, the advantages of designing a first of its kind ETM incorporating 8-hydroxyquinolato (q) and triarylboron moiety had been discussed. In particular both entities are well known for their electron accepting properties, making them particularly important candidates as ETMs, though electron mobility of such materials are still being investigated. With the discovery made by Cui and Wang, it is possible that the incorporation of a four-coordinate boron system to such triarylboron modified 8-hydroxyquinoline ligands could further enhance the system's electron accepting properties.[8]

Herein the synthesis and characterization of the first 8-hydroxyquinoline ligands modified with a triarylboron and a four-coordinate boron moiety, **B1** and **B2**, will be discussed (**Figure 3.1**). As mentioned in the previous chapter, the linkers chosen were intended to promote electron mobility. The acetylene linker in **B1** is highly planar and thus enhances the system's π-conjugation, while the thiophene linker used in **B2** has been found to facilitate electron communication within the ligand.[9,10]
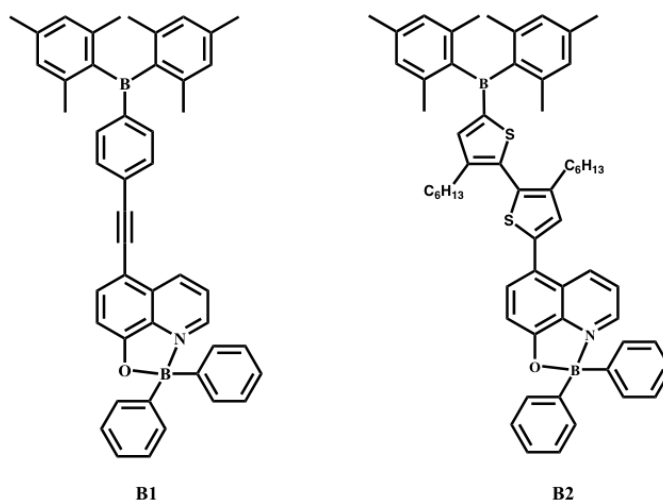
Figure 3.1. Structure of the boron chelates.

3.2 Experimental Section

Dry solvents were obtained from a solvent purification system (Innovative Technologies, Inc.). Reactions that required oxygen-free environments were conducted under an inert nitrogen

atmosphere in oven-dried glassware using standard Schlenk techniques unless otherwise stated. ^{1}H and ^{13}C NMR spectra were recorded using Bruker Avance 300, 400 or 500 MHz spectrometers. UV-Vis measurements were acquired using a Varian Cary 50 Bio Spectrometer. Excitation and emission spectra were recorded using a Photon Technologies International Quanta Master model C-60 spectrometer. High-resolution mass spectra were obtained using a Water/Micromass GC-TOF EI-MS spectrometer. Elemental analyses were conducted by Canadian Microanalytical Service Ltd. Cyclic voltammetry measurements were acquired using a BAS CV-50W analyzer with a typical sample concentration of 4 mg of sample and 50mg of NBu_4PF_6 (TBAP) as supporting electrolyte in 3 mL of DMF using a standard Ag/AgCl reference electrode, Pt working electrode, and Pt auxiliary. The ferrocenium/ferrocene couple was used as an internal standard (E_o=0.55 V). Aside from 8-hydroxyquinoline, ordered from TCI, all reagents were obtained from the Sigma-Aldrich chemical company. 5,5'-dibromo-3,3'-dihexyl-2,2'-bithiophene[11] and 5-bromo-8-(methylmethoxy)quinoline[8] were synthesized as outlined in literature.

3.2.1 Synthesis of B1

(p-iodophenyl)dimesitylborane: Diiodobenzene (3 g, 9.09 mmol) was dissolved into 60 mL of dry THF at room temperature. The temperature of the reaction flask was reduced to -78°C to which a hexane solution of nBuLi (1.6 M, 5.2 mL, 8.18 mmol) was added and the contents of the flask reacted for 2 hours. A solution of dimesitylboron fluoride (2.20 g, 8.18 mmol) in 20 mL of THF was added to the reaction flask and allowed to react for 2 hours at -78°C and then at room temperature overnight. The solvent was removed under vacuum and the product purified using

112

column chromatography on silica gel (hexane) and then recrystallized in hexane to give white crystalline product in 50% yield. ^{1}H NMR (CDCl$_3$, 25°C): δ (ppm) = 7.70 (d, J = 8.0 Hz, 2H), 7.21 (d, J = 8.0 Hz, 2H), 6.81 (s, 4H), 2.30 (s, 6H), 1.98 (s, 12H). This data matches literature spectral data.[12]

(5-ethynyl-8-quinolato)diphenylborane: Triphenylborane (712 mg, 2.94 mmol) was dissolved in 30 mL of dry THF and added via cannula into a solution of 5-bromo-8-hydroxyquinoline (600 mg, 2.67 mmol) dissolved in 30 mL of dry THF. The reaction was allowed to proceed overnight under reflux yielding **(5-bromo-8-hydroxyquinolato)diphenylborane**. The product was purified using column chromatography on silica gel (hexane:ethyl acetate 3:1) and used directly in the next step. Trimethylsilylacetylene (347 mg, 3.53 mmol) was added to a solution of (5-bromo-8-hydroxyquinolato)diphenylborane (913 mg, 2.35 mmol), [PdCl$_2$(PPh$_3$)$_2$] (18.1 mg, 0.0258 mmol), CuI (44.8 mg, 0.235 mmol) and TEA (15 mL) in THF (70 mL) at 0 ℃. The solution was then allowed to react overnight at room temperature. The THF was removed *in vacuo* and the product, **(5-trimethylsilylethynyl-8-quinolato)diphenylborane**, was extracted from water using dichloromethane and purified using column chromatography on silica gel (hexane:dichloromethane 3:1). In order to remove the TMS component, the product was dissolved in water/methanol/THF along with an excess of 18-crown-6 and KF. The mixture was alloed to react for 5 hours at room temperature. A flash column on silica gel (hexane:dichloromethane 3:1) was run to remove the crown ether yielding **(5-ethynyl-8-quinolato)diphenylborane** in an overall yield of 65%. ^{1}H NMR (CDCl$_3$, 25°C): δ (ppm) = 8.89 (d, J = 8.35 Hz, 1H), 8.70 (d, J = 5.05 Hz, 1H), 7.94 (d, J = 8.07 Hz, 1H), 7.81 (dd, J = 8.35, J = 5.05, 1H), 7.42 (d, J = 6.51 Hz, 4H), 7.29 (m, 6H), 7.15 (d, J = 7.98 Hz, 1H), 3.49 (s, 1H).

113

B1: A mixture of (5-ethynyl-8-quinolato)diphenylborane (200 mg, 0.604 mmol), (p-iodophenyl)dimesitylborane (300 mg, 0.664 mmol), Pd(PPh$_3$)$_4$ (34.9 mg, 0.030 mmol), CuI (11.5 mg, 0.06 mmol) and TEA (5 mL) was stirred in THF (40 mL) overnight at room temperature. The THF was removed *in vacuo*. Water was added to the mixture and the product was extracted with CHCl$_3$. The final product was purified using column chromatography on silica gel (hexanes:dichloromethane 3:1) resulting in a yield of 90%. ^{1}H NMR (CDCl$_3$, 25°C): δ (ppm) = 8.88 (d, *J* = 8.39 Hz, 1H), 8.70 (d, *J* = 5.06 Hz, 1H), 7.98 (d, *J* = 8.10 Hz, 1H), 7.82 (dd, *J* = 8.39, *J* = 5.06, 1H), 7.63 (d, *J* = 8.22 Hz, 2H), 7.54 (d, *J* = 8.22 Hz, 2H), 7.43 (d, *J* = 7.88 Hz, 4H), 7.29 (m, 6H), 7.20 (d, *J* = 8.10, 1H), 6.88 (s, 4H), 2.35 (s, 6H), 2.05 (s, 12H). ^{13}C {^{1}H} NMR (CD$_2$Cl$_2$, 25°C): δ (ppm) = 159.7, 141.1, 140.6, 139.3, 138.6, 137.7, 137.5, 136.5, 132.1, 132.1, 131.1, 129.4, 128.5, 128.5, 127.9, 127.8, 127.3, 126.7, 124.0, 110.0, 106.7, 93.6, 87.7, 23.4, 21.2. HRMS of C$_{48}$H$_{42}$BNO: calcd [M+H$^+$] *m/z* = 657.4565, found [M+H$^+$] *m/z* = 657.3390.

3.2.2 Synthesis of B2

5-bromo-5'-dimesitylboryl-3,3$^'$-dihexyl-2,2$^'$-bithiophene: 5,5'-dibromo-3,3'-dihexyl-2,2'-bithiophene (1.92 g, 3.89 mmol) was dissolved into 20 mL of dry THF at room temperature. The temperature of the reaction flask was reduced to -78°C to which a hexane solution of nBuLi (1.6 M, 2.55 mL, 4.08 mmol) was added and the contents of the flask reacted for ~2 hrs. A solution of dimesitylboron fluoride (1.28 g, 4.28 mmol) in 15 mL of THF was added to the reaction flask and allowed to react for 2 hours at -78 ^{o}C and then at room temperature overnight. The solvent was removed *in vacuo* and the product purified using column chromatography on silica gel using hexanes as eluent (80% yield). ^{1}H NMR (CDCl$_3$, 25°C): δ (ppm) = 7.30 (s, 1H), 6.91 (s, 1H), 6.84

(s, 4H), 2.49 (m, 4H), 1.48 (m, 4H), 1.22 (m, 12H), 0.86 (m, 6H). ^{13}C {^{1}H} NMR (CD$_2$Cl$_2$, 25 ^{o}C): δ (ppm) 145.3, 143.2, 142.7, 142.0, 141.2, 139.6, 138.8, 131.9, 128.4, 31.9, 31.8, 31.1, 30.8, 29.3, 29.0, 23.8, 22.8, 21.5, 14.3. HRMS of C$_{38}$H$_{50}$BBrS$_2$: calcd m/z = 660.2630, found m/z = 660.2645.

2: To a solution of 5-bromo-5'-dimesitylboryl-3,3'-dihexyl-2,2'-bithiophene (1.10 g, 1.66 mmol) in THF (15 mL) at -78 ^{o}C, was added nBuLi (1.6M, 1.14 mL, 1.82 mmol). The mixture was allowed to react for 2 hrs. Then 2-isopropoxy-4,4,5,5-tetramethyl-1,3,2-dioxaborolane (0.42 mL, 2.08 mmol) was added slowly at -78 ^{o}C. The reaction mixture was allowed to react for 2 hours at -78°C before it was warmed to room temperature and allowed to react overnight. The product was purified using column chromatography on silica gel using hexane and ethyl acetate sequentially, resulting in a yield of 69% of **5-pinacolboryl-5'-dimesitylboryl-3,3'-dihexyl-2,2'-bithiophene**. Into a 20 mL schlenk flask was added the above boronic ester (750 mg, 1.06 mmol), 5-bromo-8-(methoxymethoxy)quinoline (190 mg, 0.71 mmol), K$_3$PO$_4$ (567 mg, 2.13 mmol), Pd(CH$_3$COO)$_2$ (8.00 mg, 0.035 mmol), and 2-dicyclohexylphosphino-2',6'-dimethoxybiphenyl (29 mg, 0.07 mmol) in toluene (3 mL). The reaction proceeded overnight under reflux. The product was purified using column chromatography on silica gel (ethyl acetate/hexane = 1:2) to give **2-MOM** in 95% yield, which was then deprotected according to literature methods.[8] ^{1}H NMR (CDCl$_3$, 25°C): δ (ppm) = 8.83 (d, J = 4.0 Hz, 1H), 8.66 (d, J = 8.5 Hz, 1H), 7.61 (d, J = 8.0 Hz, 1H), 7.50 (dd, J = 8.5 Hz, 4.0 Hz, 1H), 7.46 (s, 1H), 7.25 (d, J = 8.0 Hz, 1H), 7.03 (s, 1H), 6.86 (s, 4H), 2.63 (m, 4H), 2.33 (s, 6H), 2.20 (s, 12H), 1.58 (m, 4H), 1.27 (m, 12H), 0.90 (m, 6H). ^{13}C {^{1}H} NMR (CD$_2$Cl$_2$, 25°C): δ (ppm) = 152.4, 149.6, 147.9, 144.6, 142.8, 142.7, 142.1, 141.0, 140.6, 138.6, 138.4, 134.7, 129.4, 129.3, 129.0, 128.3, 127.0, 123.0, 122.2, 109.7, 31.7, 31.7, 31.0, 30.9,

29.4, 29.2, 29.1, 28.9, 23.6, 22.7, 21.3, 14.2. HRMS of $C_{47}H_{56}BNOS_2$: calcd m/z = 725.3896, found m/z = 725.3905.

B2: Triphenylborane (15.8 mg, 0.065 mmol) was dissolved in 20 mL of dry THF and added via cannula into a solution of **2** (43 mg, 0.059 mmol) dissolved in 20 mL of dry THF. The reaction was allowed to proceed overnight under reflux. The product was extracted from water using dichloromethane and further purified via column chromatography using silica gel (hexanes:dichloromethane 6:1) leading to a yield of 85%. ^1H NMR (CDCl$_3$, 25°C): δ (ppm) = 8.94 (d, J = 8.8 Hz, 1H), 8.68 (d, J = 5.0 Hz, 1H), 7.85 (d, J = 7.98 Hz, 1H), 7.75 (dd, J = 8.8 Hz, 5.0 Hz, 1H), 7.45 (s, 1H), 7.36 (s, 1H), 7.27 (m, 7H), 7.13 (s, 1H), 6.88 (s, 4H), 2.66 (m, 4H), 2.34 (s, 6H), 2.19 (s, 12H), 1.61 (m, 4H), 1.28 (m, 14H), 0.89 (m, 6H). HRMS of $C_{59}H_{65}B_2NOS_2$: calcd m/z = 889.9055, found m/z = 889.4713.

3.3 Results and Discussion

3.3.1 Synthesis

3.3.1.1 Synthesis of B1

Although the overall structure of compounds **1** and **B1** are quite similar a slightly different synthetic approach was taken for the latter ligand. As illustrated by the synthetic scheme in **Figure 3.2** a boron chelate was used as protecting group rather than Boc. There were two reasons

for this decision: (1) the number of synthetic steps was reduced since the four-coordinate boron moiety was the final target and (2) piperidine was not very effective at removing the Boc protecting group. Interestingly, trifluoroacetic acid is typically a more effective agent for removing Boc, but unfortunately the ethynyl linker was found to be susceptible to reduction in the presence of acids, which would lead to a double bond.[13] Another advantage to this synthetic approach relies on the fact the four-coordinate boron moiety eliminates any possibility of the catalyst used for the Sonogoshira coupling reactions from chelating to substrate.
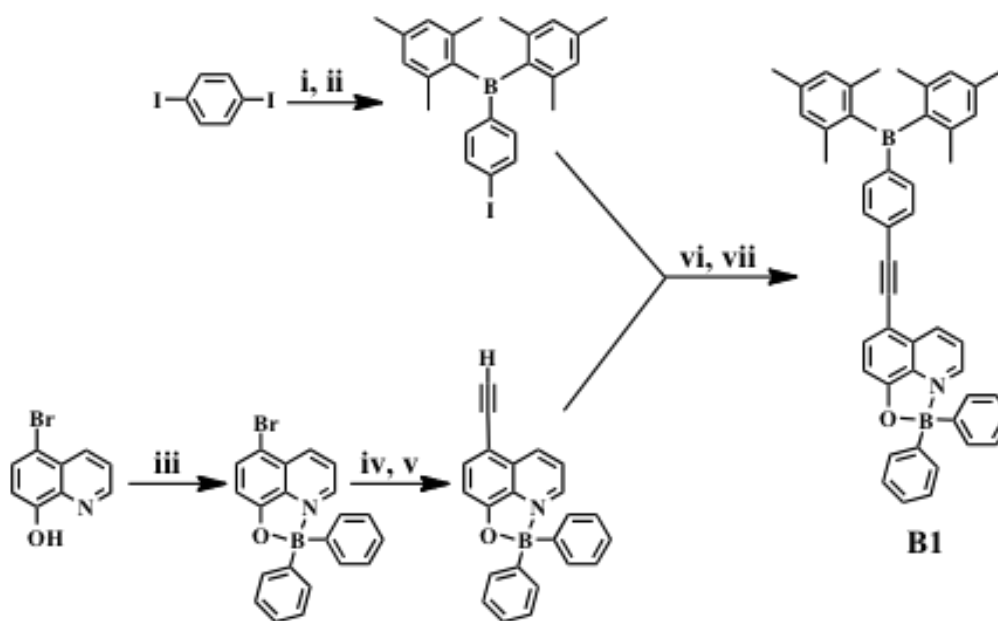
Reagents and conditions: (i) *n*-BuLi, THF, -78 °C; (ii) FBMes$_2$, THF, -78 to 25 °C, overnight; (iii) triphenylborane, THF, reflux overnight; (iv) [PdCl$_2$(PPh$_3$)$_2$], CuI, trimethylsilylacetylene, THF, TEA, reflux, overnight; (v) KF, MeOH, water, THF, r.t., 5hrs; (vi) [Pd(PPh$_3$)$_4$], CuI, THF, TEA, r.t., overnight; (vii) piperidine, dry CH$_2$Cl$_2$, r.t., overnight.

Figure 3.2. Synthetic scheme for B1.

117

3.3.1.2 Synthesis of Ligand B2

As illustrated in **Figure 3.3**, aside from the attachment of the diphenylboron moiety in the final step, the synthesis of compound **B2** is identical to that of compound **2,** which was discussed in greater detail in the previous chapter. Due to the hexyl chains on the bisthiophene linker, the final product had exceptional solubility characteristics in all solvents making it difficult to purify via re-crystallization. Again it should be noted that Dr. Yi Sun synthesized ligand **2** while I conducted the reaction to attach the boron chelate yielding ligand **B2**.
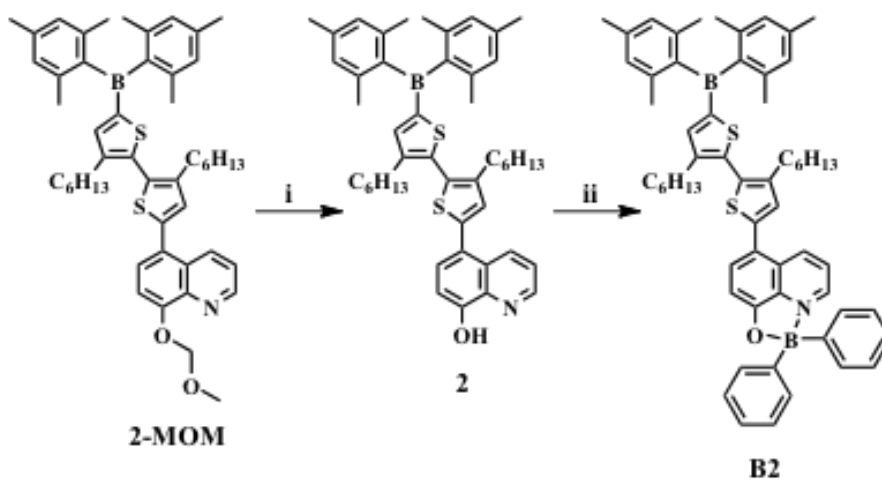
Reagents and conditions: (i) HCl, CH₃OH, reflux, (ii) triphenylborane, THF, reflux overnight.

Figure 3.3. Synthetic scheme for B2.

3.3.2 UV-Vis Absorption Spectra

UV-vis spectra were recorded for both **B1** and **B2** compounds in order to gain a better understanding of their electronic properties. The absorption spectra of compounds **B1** and **B2** are presented in F**igure 3.4**. Due to the highly conjugated nature of **B1** it shows more intense absorption peaks than compound **B2** over the same wavelength range. The peaks at ~272 nm, ~360 nm and ~435 nm for both compounds can be attributed to the π-π^* transition within the quinoline moiety, a π-π^* transition involving the triarylboron moiety and a π-π^* transition involving the four-coordinate boron system, respectively. These assignments will be supported by fluoride titrations that will be discussed later in the chapter. The absorbance profile of compound **B2** is slightly red-shifted compared to compound **B1**, which can be attributed to the larger size of the former compound resulting in a slight narrowing of the bandgap.
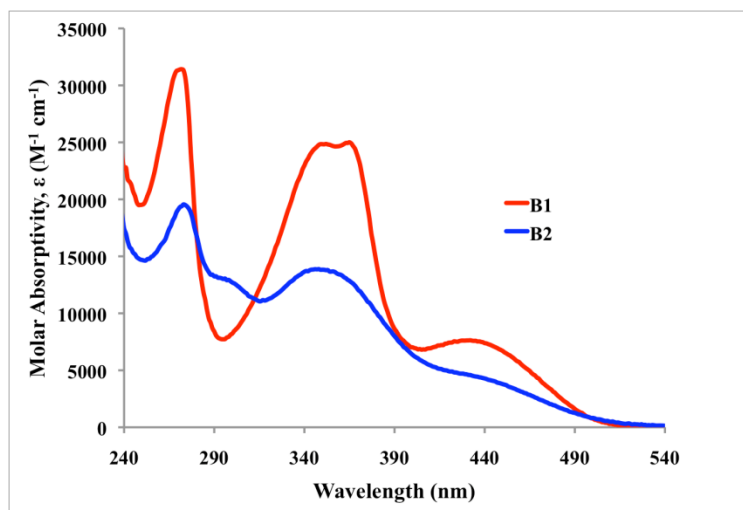
Figure 3.4. The UV-vis absorption spectra of compounds B1 and B2 in ether.

119

3.3.3 Luminescence Properties

Under UV irradiation the color of compounds **B1** and **B2** was yellow and orange, respectively. The emission spectra of the two new compounds are presented in F**igure 3.5**. In comparison to their respective ligands, **1** (λ_{max} = 413 nm) and **2** (λ_{max} = 480 nm), discussed in the previous chapter, the emission of compounds **B1** (λ_{max} = 533 nm) and **B2** (λ_{max} = 575 nm) were significantly red-shifted. This can be explained by the overall extension of the new systems as a result of the four-coordinate boron moiety, which contributes to a narrowing of the bandgap.[8] A similar explanation applies to the red-shifted nature of the emission of **B2** compared to **B1**, since the former compound has a more extended π-skeleton.
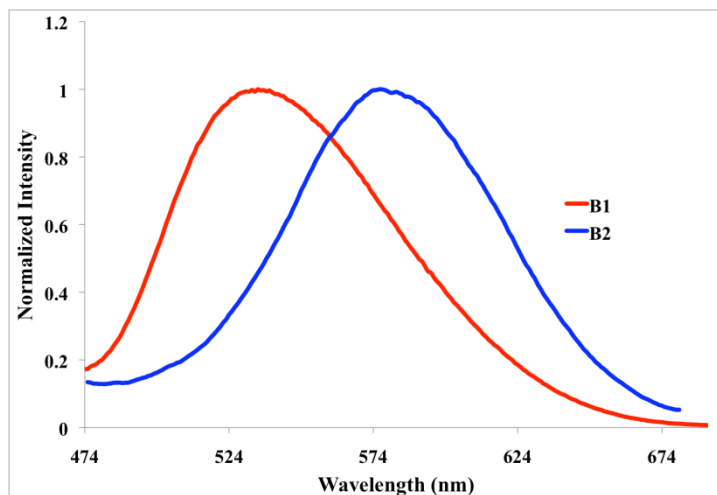
Figure 3.5. A normalized emission spectra of compounds B1 and B2 in ether at room temperature.

In addition, the emission of compound **B1** is red-shifted as the solvent polarity is increased with the λ_{max} shifting from 413 nm in ether to 458 nm in ethanol (λ_{ex} = 363 nm), indicating an intramolecular CT that yields a polarized excited state (**Figure 3.6**).[5,8] On the contrary, **B2** does not seem to be affected by the polarity of the solvent and shows signs of decomposition in DMF (**Figure 3.7**). The quantum yield of **B1** (Φ = 0.058) was much lower than **B2** (Φ = 0.019), measured using 9,10-diphenylanthracene as the standard. For comparison, the quantum yield of BPh$_2$q is 0.03 relative to 9,10-diphenlyanthracene in CH$_2$Cl$_2$ at room temperature.[14] It is unknown why the quantum yields of the two new analogues of BPh$_2$q are significantly lower, and further investigations are required. A lower quantum yield for **B2** is expected as a result of its larger degree of flexibility from the hexyl chains, which contributes to a larger number of pathways for non-radiative decay. A summary of the photophysical properties of **B1** and **B2** is presented in **Table 3.1**.
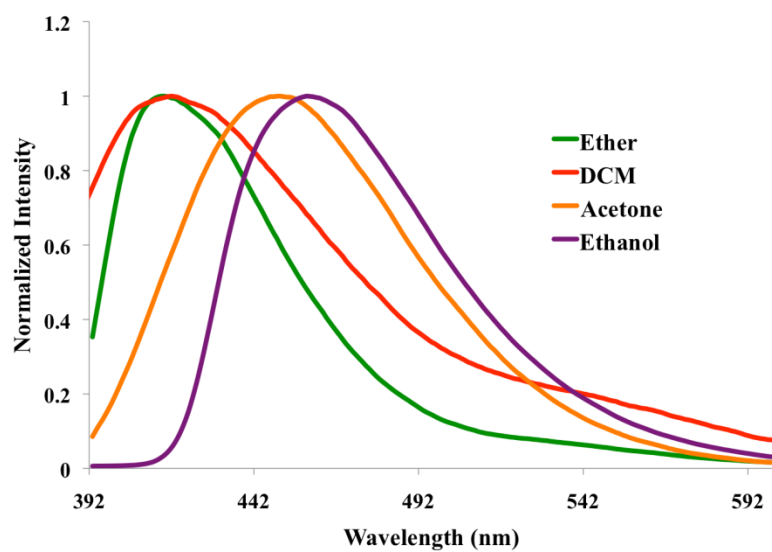
Figure 3.6. The emission spectra of B1 in various solvents at room temperature ($\lambda_{ex} = 363$ nm; 1.0×10^{-5} M).

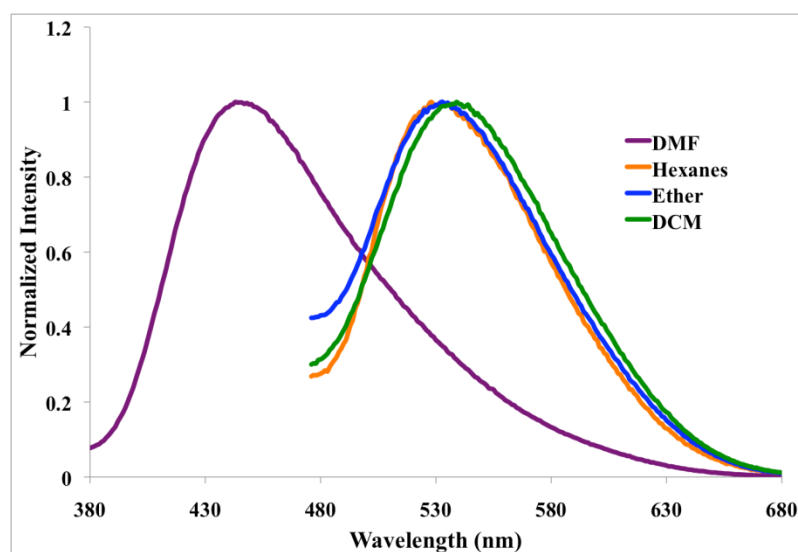**Figure 3.7. The emission spectra of B2 in various solvents at room temperature ($\lambda_{ex} = 369$ nm; 1.0×10^{-5} M).**

Table 3.1. Absorption and luminescent properties of compounds 3 and 4.

| Compound	λ_{abs}/nm (log ε/M^{-1} cm^{-1})	λ_{em}/nm[a]	$\Phi_{solution}$[b]
B1	272 (4.50), 360 (4.39), 435 (3.88)	576	0.058
B2	276 (4.28), 352 (4.14), 447 (3.84)	532	0.019

[a] In ether at 1.0×10^{-5} M. [b] Relative to 9,10-diphenylanthracene.

3.3.4 Electrochemical Properties

Cyclic voltammetry measurements were all made in dry DMF with NBu_4PF_6 as the electrolyte and using scan rates of 200-500 mV/s.

In order to gain a better understanding of the electrochemical properties of the two new compounds measurements were conducted using cyclic voltammetry. The reduction profiles are presented in **Figure 3.8** and the $E_{1/2}^{red}$ values are summarized in **Table 3.2**. Interestingly, both compounds **B1** and **B2** have two reduction peaks that were quite similar to one another. The first $E_{1/2}^{red}$ peaks at -1.84 V and -1.85 V for **B1** and **B2**, respectively, are attributed to the BPh_2-q moiety, which is consistent with literature.[8] An explanation for the slightly more positive reduction potential of **B1** is likely due to its rigidity and conjugated π-skeleton as well as a shorter length, all of which help enhance the effects of the electron deficient triarylboron moiety. The triarylboron moieties led to the second set of reduction peaks at -2.42 V and -2.36 V of **B1** and **B2**, respectively, which are similar to $BMes_2Ar$ reduction potentials in the literature.[8]
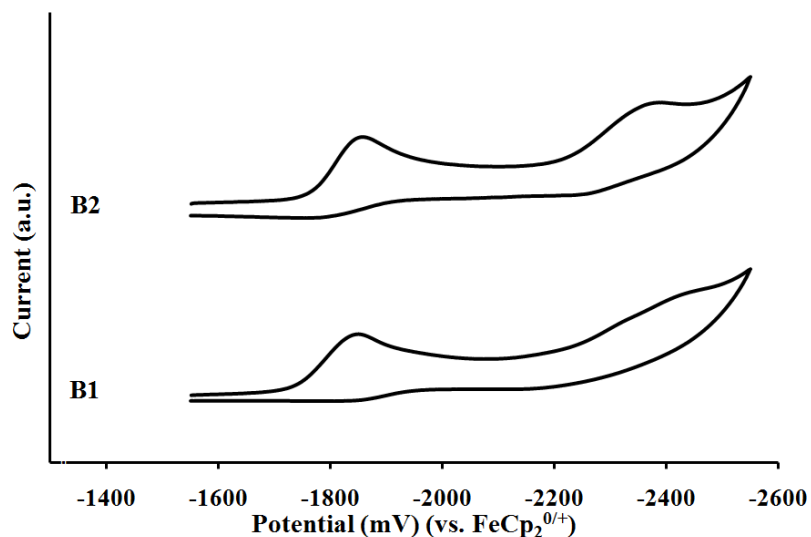
Figure 3.8. The CV diagrams of compounds B1 and B2 recorded in DMF.

The HOMO and LUMO energy levels of **B1** and **B2** are presented in **Table 3.2**. In comparison to **1** ($E_{1/2}^{red}$ = -2.22 V) and **2** ($E_{1/2}^{red}$ = -2.27 V) and their respective aluminum complexes Al(**1**)$_3$ ($E_{1/2}^{red}$ = -2.11 V) and Al(**2**)$_3$ ($E_{1/2}^{red}$ = -2.22 V) discussed in the previous chapter, compounds **B1** and **B2** both possess more positive reduction potentials and thus better electron accepting abilities. This is attributed to a stronger covalent bond between four-coordinate boron and the quinoline moiety compared to the respective aluminum (III) quinolato systems, leading to enhanced π-conjugation and a lower LUMO energy level.[5,6] The energy levels of the free ligands, their respective aluminum and boron chelate compounds, and Alq$_3$ are displayed in **Figure 3.9**. Interestingly, not only do the boron chelate compounds have better electron accepting properties than their respective aluminum complexes but they are also better than Alq$_3$, making them promising candidates as ETMs.

Table 3.2. The Reduction Potentials and HOMO/LUMO Energy of Compounds 3 and 4.

Compound	$E_{1/2}^{red\ a}$/V	HOMO[b]/eV	LUMO/eV	Band Gap/eV
B1	-1.85	-5.33	-2.95	2.38
B2	-1.86	-5.36	-2.96	2.40

[a] Measured in DMF relative to $FeCp_2^{0/+}$. [b] Determined from the reduction potential and the optical energy gap.
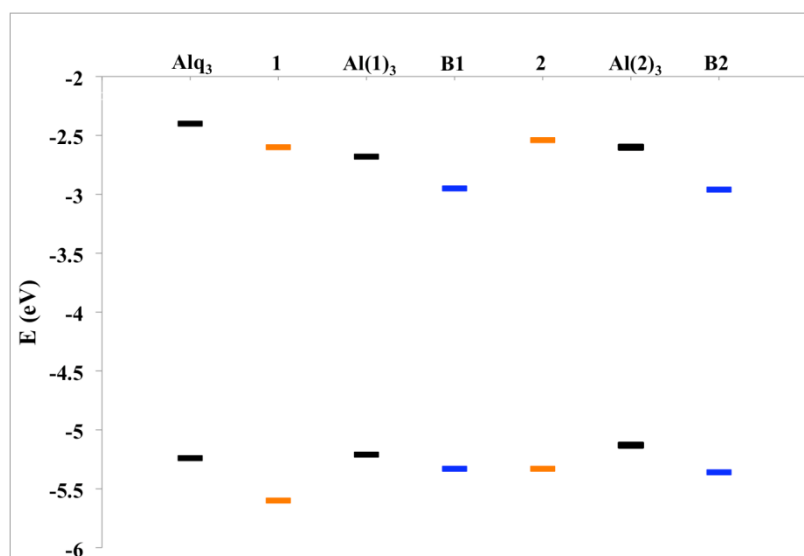
Figure 3.9. The experimental HOMOs and LUMOs of the free ligands, their respective aluminum and four-coordinate boron systems, and Alq$_3$.

3.3.5 Molecular Orbitals

DFT calculations were conducted on the boron chelate systems to gain a better understanding of their electronic transitions. The frontier molecular orbitals of **B1** and **B2** are presented in

125

Figure 3.10 and **Figure 3.11**, respectively. As expected the HOMO and LUMO of both compounds were predominantly located on the phenoxide and pyridyl parts of the quinoline moiety, respectively.[15] Additionally, the HOMO of **B1** and **B2** was also found on the acetylene linker and the first thiophene ring adjacent to q, respectively. Interestingly, although the three-coordinate boron center on **B1** also contributed to the respective LUMO, the same was not the case for **B2**. This supports the reasoning that the lower reduction potential of **B1** compared to **B2** was due to the contribution of the electron deficient triarylboron center on the LUMO. The energy levels of the HOMOs and LUMOs are presented in **Table 3.3**.

HOMO   LUMO
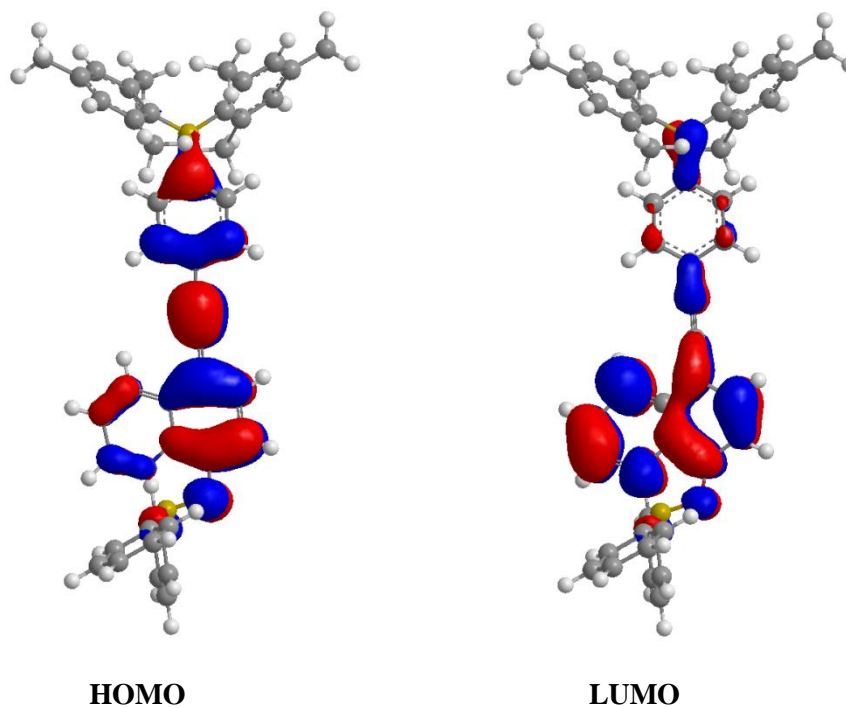
Figure 3.10. Frontier molecular orbitals of B1.

HOMO **LUMO**
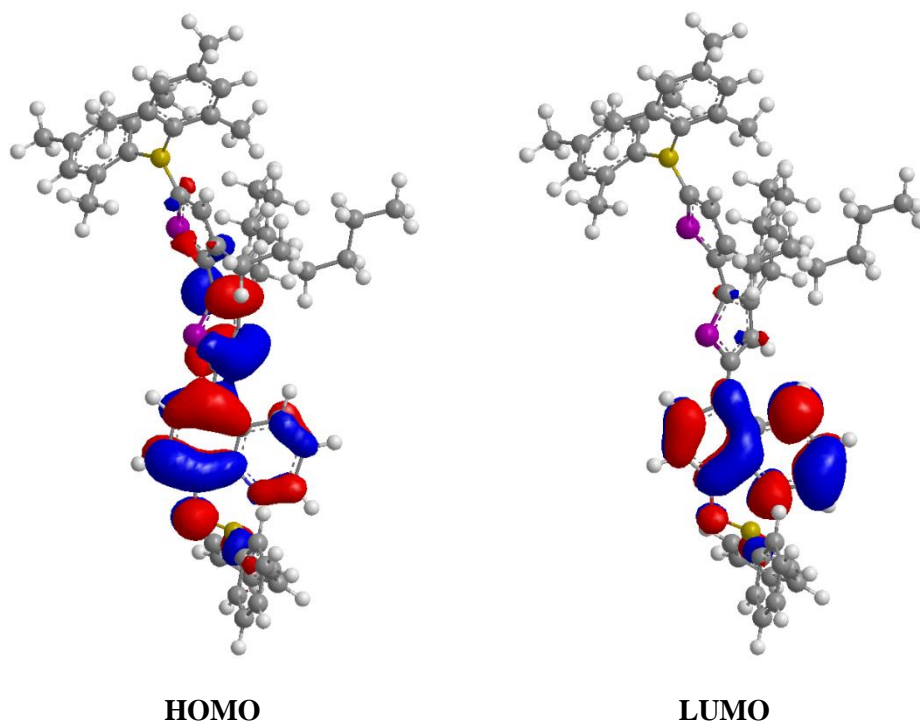
Figure 3.11. Frontier molecular orbitals of B2.

Hence the lowest electronic transition for **B1** occurs between the acetylene linker/phenoxide side of q and the p_π orbital of the boron center/pyridyl side of q. Upon excitation **B1** is polarized resulting in a boron center that is partially charged. The boron center is conjugated to electron-rich substituents that cannot stabilize this charge resulting in the solvent dependent emission observed. On the other hand, the lowest electronic transition for **B2** occurs between the first thiophene ring/phenoxide part of q and the pyridyl part of q. Since the LUMO is predominantly found on the pyridyl ring the dipolar nature of the system upon excitation is better stabilized leading to a neutral excited state that is unaffected by the solvent polarity.

Table 3.3. The calculated energy levels of the HOMOs and LUMOs of B1 and B2.

[a]Calculated Energy Levels (eV)		
Compounds	**HOMO**	**LUMO**
B1	-5.46	-2.44
B2	-5.49	-2.30

[a] Obtained at the B3LYP/6-31G* level of theory.

3.3.6 Lewis Acidity: Properties

All fluoride titrations were conducted in dry methylene chloride using TBAF as the fluoride source. Furthermore, the concentration of the free ligands in solution was 1.0×10^{-5} M in each case.

3.3.6.1 UV-Vis spectral titration of the Boron Chelates by Fluoride

Upon titration with TBAF the broad absorbance peak at 360 nm, attributed to the π to p_π^* transition, was quenched by 92% upon saturation (**Figure 3.12**). In addition, the absorption band at 430 nm attributed to the π-π^* transition of the four-coordinate boron moiety was red-shifted to 458 nm. Meanwhile during the course of the titration a new peak at ~300 nm emerged, increasing in intensity by 29%, signifying the presence of a new low electronic transition. The fact that the amount of TBAF required to reach saturation exceeded the expected amount by approximately five times indicates that the binding constant between the triarylboron center and the fluoride

anion is quite weak. On the contrary, during the titration of **B2** the saturation point was reached at 3.2 eq. of TBAF signifying a slightly stronger binding constant between the fluoride anion and triarylboron center (**Figure 3.13**). Although the changes to the absorbance profile of **B2** during the course of the TBAF titrations were quite similar to those of **B1**, the magnitude was not as large. For instance, the broad absorbance peak at ~360 nm was only quenched by 40%, while the emerging peak at ~300 nm only increased by 3%. Additionally, in the case of **B2,** the shoulder at 440 nm did not red-shift but simply appeared to be quenched.
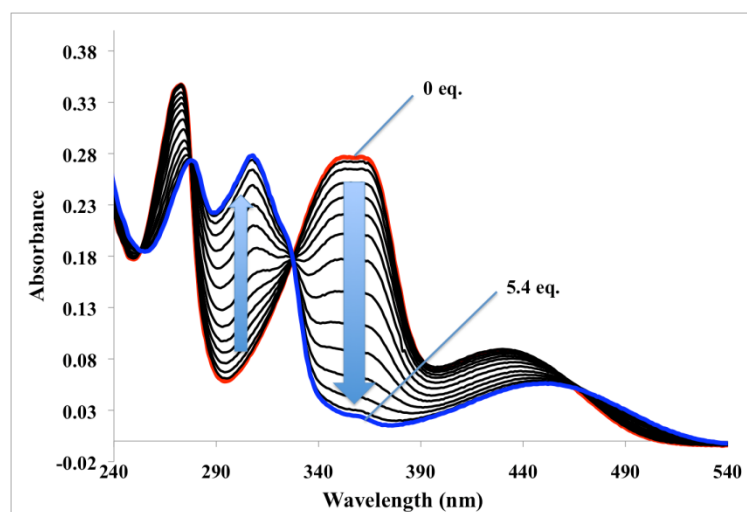
Figure 3.12. The UV-vis titration spectrum of B1 with TBAF in CH$_2$Cl$_2$ (1.0 x 10^{-5} M).
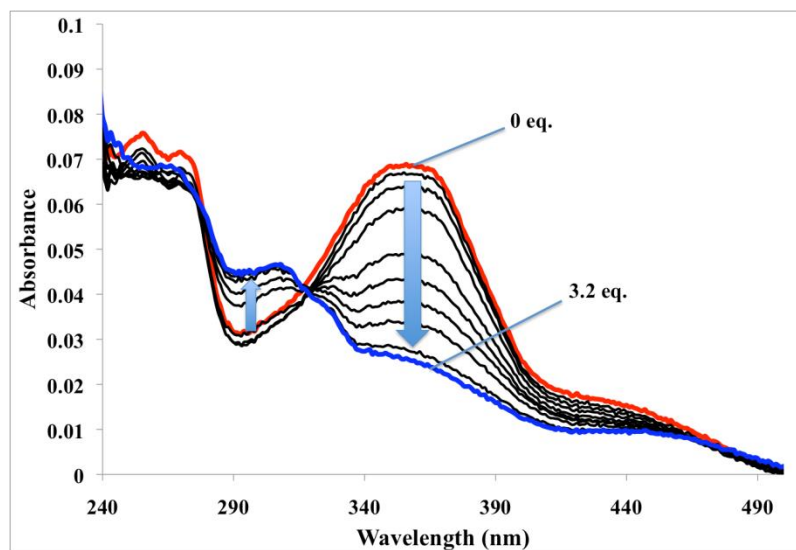
Figure 3.13. The UV-vis titration spectrum of B2 with TBAF in CH$_2$Cl$_2$ (1.0 x 10^{-5} M).

3.3.6.2 Fluorescence titration of Boron Chelates by Fluoride

The fluorescence titration spectra of **B1** and **B2** are presented in **Figure 3.14** and **Figure 3.15**, respectively. It is expected that as the fluoride anion binds to the empty p$_\pi$ orbital of the boron center the respective intramolecular CT will be inhibited and subsequently quenching the emission of the compound. The observations were consistent with the theoretical expectations as both compounds exhibited luminescent quenching. It should be noted that the luminescent quenching of **B1** upon saturation with TBAF was more extensive than that of **B2**.
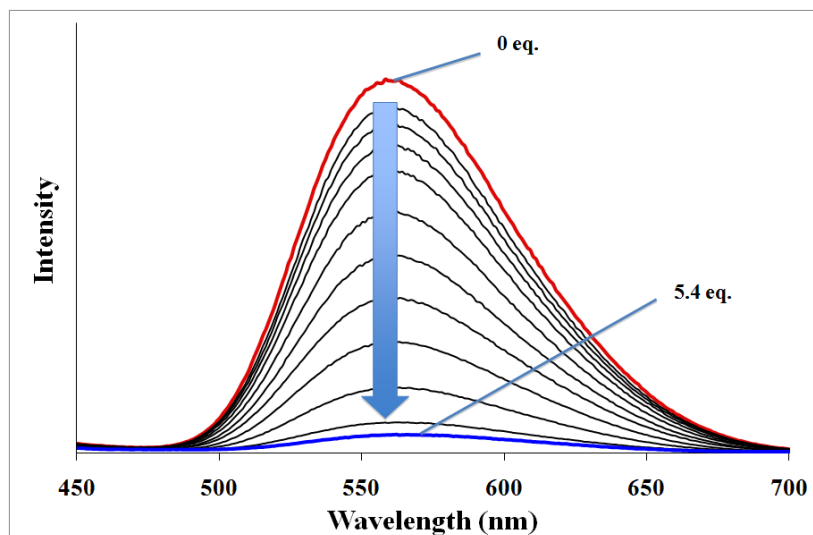
130

Figure 3.14. The fluorescent titration spectrum of B1 with TBAF in CH$_2$Cl$_2$ (1.0 x 10^{-5} M).

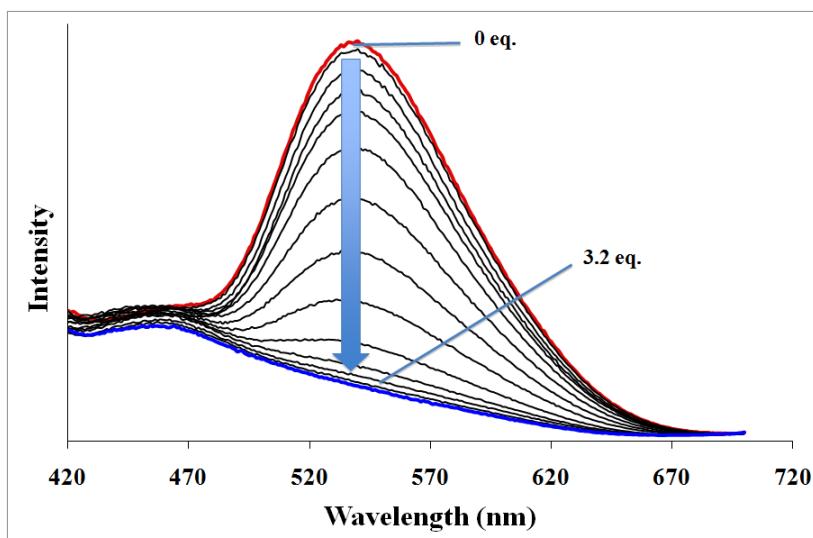**Figure 3.15. The fluorescent titration spectrum of B2 with TBAF in CH$_2$Cl$_2$ (1.0 x 10^{-5} M).**

Interestingly, according to the Stern-Volmer plots of both boron chelate systems there appears to be two binding events occurring (**Figure 3.16**). Unfortunately, both compounds only have one available site that can bind to a fluoride anion, so the second binding event must be occurring outside the system. The most likely explanation is that there was a small amount of water present in the stock solutions. As a result initially there would be competition between binding to the p_π orbital on the boron center and the water present in solution, giving the illusion of a weak binding event represented by the first shallow slope. Once all of the water has been consumed, the fluoride would then only interact with the boron center, leading to the second binding event, as observed. If this were the case, the second slope would be a result of fluoride only binding to the boron center. Another explanation that was given thought was the possibility of the fluoride anion attacking the four-coordinate boron center. There do not seem to be any similarities between the UV-Vis spectra of the free ligands **1** and **2** and the final absorption profiles of **B1** and **B2**, respectively, upon saturation. Furthermore, there are no similarities between the UV-Vis titration spectra of **B1** and **B2** to those of **1** and **2**, respectively, upon titration with TBAF. Therefore, there is likely no interaction between the fluoride anion and the four-coordinate boron center. In order to investigate this further BPh$_2$-q, an analogue of **B1** and **B2** that lacks a three-coordinate boron center, was titrated with TBAF. During the course of the titration there were no changes to the absorbance (**Figure 3.17**) and fluorescence (**Figure 3.18**) profile, supporting the conclusion that there is in fact no interaction between the 4-coordinate boron moiety and the fluoride anion. Based on the Stern-Volmer it would appear that while the luminescence of **B1** was quenched to a larger degree than **B2**, the latter was quenched more rapidly.
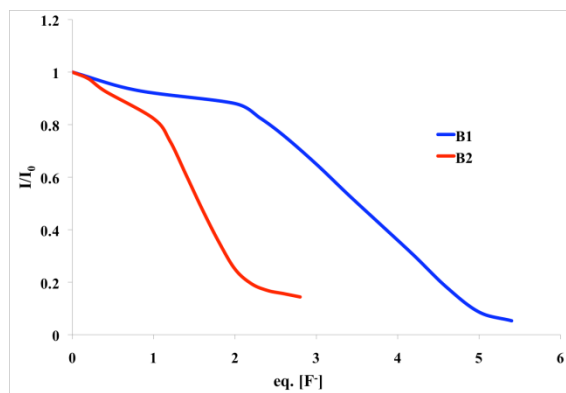
Figure 3.16. Stern-Volmer plots of B1 (λ_{max} = 558 nm) and B2 (λ_{max} = 536 nm) in CH$_2$Cl$_2$.
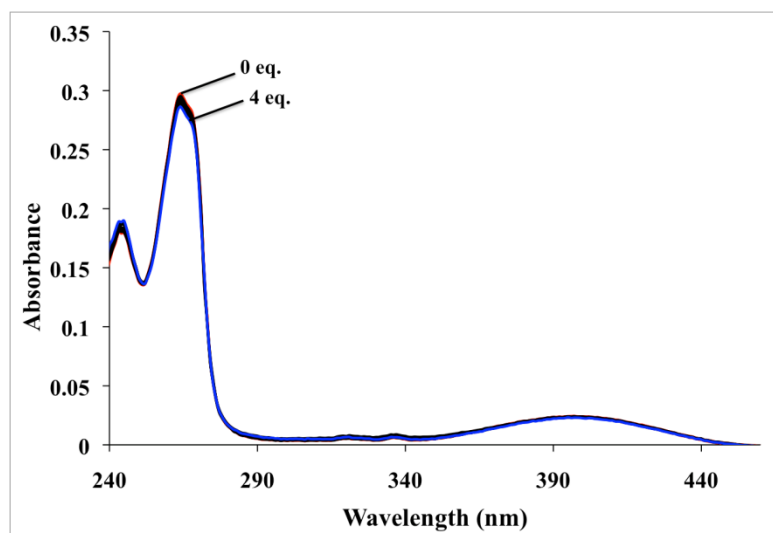
Figure 3.17. UV-Vis titration spectrum of BPh$_2$-q with TBAF in CH$_2$Cl$_2$ (1 x 10^{-5} M).

133
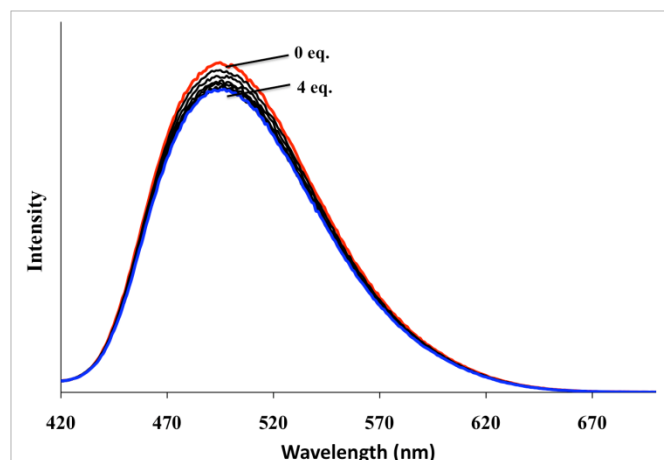
Figure 3.18. Fluorescent titration spectrum of BPh$_2$-q with TBAF in CH$_2$Cl$_2$ (1 x 10^{-5} M).

3.3.7 Conclusion

Compounds **B1** and **B2** are the first examples of diboron-functionalized 8-hydroxyquinoline compounds. Consistent with literature, it was anticipated that the electron accepting abilities of the free ligands could be enhanced upon coordination to a four-coordinate boron moiety, while retaining the luminescence of the chromophore. Not only were the reduction potentials of the boron-chelates lower than Alq$_3$ but also considerably lower than those of their aluminum analogues, making them more favorable as ETM candidates for OLEDs. As such this further supports the findings that the -BPh$_2$ moiety is able to lower the LUMO of the corresponding system, likely a result of the stronger covalent bonds that enhance the overall π-conjugation of the compound. Interestingly, although it was expected that the empty p$_\pi$-orbital on the boron center would make a significant contribution to the LUMO of both compounds, DFT calculations indicated that this was only the case for **B1**. It is believed that the shorter and highly conjugated π-skeleton of **B1** resulted in the greater effect experienced by the triarylboron moiety.

Alternatively, due to the steric hindrance from the hexyl chains on the thiophene rings of **B2** the linker took on a staggered conformation that effectively diminished the π-conjugation of system and thus reduced the effect of the triarylboron center. These conclusions are further supported by the slightly lower reduction potential of **B1** compared to the other systems investigated. According to the solid-state quantum yields, **B2** had weaker luminescent properties than **B1** attributed to the same reasons that were provided in the previous chapter regarding the flexibility of the linker in **B2**. These diboron compounds also showed potential as fluoride sensors.

3.3.8 References

1) C. D. Entwistle and T. D. Marder, *Angew. Chem. Int. Ed.*, **2002**, 41, 2927.

2) S. Wang, *Coord. Chem. Rev.*, **2001**, 215, 79.

3) A. Fukazawa and S. Yamaguchi, *Chem. —Asian J.*, **2009**, 4, 1386.

4) F. Jäkle, *Coord. Chem. Rev.*, **2006**, 250, 1107.

5) Y.-L. Rao and S. Wang, *Inorg. Chem.*, **2011**, Article Asap.

6) Q. Wu. M Esteghamatian, N.-X. Hu, Z. D. Popovic, G. Enright, S. R. Breeze and S. Wang, *Angew. Chem. Int. Ed. Engl.*, **1999**, 38, 985.

7) A. Wakamiya, T. Taniguchi and S. Yamaguchi, *Angew. Chem. Int. Ed.*, **2006**, 45, 3170.

8) Y. Cui and S. Wang, *J. Org. Chem.*, **2006**, 71, 6485.

9) A. J. Mäkinen, I. G. Hill, M. Kinoshita, T. Noda, Y. Shirota and Z. H. Kafafi, *J. Appl. Phys.*, **2002**, 91, 5456.

10) Y. Shirota, *J. Mater. Chem.*, **2000**, 10, 1.

11) M. Takahashi, K. Masui, H. Sekiguchi, N. Kobayashi, A. Mori, M. Funahashi and N. Tmaoki, *J. Am. Chem. Soc.*, 2006, **128**, 10930.

12) Z. Yuan, C. D. Entwistle, J. C. Collings, D. Albesa-Jové, A. S. Batsanov, J.A.K Howard, N.J. Taylor, H. M. Kaiser, D. E. Kaufmann, S. -Y. Poon, W. -Y. Wong, C. Jardin, S. Fathallah, A. Boucekkine, J.-F. Halet and T.B. Marder, *Chem. Eur. J.*, 2006, **12**, 2758.

13) V. A. Montes, R. Pohl, J. Shinar and P. Anzenbacher Jr., *Chem. Eur. J.*, **2006**, 12, 4523.

14) Y. Cui, Q.-D. Liu, D.-R. Bai, W.-L. Jia, Y. Tao and S. Wang, *Inorg. Chem.*, **2005**, 44, 601.

15) (a) J. Zhang and G. Frenking, *J. Phys. Chem. A.*, **2004**, 108, 10296. (b) A. Curioni, M. Boero and W. Andreoni, *Chem. Phys. Lett.*, **1998**, 294, 263. (c) A. Irfan, R. Cui, J. Zhang and C. Hao, *Chem. Phys.*, **2009**, 364, 39.

Chapter 4

Summary and Future Work

4.1 Summary

This thesis presents the synthesis and investigation of the first triarylboron-functionalized 8-hydroxyquinoline (q) ligands, **1** and **2**, their respective aluminum (III) complexes, Al(**1**)$_3$ and Al(**2**)$_3$, and diboron analogues, **B1** and **B2**. Tris(8-hydroxyquinoline)aluminum (Alq$_3$) is a well-known electron transport material that has been used in OLEDs for many years and for this reason was chosen as the parent complex for modifications intended to improve its electron accepting abilities.

In order to facilitate electron communication between the triarylboron and q moieties two different linkers were investigated. In ligand **1** a highly planar and conjugated acetylene linker was employed while ligand **2** used an oligothiophene linker that has been demonstrated to exhibit excellent electron mobility. Unfortunately, the flexible nature of the oligothiophene system reduced the quantum yield of its respective compounds, Al(**2**)$_3$ and **B2**, compared to compounds Al(**1**)$_3$ and **B1** with the acetylene system. Furthermore, the staggered and extended nature of the oligothiophene linker diminished the contribution of the electron deficient boron center to the LUMO of **B2**. Therefore, both in terms of luminescent properties and electron mobility the use of a shorter planarized and highly conjugated system is more favorable for facilitating electron mobility between the boron center and the q moiety.

The photophysical properties of the aluminum complexes were investigated using UV-Vis absorbance and fluorescence measurements. Under UV light the colors of Alq$_3$, Al(**1**)$_3$ and Al(**2**)$_3$ were green, yellow and orange, respectively. The red-shifting in emission properties was

consistent with a narrowing of the band-gap due to: (1) the triarylboron moiety lowering the LUMO level, and (2) the attachment of an overall electron donating group to the phenoxide part of q, which increased the HOMO energy level. Additionally, according to the DFT calculations the HOMO was predominantly found on the phenoxide part of q, while the LUMO was found on both the boron center and the pyridyl part of q.

Most importantly, CV measurements conducted on Al($\mathbf{1}$)$_3$ and Al($\mathbf{2}$)$_3$ indicated that both complexes possessed better electron accepting abilities than Alq$_3$, making them strong candidates as new electron transport materials.

Using ^{1}H NMR, ^{11}B NMR and spectrophotometric measurements it was discovered that the aluminum complexes were not stable in the presence of strong lewis bases such as fluoride, as the anion coordinated with the aluminum center and ejected the ligand. Therefore, Al($\mathbf{1}$)$_3$ and Al($\mathbf{2}$)$_3$ could only be used as sensors towards weak lewis bases such as cyanide.

Interestingly, based on CV measurement the diboron compounds had better electron accepting abilities than the aluminum complexes making them more favorable candidates as ETMs. The lower LUMO energy levels of **B1** and **B2** could be attributed to q having stronger and more stable coordination to the four-coordinate boron moiety as opposed to the aluminum center. In order to gain a better understanding of the electronic transitions DFT calculations were conducted on the new compounds. Similar to the Al($\mathbf{1}$)$_3$ and Al($\mathbf{2}$)$_3$, the HOMOs and LUMOs were located on the phenoxide and pyridyl parts of the q ring, respectively. Though only **B1** experienced contribution to its LUMO by the triarylboron moiety, resulting in its slightly lower reduction potential compared to **B2**.

In addition, the diboron compounds could be used as anion sensors towards both strong and weak lewis acids. This further supports the concept that q coordinated more strongly to the four-coordinate boron moiety as opposed to the aluminum center.

4.2 Future Work

At this point in time none of the compounds presented in this thesis have undergone device testing. Therefore, based on the superior electron accepting abilities of **B1** and **B2** it is prudent that these compounds undergo testing as potential ETMs in OLEDs.

Further development of this series of molecules would be promising. It is believed that by using shorter and more highly conjugated linkers that the electron communication between the three-coordinate boron moiety and q can be further enhanced. To this end, there are currently investigations into the development of ligands using a phenyl ring and a vinyl moiety as linkers (**F**igure 4.1).
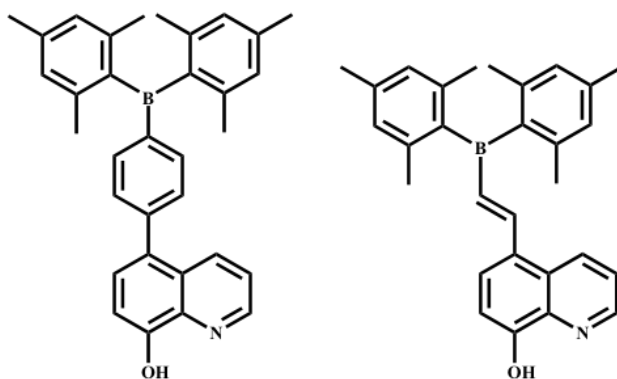

Figure 4.1. Prospective ligands as ETMs.

In addition, further investigations will be required to determine why the reduction peaks for the aluminum complexes are not reversible. It is possible that the materials lack stability in the presence of air, which is a common problem with Alq$_3$.

Finally, it is unclear why the quantum yields of both **B1** and **B2** are considerably lower than the parent system, BPh$_2$q, and more detailed experiments will be needed.